Max-Planck-Institut für Meteorologie
Max Planck Institute for Meteorology

MAX-PLANCK-GESELLSCHAFT

Regional Modeling of Inorganic and Organic Aerosol Distribution and Climate Impact over Europe

Elina Marmer

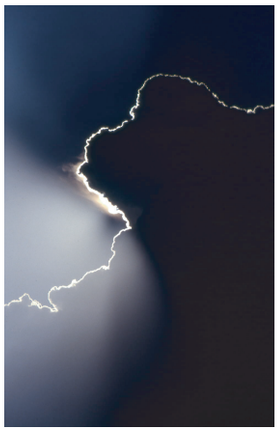

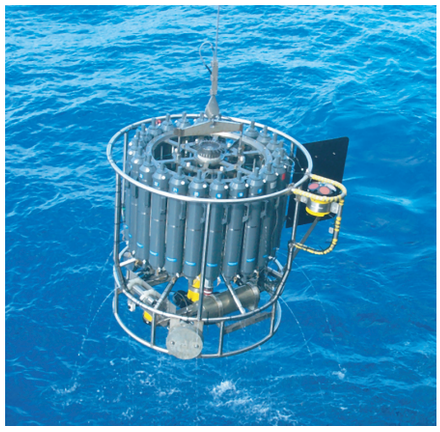

Berichte zur Erdsystemforschung 24/2006

Reports on Earth System Science

Hinweis

Die Berichte zur Erdsytemforschung werden vom Max-Planck-Institut für Meteorologie in Hamburg in unregelmäßiger Abfolge herausgegeben.

Sie enthalten wissenschaftliche und technische Beiträge, inklusive Dissertationen.

Die Beiträge geben nicht notwendigerweise die Auffassung des Instituts wieder.

Die "Berichte zur Erdsystemforschung" führen die vorherigen Reihen "Reports" und "Examensarbeiten" weiter.

Notice

The Reports on Earth System Science are published by the Max Planck Institute for Meteorology in Hamburg. They appear in irregular intervals.

They contain scientific and technical contributions, including Ph. D. theses.

The Reports do not necessarily reflect the opinion of the Institute.

The "Reports on Earth System Science" continue the former "Reports" and "Examensarbeiten" of the Max Planck Institute.

Anschrift / Address

Max-Planck-Institut für Meteorologie
Bundesstrasse 53
20146 Hamburg
Deutschland

Tel.: +49-(0)40-4 11 73-0
Fax: +49-(0)40-4 11 73-298
Web: www.mpimet.mpg.de

Layout:

Bettina Diallo, PR & Grafik

Titelfotos:
vorne:
Christian Klepp - Jochem Marotzke - Christian Klepp
hinten:
Clotilde Dubois - Christian Klepp - Katsumasa Tanaka

Berichte zur Erdsystemforschung 24/2006

Regionalmodellierung anorganischer und organischer Aerosole und deren direkten Strahlungsantriebs über Europa

Regional Modeling of Inorganic and Organic Aerosol Distribution and Climate Impact over Europe

Dissertation zur Erlangung des Doktorgrades der Naturwissenschaften
im Fachbereich Geowissenschaften der Universität Hamburg
vorgelegt von

Elina Marmer
aus Riga

Hamburg 2006

Reports on Earth System Science 24/2006

ISSN 1614-1199

Elina Marmer
Max-Planck-Institut für Meteorologie
Bundesstrasse 53
20146 Hamburg
Germany

Als Dissertation angenommen
vom Fachbereich Geowissenschaften der Universität Hamburg

auf Grund der Gutachten von
Prof. Dr. Hartmut Graßl
und
und Dr. Habil. Bärbel Langmann

Hamburg, den 2. Mai 2006
Professor Dr. Helmut Schleicher
Dekan des Fachbereiches Geowissenschaften

ISSN 1614-1199

Regional Modeling of Inorganic and Organic Aerosol Distribution and Climate Impact over Europe

Elina Marmer

Hamburg 2006

Contents

Abstract

Aerosol distribution over Europe and its direct radiative forcing have been simulated utilizing a regional atmosphere-chemistry model and an off-line radiation transfer model. Three complementary studies have been performed:
1) A simulation of air pollution causes and effects over Europe focusing on the Mediterranean region,
2) An evaluation of the historical (1900–2000) direct radiative forcing of sulfate aerosol over Europe,
3) An assessment of the relative importance of carbonaceous aerosols for air pollution and direct radiative forcing over Europe.

In the first study, the simulated peak sulfate aerosol concentration over the summertime Mediterranean Sea could be confirmed by comparison with available observations. The summer mean sulfate aerosol column burden over the Mediterranean is shown to be 7.8 mg(m^{-2}) and significantly higher than the European mean of 4.7 mg(m^{-2}). Partitioning of the SO_x emissions into land and water sources has demonstrated that ship emissions contribute 54 % to the summertime sulfate aerosol burden in the Mediterranean. The influence of the meteorological conditions characteristic for this region (high solar radiation intensity and the semi-aridity) are demonstrably the reason for the enhanced summertime pollution. Under summertime Mediterranean conditions, ship emissions of NO_x largely contribute to the formation of ozone and hydroxy radicals, which participate in the sulfate aerosol formation. Simulations excluding the ship emissions showed significantly reduced near surface concentrations of sulfate, ozone and hydroxy radicals, as well as nitric acid and formaldehyde. According to their contribution to the aerosol burden, ship emissions are shown to be responsible for over 50 % of the sulfate aerosol direct radiative forcing in the summertime Mediterranean. They account for –1 Wm^{-2} averaged over the whole region, and for –2 Wm^{-2} over the western Mediterranean Sea.

The second study simulating the historical (1900–2000) atmospheric distribution of sulfate aerosol over Europe has shown that the Mediterranean region has not always been the most polluted area in the summertime Europe. The European mean sulfate aerosol burden doubled in the first half of the 20th century, and then doubled again between the 1950's and the 1970's. Sulfate aerosol burden and its direct radiative forcing reached their peak in the 1980's. Since then, environmental policies regulating SO_x emissions successfully reduced the atmospheric load, creating a reduction in the direct radiative forcing. Averaging over Europe, the sulfate burden and forcing of the year 2000 equals that of the 1950's. Spatially, the forcing maxima of the sulfate aerosol pollution and the direct radiative forcing experienced a shift from the northwest to the southeast of Europe during the century. In the first half of the last century sulfate aerosol burden over the Mediterranean Sea was dominated by the volcanic degassing of Mt. Etna while anthropogenic sulfur sources gained importance in the second half. Policies regulating sulfur content in fossil fuel did not apply to ship emissions. Since the 1980's, ship emissions account for the only growing sulfur emission sector in Europe.

In the third study, the inclusion of both primary and secondary carbonaceous aerosols in the model has substantially altered the direct aerosol forcing estimates. Under present day conditions, highly absorbing black carbon produces a positive forcing over eastern Europe in winter and spring of +0.5 Wm^{-2} to +1 Wm^{-2}, depending what aerosol mixing state assumption is applied. The mixing state of aerosols, externally or internally, is shown to influence the strength, regional distribution and the sign of radiative forcing, thereby regulating the forcing efficiency. The modeled ground level concentrations of carbonaceous aerosols are underestimated as compared with measurements by a factor of 2–5 for black carbon and a factor of 10 for organic carbon. This underestimation most likely results from the lack of biomass burning emissions in the emission inventory. Unknown formation processes of secondary aerosol production could present an additional explanation of such a high underestimation of the organic carbon. A study scaling the carbonaceous aerosols to the levels seen in observations showed a distinct increase in both positive and negative forcing, regionally ranging from –9.5 Wm^{-2} to +13 Wm^{-2} in spring 2002 and from –11 Wm^{-2} to + 1.5 Wm^{-2} in summer 2003. Based on these two substantially different meteorological years, the inter-annual variability of aerosol burden and the direct aerosol forcing over Europe was demonstrated. General weather conditions are found to govern the aerosol life time and aerosol formation as well as sign and intensity of the direct aerosol forcing.

Zusammenfassung

Ein regionales Atmosphären-Chemie-Aerosol-Modell und ein diagnostisches Strahlungstransportmodell wurden angewandt, um die regionale Aerosolverteilung über Europa und den direkten Strahlungsantrieb von Aerosolen zu untersuchen. Folgende Themen behandelt:
1. Die Luftverschmutzung der sommerlichen Mittelmerratmosphäre;
2. Die Historischen Entwicklung des atmosphärischen Sulfataerosolgehalts und seines direkten Strahlungsantriebs über Europa im 20. Jahrhundert;
3. Die relative Bedeutung der kohlenstoffhaltigen Aerosole für die regionale atmosphärische Belastung und den direkten Strahlungsantrieb über Europa.

Die Simulation von Sulfataerosol in der ersten Studie ergab ein Immissionsmaximum in der sommerlichen Mittelmeeratmosphäre, welches durch einen Vergleich mit verfügbaren Messdaten bestätigt werden konnte. Der mittlere Sulfatgehalt der Atmosphäre über dem Mittelmeer im Sommer betrug 7,8 mg(m^{-2}) und lag wesentlich höher als das europäische Mittel von 4,7 mg(m^{-2}). Eine Aufteilung der Schwefelemissionen in Land- und Wasserquellen ergab, dass die Schiffemissionen einen wesentlichen Beitrag zum atmosphärischen Sulfatgehalt leisten, und zwar 54 %. Die außerordentliche Belastung in dieser Jahreszeit begründet sich im Einfluss, den die besonderen regionalen meteorologischen Bedingungen (hohe Intensität der solaren Einstrahlung und Semiaridität) auf die Atmosphärenchemie und die Verweildauer der Aerosole in der Atmosphäre ausüben. Unter diesen Bedingungen bewirken die Schiffemissionen von NO_x eine erhöhte Produktion von Bodenozon und Hydroxylradikalen, die ihrerseits zur Sulfatbildung beitragen. Eine Simulation ohne Schiffemissionen ergab eine erhebliche Reduktion von Sulfat, Bodenozon und Hydroxylradikalen, sowie Salpetersäure und Formaldehyd. Entsprechend ihrem Beitrag zum atmosphärischen Sulfatgehalt, sind die Schiffemissionen für 50 % des direkten Strahlungsantriebs über dem Mittelmeer im Sommer verantwortlich. Ihr Beitrag beläuft sich auf –1 Wm^{-2} im regionalen Mittel, im westlichen Mittelmeer sind es gar –2 Wm^{-2}.

Die Mittelmeeratmosphäre gehörte nicht immer zu den am meisten verschmutzten Regionen Europas, wie historische Simulationen des letzten Jahrhunderts in der zweiten Studie zeigen. Im europäischen Mittel verdoppelte sich der atmosphärische Sulfatgehalt in den ersten 50 Jahren, in den darauf folgenden 20 Jahren verdoppelte es sich nochmals. Der mittlere Sulfatgehalt und der mittlere direkte Strahlungsantrieb erreichten ihren Spitzenwert in den 1980er Jahren. Seitdem wurde der Schwefelgehalt im fossilen Treibstoff erfolgreich reduziert. Daher verminderte sich sowohl die atmosphärische Belastung als auch der direkte Strahlungsantrieb von Sulfataerosol und erreichte im Jahre 2000 etwa den Stand von 1950. Das Belastungsmaximum sowie das Strahlungsantriebsmaximum von Sulfataerosol verschoben sich im Laufe der zweiten Jahrhunderthälfte vom Nordwesten nach Südosten Europas. Während in der ersten Hälfte des 20. Jahrhunderts die Vulkanemissionen des Ätna die Sulfatbelastung der Mittelmeeratmosphäre hauptsächlich bestimmten, spielten anthropogene Emissionen in der zweiten Jahrhunderthälfte eine zunehmende Rolle.

Hinzu kommt, dass die erfolgreiche Treibstoffentschwefelung den Schiffverkehr nicht betraf. Somit sind die Schiffemissionen der europaweit einzige wachsende Emissionssektor von Schwefel seit den 1980er Jahren.

Der direkte Strahlungsantrieb veränderte sich deutlich unter Berücksichtigung von kohlenstoffartigen Aerosolen in der dritten Studie. Die entscheidende Rolle spielte hierbei das Sonnenlicht absorbierende Rußaerosol. Es bewirkte einen positiven direkten Strahlungsantrieb über Osteuropa im Frühjahr und Winter. Dieser betrug, je nach Mischungsansatz (extern oder intern), zwischen +0,5 und +1 Wm^{-2}. Der Mischungsansatz erwies sich als entscheidend für die Intensität, regionale Verteilung und das Vorzeichen des Strahlungsantriebs. Der Vergleich der modellierten bodennahen Konzentration von kohlenstoffhaltigen Aerosolen mit verfügbaren Messungen hat allerdings ergeben, dass diese vom Modell erheblich unterschätzt wurden. Diese Unterschätzung wurde auf etwa einen Faktor 2-5 für Ruß, und einen Faktor 10 für organisches Aerosol geschätzt. Unsere Ergebnisse weisen darauf hin, dass die Ursache hierfür möglicherweise in der Vernachlässigung von Biomasseverbrennung bei der Simulation begründet ist. Eine weitere Ursache wird in den wenig verstandenen Bildungsprozessen vom sekundärem organischen Aerosol vermutet. Versucht man, dieser Unterschätzung grob Rechnung zu tragen, erhöht sich der direkte Strahlungsantrieb dramatisch – der berechnete Antrieb lag regional im Bereich von –9.5 bis +13 Wm^{-2} im Frühjahr 2002 und von –11 bis +1.5 Wm^{-2} im Sommer 2003. Die zwischenjährliche Variabilität sowohl des Strahlungsantriebs als auch der regionalen Verteilung und der atmosphärischen Belastung von Aerosolen wurde an Hand der meteorologisch sehr unterschiedlichen Jahre 2002 und 2003 untersucht. Entscheidende Rolle spielen dabei die Großwetterlagen, die die Verweildauer von Aerosolen in der Atmosphäre, die Bildung von sekundären Aerosolen sowie das Vorzeichen und die Intensität des Strahlungsantriebs von Aerosolen zum Teil erheblich beeinflussen.

Chapter 1

Introduction

Atmospheric aerosol is defined as a suspension of liquid and solid particles in air. We distinguish between primary aerosols, which are directly emitted in the atmosphere in particulate form, and secondary aerosols, which are formed in the atmosphere from gaseous precursor molecules by gas and aqueous phase reactions. The size of atmospheric aerosol particles ranges from nanometers to several tens of micrometers. For measurements and environmental regulations, aerosols are often divided into three major size categories: PM_{10} includes aerosol particles smaller than 10 μm, $PM_{2.5}$ includes particles smaller than 2.5 μm and PM_1 particles smaller than 1 μm.
The main components of atmospheric aerosol are sulfate, carbonaceous substances, ammonium, nitrate, mineral dust and sea salt. Mineral dust is emitted by wind-driven mobilization of erodible soil dust particles. In Europe, mineral dust was observed to be a major contributor to PM_{10} at roadside sites (20 %) (Putaud et al., 2004), indicating the importance of anthropogenic activities for mineral dust emissions. Sea salt aerosol is produced by bursting of air bubbles produced by breaking waves (e.g. Blanchard, 1963) and is an important contributor to atmospheric aerosol at European coastal sites. The main type of aerosol found at European urban and near-city sites is organic aerosol, with an average contribution of 20 %; under polluted conditions ($PM_{10} > 50$ $\mu g(m^{-3})$), the contribution of nitrate becomes very important (Putaud et al., 2004). Nitrate aerosols are formed in conditions with excess ammonia to neutralize all sulfuric acid to ammonium sulfate (Seinfeld and Pandis, 1998). At natural and rural background European sites, non-sea-salt sulfate aerosol was found to be the main contributor to aerosols sampled (30 %); black carbon contributes 5–10 % to the atmospheric aerosol (Putaud et al., 2004).
Following is a more detailed introduction about the aerosol species considered in the model studies of this work, their sources and sinks, measurements, previous modeling efforts, and lastly the effects of these aerosols on human health and climate.

1.1 Sulfate aerosol

Sulfate is a secondary aerosol, which is produced in the atmosphere from gaseous precursor molecules, sulfur dioxide (SO_2) and dimethyl sulfide (DMS), via chemical reactions

(except for sulfate aerosol from sea salt and gypsum dust). The oxidation of SO_2 can take place in the gas phase, or after SO_2 becomes dissolved in cloud droplets (aqueous production). In an intercomparison study of global models, 12 % of SO_2 were found to be oxidized in the gas phase and 45 % in the aqueous phase (Penner et al., 2001). The main oxidation pathways of SO_2 to sulfate are the oxidation by hydroxy radicals (OH) in the gas phase and the oxidation by hydrogen peroxide (H_2O_2) and ozone (O_3) in the aqueous phase. During summer in southern Europe, there are only few clouds but high OH concentrations, resulting in the main path of sulfate aerosol production via the oxidation of SO_2 by OH in the gas phase (Bardouki et al., 2003). Both pathways produce sulfate aerosols in the submicron size range that are efficient sun light scatterers. Positively charged ions must be present on sulfate aerosols to neutralize the sulfate anions. Thus, the sulfate in aerosol particles is mainly present as sulfuric acid (H_2SO_4), ammonium sulfate $(NH_4)_2SO_4$, or ammonia hydrogen sulfate, depending on the availability of gaseous ammonia to neutralize the sulfuric acid formed from SO_2.
The calculated residence times of SO_2, defined as the global burden divided by the global emission flux, range from 0.6 to 2.1 days (Penner et al., 2001). Only 46-82 % of the emitted SO_2 undergoes chemical transformations and forms sulfate, because of losses due to SO_2 deposition. The residence time of sulfate is mainly determined by wet removal and is estimated to be between 2.7 and 7.2 days (Penner et al., 2001).

1.2 Carbonaceous aerosol

Carbonaceous aerosol is increasingly recognized as an important atmospheric constituent (Hansen et al., 2004). Primary carbonaceous aerosol is produced by incomplete combustion of fossil fuels, biofuels, and biomass that generally form through condensation of vaporized organic compounds (Chylek et al., 2003). Biogenic emissions from vegetation and animals are also important sources of carbonaceous aerosols. Black carbon, in the form of graphite, is the main cause of the blackness of soot; it strongly absorbs sunlight almost uniformly across the solar spectrum. Carbonaceous aerosol includes an enormous variety of carbon containing organic compounds. Carbonaceous aerosol is usually divided into categories of black carbon (BC) and water soluble and water insoluble organic carbon (OC). This partitioning is based on the aerosol optical properties. The carbonaceous aerosol that strongly absorbs visible radiation is defined as BC, the remaining fraction as OC. OC aerosols may mainly scatter visible light, with weak absorption usually increasing toward ultraviolet wavelengths (Hansen et al., 2004).
Besides primarily released organic carbon (POC), secondary organic aerosol (SOA) is formed in the atmosphere by photo-oxidation of reactive volatile organic compounds (VOC). The formation of SOA involves two crucial steps: First volatile organic precursor gases are oxidized mainly by O_3, NO_3 and OH to form semi-volatile organic carbon with saturation vapor pressures below a certain threshold (Turpin et al., 2000). Those semi-volatile organic compounds then partition between the gas aerosol phase. Three main aerosol formation processes are discussed in the literature: condensation, adsorption (accumulation of a gas onto a particle surface) and absorption (dissolving of a gas into an

aerosol particle), with condensation being considered the most important process (Odum et al., 1997a,b). The production of SOA is highly temperature dependent. A model study (Strader et al., 1999) suggests that the ideal temperature for SOA formation lies between 15 and 20 °C, where the temperature is high enough for fast oxidation and low enough for effective condensation.
The atmospheric contribution of BC, POC and SOA to the carbonaceous aerosol is up to day very uncertain. The EU project CARBOSOL was established to gain a deeper insight into the sources, composition and formation processes of carbonaceous aerosols over Europe. During the project, iterative use of models and measurements has been applied to estimate the relative contribution of natural versus anthropogenic and primary versus secondary organic carbon (Gelencsér et al., 2006; Pio et al., 2006).

1.3 Emissions

Reliable emission inventories of primary aerosols and the gaseous precursors to secondary aerosols are the key to accurate modeling of atmospheric aerosol distribution. Historical emission inventories are needed to investigate the possible role of aerosols in past climate change.
The two main sulfate precursor substances are SO_2, released from anthropogenic sources and volcanos, and dimethyl sulfide (DMS) from biogenic sources, especially marine plankton. Extrapolations from measurements to emission factors result in widely variable estimates of total natural emissions of SO_2 and DMS (Mylona, 1996). European volcanic emissions of SO_2 are dominated by the degassing of Italian and Iceland volcanos. Emissions of DMS make only a small fraction of total emission of sulfate aerosol precursors in Europe. Anthropogenic sulfur emissions mainly originate from the combustion of fossil fuels (coal and petroleum). Additional releases occur during petroleum refining, the roasting and smelting of sulfidic ores in the production of copper, lead, zinc and nickel, the production of sulfuric acid and sulfur, the conversion of pulp into paper and refuse incineration (Mylona, 1996). Sulfur dioxide is also released during fuel wood burning (Mylona, 1996). A large fraction of SO_2 is emitted from high stack chimneys, and thus can be transported over long distances in the atmosphere (Fabian, 1993). The source strengths for anthropogenic SO_2 gas are fairly well known compared to other aerosol precursor gases, and recent global estimates differ by no more than 20–30 % (Penner et al., 2001). During the first half of the last century, Europe was one of the strongest SO_2 emitters world-wide. The awareness of the health risks and environmental impacts of the atmospheric sulfate aerosol pollution resulted in efficient emission control since the late 1970's, leading to a constant and significant reduction of anthropogenic SO_2 emissions (Mylona, 1996).
Primary carbonaceous aerosols BC and POC are emitted by incomplete combustion of fossil fuels, biofuels, and biomass (Chylek et al., 2003). A recent and extensive analysis of BC and POC emissions is provided by Bond et al. (2004), using energy statistics for the year 1996. Main uncertainties are associated with the choice of emission factors that depend on the fuel burnt and the type of combustion. Biofuel consumption for domestic use is the source category associated with the highest uncertainty due to the difficulty in getting reliable statistics. A recent study by Schaap et al. (2004) suggests that in

Europe the BC emissions of this inventory may be underestimated by a factor of two. Novakov et al. (2003) estimated global historical trends in fossil fuel BC emissions since 1875. These trends show rapid increase in the latter part of the 1800's and levelling off in the first part of 1900's. These changes that have caused regionally large temporal modifications in aerosol absorption might be accompanied by similar trends in POC emissions. These emission trends and associated climate impacts are still rather uncertain and need further evaluation (Kanakidou et al., 2004).
Precursor gases for the formation of SOA, VOCs, are emitted from anthropogenic (fossil fuel and wood combustion, biomass burning, solvent use) and natural sources (e.g. Seinfeld and Pandis, 1998; Jacobson et al., 2000). On a global basis the emissions of biogenic VOCs, which are emitted mainly by vegetation, are estimated to exceed those from anthropogenic emissions (Guenther et al., 1991, 1993). Isoprene accounts for about half of all natural VOC emissions and is, on a mass basis, the dominant emitted biogenic VOC component (Wiedinmeyer et al., 2004).Claeys et al. (2004) proposed that a small fraction of isoprene may be converted into SOA However, isoprene is generally not considered as a major producer of SOA, but it is generally not considered a major producer of SOA. Globally, woods, crops and shrubs contribute 55 %, 15 % and 14 % respectively to the non-isoprene biogenic emissions. The main external factors influencing biogenic VOC emissions are temperature, light and water stress (Kanakidou et al. (2004) and references therein). The overall uncertainties of emissions both of primary carbonaceous particles and of gaseous precursors of SOA range between a factor of 2 and 5 (Kanakidou et al., 2004).
Emissions of NO_x (NO and NO_2) play an important role in the atmospheric chemistry, contributing to the secondary aerosol formation. In Europe, NO_x are predominantly emitted form road and ship traffic and from industrial combustion and production processes. Lightning is a natural emission source of NO_x, but it is negligible over Europe.

1.4 Aerosol deposition

Aerosols are removed from the atmosphere by dry and wet deposition. Dry deposition depends on surface friction, boundary layer stability and gravitational settling and is less important than wet deposition by scavenging, which presents the main sink of atmospheric aerosol.
Aerosol is scavenged within a cloud and below a cloud. The wet scavenging of aerosol depends on large-scale features such as cloud formation, the conversion of cloud droplets into rain drops, sedimentation and evaporation of rain. In addition to large scale cloud and rain processes, the wet scavenging also depends on microphysical properties of the aerosol, determining its ability to get included in cloud and rain droplets. Kasper-Giebl et al. (2000) have measured the scavenging efficiency of different organic compounds at Mt. Sonnblick, Austria. Dicarboxylic acids were found to be the most efficient class of organics to be scavenged, with an efficiency similar to that of sulfate. Scavenging efficiency also depends on the liquid water content of the cloud. Scavenging efficiency of black carbon was measured by Hitzenberger et al. (2000) and was found to be lower than that of OC and sulfate. The scavenging efficiency is directly related to the hygroscopicity

of the particles. While sulfate aerosol is assumed to be highly hygroscopic, freshly released carbonaceous aerosols are more hydrophobic, becoming more hygroscopic with time by chemical and physical aging. Chemical aging refers to chemical modifications of the aerosol components due to heterogeneous and liquid phase reactions, thereby modifying the hygroscopicity of the particles. Physical aging is due to mixing processes such as coagulation and condensation adding more soluble material, thereby increasing the overall solubility and hygroscopicity of the particles. The aerosol aging that converts aerosol properties from hydrophobic to hygroscopic is a key process determining the wet removal, and hence the residence time and atmospheric burden, of aerosols in the atmosphere (Kanakidou et al. (2004) and references therein).
Precipitation cleans the atmosphere of anthropogenic and natural pollution by depositing aerosol, but high concentration of sulfate in rain water – so called "acid rain" – causes acidification of surface waters and soil, disturbing vegetation and forest ecosystems (Likens and Bohrmann, 1974). This problem was recognized in Europe and the United States in the 1970's, and became one of the reasons for sulfur emission reduction strategies (Stoddart et al., 1999). In Asia, where sulfur emissions remain uncontrolled, they cause increasing acidification of water and soil (Lin and Gao, 2002).

1.5 3-Dimensional aerosol modeling

3D atmosphere aerosol models are important tools for determining aerosol load distribution because of the the sparseness of measurements and large aerosol spatial inhomogeneity.
Aerosols generally show large spatial variability because of spatial variability of their sources combined with their short atmospheric life times and their rapid chemical and microphysical transformations, transport, and removal processes. As a result, the effects of anthropogenic aerosols are expected to be particularly relevant at the regional scale (Solmon et al., 2006). Recent development of high-resolution regional aerosol climate models offers useful tools to assess the regional impacts of anthropogenic aerosols. Compared to global climate models the relatively high-resolution and detailed physical parameterizations offered by regional models are particularly suitable to describe the complexity of aerosol processes (Solmon et al., 2006). For example, Giorgi et al. (2002, 2003) and (Qian et al., 2003) assessed the regional climatic impacts deriving from the direct and indirect effects of anthropogenic aerosol over East Asia and found that these effects can help to explain a cooling trend over various regions of China during the last decades of the 20th century. Ekman and Rodhe (2003) carried out a similar study for Europe and found that anthropogenic sulfate can induce a cooling of more than 1 K. Menon et al. (2002) found substantial regional climatic effects induced by large BC aerosol forcing over South Asia.
In high emission areas, such as Europe, an accurate description of regional aerosol burdens and their chemical nature is still a key issue with regard to the effectiveness of emission reduction policies (Solmon et al., 2006). Several European Air Quality Models have been upgraded toward a more detailed description of tropospheric aerosols. Six of these models have been intercompared within the EUROTRAC 2 project (Hass et al.,

2003). The aerosol process treatment by the models varies substantially. All models include sulfate aerosol, while only some include nitrate. Primary carbonaceous aerosols are only included in EURAD (Hass et al., 1993, 1995) and LOTOS (van Loon et al., 2000): these are the only models explicitly treating secondary aerosol production utilizing the SORGAM module (Schell, 2000). The size distribution of aerosols within these models is either modal or sectional; two models consider aerosol as a bulk mass. The aerosol modul MADE (Ackermann et al., 1998), incorporated in EURAD, provides detailed information about the chemical composition and the size distribution of the particles as well as the dynamic processes influencing the particle population. The aerosol climate model ECHAM5-HAM with the aerosol module M7 is one of the recent developments on the global aerosol modeling scale. It predicts the evaluation of an ensemble of microphysically interacting internally and externally mixed aerosol population as well as their size distribution and chemical composition (Stier, 2004).
Due to the complexity of the formation mechanism of SOA and the great number of individual chemical species involved, it is especially challenging to incorporate secondary organic particles into aerosol climate models (Dusek, 2000). Both the actual gas-phase reaction pathways and the condensation mechanisms of secondary aerosol formation, however, are still rather speculative. In SOA models, the aerosol formation potential of important precursor gases is characterized by establishing empirical expressions for the total amount of aerosol formed by the oxidation of precursor gas. The aerosol formation potential is expressed either by the fractional aerosol coefficient or the aerosol yield (Dusek, 2000). Most of the experiments of the atmospheric chemistry for quantification of SOA yields, fractional aerosol coefficients and its molecular composition have been performed in smog chambers. Chamber experiments have inherent difficulties associated with the chemistry of SOA formation when extrapolating the results to atmospheric conditions (Kanakidou et al., 2004).

1.6 Aerosol measurements

The accuracy of aerosol emission scenarios and the capability of atmospheric aerosol models need to be continuously evaluated and improved using a variety of observational data. Satellite data and ground-based networks can be used to evaluate emission inventories and modeling processes. Continuous ground based measurements of sulfate aerosol in air and rain water exist in Europe for several decades. The largest European network is operated by EMEP (Co-operative program for monitoring and evaluation of the long-range transmissions of air pollutants in Europe, http://www.nilu.no/projects/ccc/emepdata.html). During the last decade, organic and black carbon started to be more commonly measured over longer time periods. Measurements of carbonaceous aerosols were included in decadal data sets produced in Europe (Putaud et al., 2004). Recently, OC measurements have been added to the EMEP monitoring program. A source-apportionment analysis of continuous aerosol samples from six European sites samples was recently performed by Gelencsér et al. (2006). The sampled carbonaceous species were specified as emitted from fossil fuel combustion and from biomass burning; organic carbon was additionally

specified as primary and secondary.
Uncertainties in determining the black and organic carbon concentration from aerosol samples arise from the difficulty of separating BC and OC (Kanakidou et al., 2004). The distinction between these two species is only instrumentally defined. The transformation of OC to BC during thermal analysis which is dependent on analytical conditions and sampling substrate nature, all of which can strongly affect the reported OC/BC partitioning. As a consequence, the difference in OC determination from two different techniques can be as high as a factor of 2. OC measurements may be seriously affected by various artifacts at the sampling and analysis stages (Turpin et al., 2000). Several sampling methods compared in Hering et al. (1990) showed up to 70 % differences in a single sample (Kanakidou et al., 2004).
Remote sensing of aerosols has made significant progress in the past years (e.g. King et al., 1999; Kaufman et al., 2002; Veefkind et al., 1999; Bellouin et al., 2005), but uncertainties also exist in satellite products and algorithm parameters (Bellouin et al., 2005): Satellite measurements over land are unreliable, especially the PM_1 fraction, which dominates the anthropogenic aerosols. The parameter retrieved from satellite is the aerosol optical thickness, which has to be converted to the actual aerosol burden assuming aerosol specific extinction. Large deviations can result from different assumptions (Section 1.7). An additional difficulty is that different aerosol species can not be distinguished.

1.7 Aerosol optical properties

Aerosol optical properties, such as optical thickness (AOT) and single scattering albedo (ω) have to be determined in order to quantify the direct aerosol radiative forcing. AOT is the extinction resulting from absorption and scattering of radiation by the aerosols in a column and is directly dependent on the aerosol column burden. The spectral characteristics of AOT are required to model the radiative forcing and to retrieve aerosol parameters from satellite remote sensing. ω is defined as

$$\omega = \frac{Q_{scat}}{(Q_{scat} + Q_{abs})} \tag{1.1}$$

where Q_{scat} and Q_{abs} are the scattering and absorption efficiencies of the aerosol respectively. Q_{scat} and Q_{abs} are commonly calculated by Mie theory assuming a spherical aerosol shape and depending on the aerosol complex index of refraction and a size distribution. The complex index of refraction $N(\lambda)$ is given by

$$N(\lambda) = n(\lambda) + ik(\lambda) \tag{1.2}$$

$k(\lambda)$: wavelength dependent absorption index
$n(\lambda)$: wavelength dependent refractive index

A single scattering albedo ω=1 indicates an aerosol with 100 % scattering properties.
The optical properties of sulfate, which mainly scatters shortwave radiation, are reasonably well known compared with other types of aerosols (Li et al., 2001). Only BC

aerosol is known to be highly absorbing. The optical properties of organic carbon are not well established. Myhre and Nielsen (2004) studied the complex index of refraction of various organic aerosol components and mixtures at concentrations representative for tropospheric particulate matter and found that all the investigated organic acids scatter solar radiation similar to sulfate aerosol.
One of the major uncertainties associated with deriving aerosol optical properties results from assumption regarding the mixing state. The diversity of aerosol types results in a complex mixture of aerosol components that reside in the atmosphere. The different molecular compositions influence the aerosol size distribution, particle shape, water solubility, hygroscopicity, and refractive index (Lesins et al., 2002). Aerosol components can be either assumed to be physically separated creating an external mixture of chemically pure modes, or the aerosols can be assumed to be internally mixed as a homogeneous material reflecting the chemical and physical average of all contributing components. A third assumption is that hydrophobic particles, such as black carbon, get coated with sulfate or SOA aerosols. Internally mixed primary aerosols can be produced at the source if more than one component is involved in the formation process of the aerosol. This can be expected in the combustion of complex mixtures of materials such as fossil fuels and biomass. Even if the particles are individually pure when first produced, there are numerous processes in the atmosphere that can convert an external mixture to an internal mixture. Coagulation increases the average aerosol size and is particularly effective if there is a large size difference between the colliding particles. The cycling of aerosols through a cloud where condensation is followed by evaporation can produce larger heterogeneous particles from all the aerosols collected by scavenging or accumulated as the cloud droplets coalesced. Aqueous phase reactions may also enhance the oxidation rate of dissolved gases that can combine with other aerosols to form internal mixtures. Initially hydrophobic particles such as black carbon may eventually be incorporated in cloud droplets. Gas-to-particle reactions onto existing particles will also create composite mixtures (Lesins et al., 2002).

1.8 Climate impacts

Atmospheric aerosols influence the radiative budget of the Earth-atmosphere system in two different ways. The direct forcing results from scattering and absorbing of the solar and thermal infrared radiation by aerosol particles, thereby altering the planetary albedo. The indirect forcing results from modification of microphysical and radiative properties and lifetime of clouds by aerosols (Haywood and Boucher, 2000). Radiative calculations are performed excluding and including the aerosol perturbation. The difference in the net radiation at the top of the atmosphere yields the TOA radiative forcing, while the difference in the net surface radiation, the bottom of the atmosphere, yields the BOA radiative forcing. The difference between BOA and TOA corresponds to the energy absorbed in the aerosol layer (Gilgen et al., 1998). Aerosol scattering and absorption reduces the incoming short wave radiation at the surface (Gilgen et al., 1998). This reduction is partly balanced by reductions in the fluxes of latent and sensible heat. The

resulting reduction of evaporation and evapotranspiration is dampening the hydrological cycle (Liepert et al., 2004; Feichter et al., 2004; Hohenegger and Vidale, 2005). Aerosols also interact with the chemistry of the atmosphere, influencing the radiative effects of other chemical species, such as ozone (Crutzen, 1996; Ravishankara, 1997; Andreae and Crutzen, 1997).

1.8.1 Direct radiative forcing

The Intergovernmental Panel on Climate Change (IPCC, 2001) considered the direct radiative forcing from sulfate, fossil fuel back carbon and biomass-burning aerosols. The subjective confidence level of IPCC (2001) was found to be "low" for sulfate aerosol and "very low" for other aerosol species. The direct radiative forcing depends on the atmospheric column burden of particulate aerosol species, the aerosol size distribution, the chemical composition and the mixing state of the aerosols, as well as on the albedo of the underlying surface and clouds, the relative humidity for hygroscopic aerosols and the radiation. Sulfate and organic aerosols are found to be mainly scattering (Section 1.7 and references therein). Enhanced aerosol scattering of solar radiation back into space increases the planetary albedo and is therefore associated with cooling. Black carbon is a strong absorber of solar radiation and is therefore associated with warming (Hess et al., 1998). Enhanced absorption of atmospheric aerosols and hence radiative heating due to internal mixing with black carbon was found by Jacobson (2001) and Schnaiter et al. (2005). Sulfate and carbonaceous aerosols have negligible radiative effects in the infrared spectrum. Mineral dust is predominantly scattering in the visible spectrum. Because mineral dust particles are of a large size, they may exert a significant thermal infrared radiative forcing, which is positive, because mineral dust is absorbing in infrared (Sokolik and Toon, 1996). The sensitivity of the modeled European climate to a change in its aerosol direct forcing due to different aerosol distributions was investigated by Hohenegger and Vidale (2005).

1.8.2 Indirect radiative forcing

Aerosols can serve as cloud condensation and ice nuclei. An increase in aerosol concentration can modify the microphysical and radiative properties of clouds, resulting in more but smaller cloud droplets (Twomey, 1974), defined as the first indirect effect. Smaller cloud droplets can suppress precipitation in warm clouds, prolonging the life time of the cloud and the aerosol (Albrecht, 1989; Rosenfeld, 1999; Khain et al., 2001), defined as the second indirect effect. Absorption of solar radiation by black carbon particles in clouds can evaporate cloud droplets reducing cloud cover (Ackerman et al., 2000), defined as the semi-indirect effect. Additionally, black carbon particles can act as ice nuclei (DeMott et al., 1999), enhancing the precipitation formation in mixed phase clouds and reducing the cloud life time (Lohmann, 2002), defined as the glaciation indirect effect. Further, black carbon particles in cloud droplets can reduce the cloud albedo (Krüger and Grassl, 2002). Significantly larger cloud droplet number concentrations and smaller cloud droplets for clouds formed in air masses of continental origin compared with air masses of marine

origin were reported by Brenguier et al. (2000). The indirect aerosol effect over Europe was demonstrated by Krüger and Grassl (2002).
According to general circulation model studies the indirect effect is similar in magnitude to the direct effect (Haywood and Boucher (2000) and references therein). Same conclusion can be drawn for Europe from the regional model study of the sulfate direct and indirect radiative forcing of Langmann et al. (1998). The aerosol indirect effect from enhanced aerosol concentrations is very difficult to measure, the model results thus can not be validated Haywood and Boucher (2000).

1.9 Health impacts

The effects of inhaling particulate matter by humans and animals has been widely studied and include: asthma, lung cancer-cardiovascular issues, and death. The size of the particle determines where in the body the particle will come to rest if inhaled. Larger particles are generally filtered by small hairs in the nose and throat and do not cause problems, but particulate matter smaller than 10 μm, PM_{10}, can settle in the bronchies and lungs and cause health problems (Pekkanen et al. (2002) and references therein). $PM_{2.5}$, can penetrate directly into the lung, whereas PM_1 can penetrate into the alveolar region of the lung and tend to be the most hazardous when inhaled. In particular, a study by Pope (2002), indicates that $PM_{2.5}$ leads to high plaque deposits in arteries, causing vascular inflammation and atherosclerosis – a hardening of the arteries that reduces elasticity, which can lead to heart attacks and other cardiovascular problems. There is evidence that particles smaller than 100 nanometers can pass through cell membranes, for example, such particles can migrate into the brain. It has been suggested that particulate matter can cause similar brain damage as that found in Alzheimer patients (Pekkanen et al. (2002) and references therein). The large number of deaths and health problems associated with particulate pollution was first demonstrated in the early 1970's (Lave and Seskin, 1973) and has been reproduced many times since. The World Health Organization (WHO, 2002) estimated that the increased mortality due to particulate matter in outdoor air to be about 100,000 people per year in Europe. The European Commission has set limits for PM_{10} in the air in directives 1999/30/EC and 96/62/EC.

1.10 Objectives and outline of this study

This study is dedicated to a better understanding of past and present day aerosol distribution and direct radiative forcing over Europe. Chapter 2 describes a present day sulfate aerosol distribution simulated by applying the regional atmosphere chemistry model REMOTE (Langmann, 2000). Emissions are based on the EMEP emission inventory (Vestreng et al., 2004). The direct radiative forcing of sulfate aerosol is estimated diagnostically with the radiation transfer model ORTM (Langmann et al., 1998). The chapter is focused on the impact of ship emissions on Mediterranean pollution and climate and has been published (Marmer and Langmann, 2005). In Chapter 3 the historical evolution of sulfate aerosol direct forcing over Europe is investigated. This study is based on

historical sulfur emissions and respective sulfate aerosol distribution simulations from the Norwegian Meteorological Institute. The evolution of the radiative forcing is calculated diagnostically utilizing the ORTM model. The temporal and regional trend of aerosol distribution and its impact on the direct radiative forcing is discussed, focusing on the change of the forcing efficiency, for the European continent, and exemplarily for selected areas. Originally, historical emissions and distribution of black carbon aerosol were supposed to be additionally included in this study. Unfortunately, difficulties in determining consistent historical black carbon emissions occurred. The study is thus meant to be a base line for additional research, which will have to include black carbon in future. In Chapter 4, carbonaceous aerosols are investigated. Primary black and organic carbon emissions were based on the EMEP emission inventory of $PM_{2.5}$. Secondary organic carbon formation in the atmosphere was implemented based on the SORGAM model (Schell, 2000). Present day distribution of sulfate and carbonaceous aerosols was simulated, and evaluated against measurements. The uncertainties of the modeled distribution are discussed based on the source-apportionment analysis of carbonaceous species (Gelencsér et al., 2006). The dependency of the spatial, seasonal and inter-annual variation of aerosol distribution on variation of emissions and general weather conditions are analyzed. Further, direct radiative forcing of these aerosols alternatively assuming external and internal mixing are estimated. The direct radiative forcing of a realistic aerosol load based on observations, is calculated in a sensitivity experiment. The dependency of the spatial, annual and inter-annual forcing efficiency on variations in aerosol burden and meteorological conditions was investigated. Chapters 3 and 4 present the manuscripts to be submitted to a special issue together with other publications resulting from the research conducted during the EU-project CARBOSOL. Chapter 5 finalizes the main findings and gives an outlook about the ongoing and future research.

Chapter 2

Impact of ship emissions on the Mediterranean summertime pollution and climate: A regional model study

[1] **Abstract**

Ship emissions contribute substantially to atmospheric pollution over the summertime Mediterranean region, thereby modifying the radiation budget through sulfate aerosol forcing. By applying a regional atmospheric-chemistry model and a radiation model we determine the seasonal variability of secondary trace gases and aerosols, their origin and impact on climate. Summer mean sulfate aerosol column burden over the Mediterranean is 7.8 mg m^{-2} and remarkably higher than the European mean of 4.7 mg m^{-2}. Partitioning SO_2 emissions into land and water sources allows to investigate their respective impact on the sulfate aerosol concentration, its total burden and direct radiative forcing. 54% of the total sulfate aerosol column burden over the Mediterranean in summer originates from ship emissions. Accordingly, they contribute over 50% to the direct radiative forcing. Running the model without ship emissions significantly reduces near surface concentration of sulfate, ozone, nitric acid, hydroxy radicals and formaldehyde. As the applied ship emission inventory is based on the year 1990 and model results tend to underestimate observed concentrations at Mediterranean locations influenced by ship emissions, we assume that increased ship emissions during the past decade contribute nowadays even stronger to secondary pollution formation and radiative forcing.

[1] published as: Marmer, E. and Langmann B., Impact of ship emissions on the Mediterranean summertime pollution and climate: A regional model study *Atmos. Environ., 39, 4659–4669, 2005.*

2.1 Introduction

The summertime Mediterranean atmosphere ranks among the most polluted regions on Earth in terms of photochemical ozone formation and aerosol loading (Kouvarakis et al., 2000; Lelieveld and Dentener, 2000). Concentrations of several trace gases (ozone, formaldehyde, peroxy radicals, nitric oxide) are considerably enhanced in the Mediterranean summer atmosphere compared with the hemispheric background (Lelieveld et al., 2002). Meteorological and chemical conditions during Mediterranean summer favor the accumulation of primary emitted pollutants and the formation of secondary gases and aerosols. Photochemical processes responsible for the production of secondary pollutants are enhanced due to high solar radiation intensity. Wash out processes are limited by summertime aridity.

Transport of air pollution from outside the Mediterranean region is one cause for increased concentrations of primary and secondary pollutants (Lelieveld et al., 2002). Several aspects of this phenomenon have been the subject of MINOS (Mediterranean Intensive Oxidant Study) campaign in August 2001 (Mihalapous and de Reus, 2004). In the summertime upper troposphere, Asian monsoon outflow transports pollution across northern Africa and the Mediterranean (Scheeren et al., 2003). In the middle troposphere, westerly winds prevail, transporting polluted air masses from Western Europe and North America. In the surface layer, land emissions from South and Central Europe are transported to the Western Mediterranean by northerly winds (Sciare et al., 2003).

Local ship emissions are important sources of the atmospheric pollution in the region. The main trace gases emitted from ships are sulfur dioxide and nitrogen oxides. Both are precursor gases of secondary pollutants. Sulfur dioxide is oxidized to sulfate aerosol. Nitrogen oxides (NO_x as sum of NO and NO_2) increase tropospheric ozone and hydroxy radical concentrations, thus increasing the oxidizing capacity of the atmosphere (Crutzen and Zimmermann, 1991), and enhancing secondary organic aerosol production. Lawrence and Crutzen (1999) demonstrated the significance of ship emissions utilizing a global atmospheric transport and chemistry model. They found a noticeable decrease of ozone (factor of 2) and hydroxyl radical (by more than 20%) concentration over the summer hemisphere oceans by switching off the NO_x ship emissions. According to (Endresen et al., 2003), 2.9% of the annual atmospheric global sulfate load originates from ship emissions. In this study we show that on regional and seasonal scales this value can be even an order of magnitude greater.

Enhanced summertime sulfate aerosol concentration contributes to the radiative forcing over the region. The direct radiative forcing is the ability of sulfate aerosols to scatter sunlight thus cooling the earth-atmosphere system. Haywood and Boucher (2000), Formenti et al. (2001) and Andreae et al. (2002) indicate that aerosol radiative forcing is among the highest in the world over the summertime Mediterranean. The global impact of SO_x ship emissions on the indirect sulfate aerosol forcing was estimated by Capaldo et al. (1999).

In this paper we study the seasonal variations of secondary pollutants focusing on the Mediterranean Sea summertime atmosphere. The numerical model tool used is the regional climate and chemistry model REMOTE (Regional Model with Tracer Extension).

Until now REMOTE has been successfully applied to simulate short-time (days or months) pollution episodes to investigate the relative contribution of individual processes such as chemical transformations, transport and deposition to total atmospheric concentration changes (Langmann, 2000), (Langmann and Bauer, 2002), (Langmann et al., 2003). A brief model description is given in Section 2.2. The results of the model simulation (Section 2.3) are analyzed particularly to determine the impact of ship emissions on the Mediterranean summertime pollution:
Investigation of the contribution of SO_x ship emissions to the sulfate aerosol concentration near the surface and at higher atmospheric levels. For this investigation, the fate of land and ship emissions was followed separately.
Running the experiment without ship emissions (SO_x, NO_x, CO, NMVOC's) to determine the reduction of secondary pollutants such as sulfate aerosols, ozone, hydroxy radicals, nitric acid and formaldehyde.
Model results are compared with observations.
An off-line radiation model is utilized to estimate the direct radiative forcing of sulfate aerosols at the top-of-the-atmosphere (TOA) over the Mediterranean region (Section 2.4). Again, we focus on the contribution of ship emissions to this forcing.

2.2 Model description

2.2.1 Atmospheric-Chemistry Model

The regional three-dimensional on-line atmosphere-chemistry model REMOTE (Langmann, 2000) determines the physical and chemical state of the model atmosphere at every time step. A terrain following, hybrid pressure-sigma coordinate is used in the vertical with 19 vertical layers of unequal thickness between the ground and the 10 hPa pressure level. The horizontal resolution for the presented investigations is 0.5° on a spherical rotated grid. The dynamical part of the model is based on the regional weather forecast model system EM/DM of the German Weather Service (Majewski, 1991). In addition to the German Weather Service physical parameterizations, those of the global ECHAM 4 model (Roeckner, 1996) have been implemented in REMOTE (Jacob, 2001) and are applied in the current study. The prognostic equations for surface pressure, temperature, specific humidity, cloud water, horizontal wind components and trace species mass mixing ratios are written on an Arakawa-C-Grid (Mesinger and Arakawa, 1976).
In the current model set-up, 63 chemical species are included. The species transport is determined by horizontal and vertical advection according to the algorithm of Smolarkiewitz (1983), convective up- and downdraft by a modified scheme of Tiedtke (1989) and vertical diffusion after Mellor and Yamada (1974). Dry deposition velocities are computed as in Wesley (1989) dependent on the friction velocities and stability of the lowest model layer. Wet deposition is computed according to Walcek et al. (1986) by integrating the product of the grid-averaged precipitation rate and the mean cloud water concentration. The gas-phase chemistry package RADM II (Stockwell et al., 1990) is implemented with a quasi-steady-state approximation (QSSA) solver (Hesstvedt et al., 1978). Forty-three

longer-living prognostic species and 20 short living diagnostic molecules react in the gas phase. The photochemical gas phase mechanism consists of 158 reactions. Clear sky photolysis rates are calculated by a climatological preprocessor model (Madronich, 1987). The presence of clouds modifies photolysis rates as described by Chang et al. (1987).

2.2.2 Initial and boundary conditions

At the first time step, REMOTE is initialized using meteorological analysis data of the European Center for Medium Range Weather Forecast (ECMWF), which also serve as lateral boundary conditions every 6h. Chemical initial and boundary concentrations are prescribed by the model results of the global chemistry transport model MOZART (Horowitz et al., 2003) for 14 species including PAN, HNO_3, H_2O_2, CO, NO, NO_2, O_3 and 7 hydrocarbons. Concentrations of the other species are derived from available measurements (Chang et al., 1987), and references therein, and are held constant at the lateral model boundaries throughout the simulation. The REMOTE model was applied in the so called 'climate mode', which means that it was started on 1.01.2002 with the ECMWF analyses data for meteorological initialization and with chemical initialization from MOZART and then applied continuously for the period of 21 months.

2.2.3 Emissions

Emission data for SO_x (Figure 2.1), NO_x, NH_3, CO and anthropogenic NMVOC are provided by the EMEP emission inventory (Vestreng et al., 2004). We assume that 96% of the total SO_x is emitted as SO_2 and 4% as $SO_4{}^{2-}$. SO_x is emitted from natural and anthropogenic sources with DMS treated as SO_2. Natural sources of NO_x are not considered. SO_x and NO_x emissions from point sources are distributed vertically between the seven lowest model levels following Memmesheimer et al. (1991). Anthropogenic NMVOC emissions are prescribed by the EMEP inventory and are distributed in 12 different classes of volatile organic compounds (VOC), according to Memmesheimer et al. (1991). Biogenic emissions of isoprene and monoterpenes are calculated at every model time step as a function of temperature, solar radiation and landuse, calculations are based on Guenther et al. (1991, 1993).

2.2.4 Radiation Transfer Model

The direct radiative short wave forcing of sulfate aerosols was calculated using an Off-line Radiation Transfer Model (ORTM) described by Langmann et al. (1998). It estimates the direct and indirect short wave forcing of sulfate aerosols based on the variable sulfate mass distribution and meteorological input data. The delta-Eddington approximation includes single as well as multiple scattering. Only the short wave part of the solar spectrum 0.2–5 μm, subdivided into 18 wavelength intervals, is considered, because sulfate aerosols have

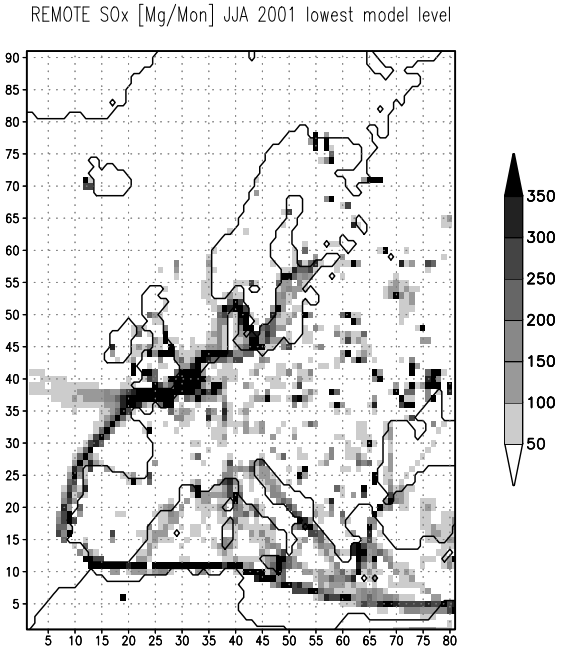

Figure 2.1: EMEP emission inventory (Vestreng et al., 2004): SO_x emissions [Mgmon^{-1}], lowest model level.

a negligible radiative effect in the infrared. Optical properties of the dry sulfate aerosol are determined form the Mie theory calculations. The modification of aerosol specific extinction due to relative humidity of the ambient air is considered using a simple approximation adapted from the data given by Nemesure et al. (1995).

2.3 Mediterranean summer smog — model results and validation

2.3.1 Base case model results — origin of sulfate aerosols

For the base case study REMOTE was set up to run for a 21 months long simulation period from January 2002 to September 2003, which presents the first long term simulation case with REMOTE photochemistry. In order to investigate the contribution of local ship emissions to the sulfate aerosol concentration in the boundary layer, SO_x emissions were artificially partitioned in four categories:
$SO_{2,l}$: SO_2 emitted on land,
$SO_{2,w}$: SO_2 emitted from the sea and
$SULF_{,l}$ and $SULF_{,w}$: for sulfate aerosols emitted from land and water respectively.
Secondary sulfate aerosols formed from land emissions are marked as '$SULF_{,l}$', while aerosols formed from ship precursors are marked as '$SULF_{,w}$'. This partitioning allows

us to follow the fate of SO_x emissions released from ships.
Ship traffic emissions are based on Lloyd's Register of Shipping and refer to 1990 (Vestreng, 2003). Emissions are probably underestimated for the years 2002-03 (Corbett and Koehler, 2003). Shipping routes can be clearly distinguished from the emission map (Figure 2.1). The total SO_x emission flux from the ship traffic in the Mediterranean Sea is 1189 Gg Yr^{-1}, which is quite remarkable compared with the 1640 Gg Yr^{-1} combined ship emissions of the Baltic, North and Black Sea and the North-East Atlantic Ocean. Total DMS emission flux is 743 Gg Yr^{-1}, with only 80.7 Gg Yr_{-1} emitted from the Mediterranean Sea (Vestreng et al., 2004). It is included within $SO_{2,w}$, but its impact is neglected here.
Model results show enhanced concentrations of sulfate aerosols (Figure 2.2) and other

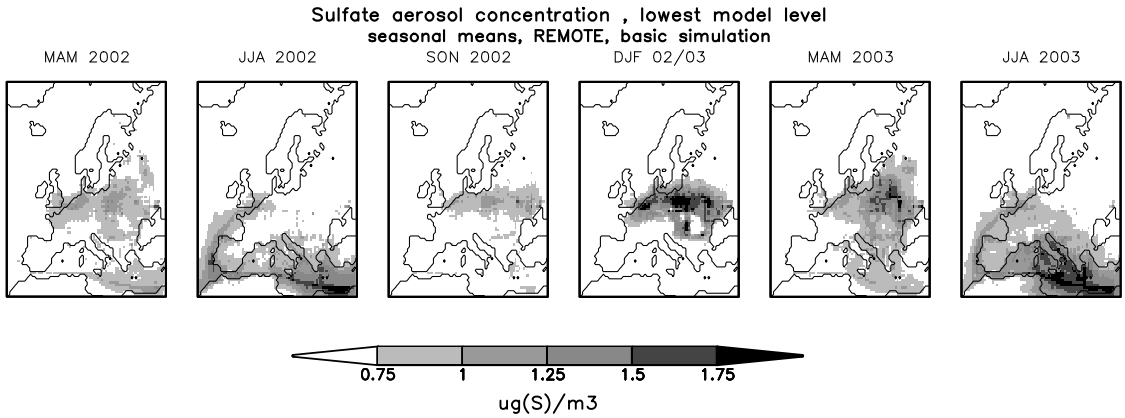

Figure 2.2: REMOTE base case, 2002-2003: Seasonal means of sulfate aerosol concentration [μg(S) m^{-3}], lowest model level.

secondary pollutants, such as OH, HNO_3, HCHO and O_3 (Figure 2.3), in the Mediterranean summer atmosphere. The pollution is concentrated in the lower atmospheric layers, mainly near the surface. Pronounced seasonal cycles look very similar for concentrations of OH, H_2O_2, HNO_3, HCHO and sulfate averaged over the Mediterranean region (Figure 2.4). Lowest concentrations were simulated in winter 2002/2003, while peaks appear in both summers (2002 and 2003). Ozone is an exception with peaks in both springs (2002 and 2003). We have chosen summer 2002 for a more comprehensive investigation of this phenomenon.

Mean concentration of sulfate aerosol in the lowest level in summer 2002 is 1.1μg(S) m^{-3} and almost four times higher then in winter 02/03. As the emissions in this area are assumed to be constant throughout the year they cannot explain such high concentration variation. The meteorological conditions during summer 2002 clearly favor the production

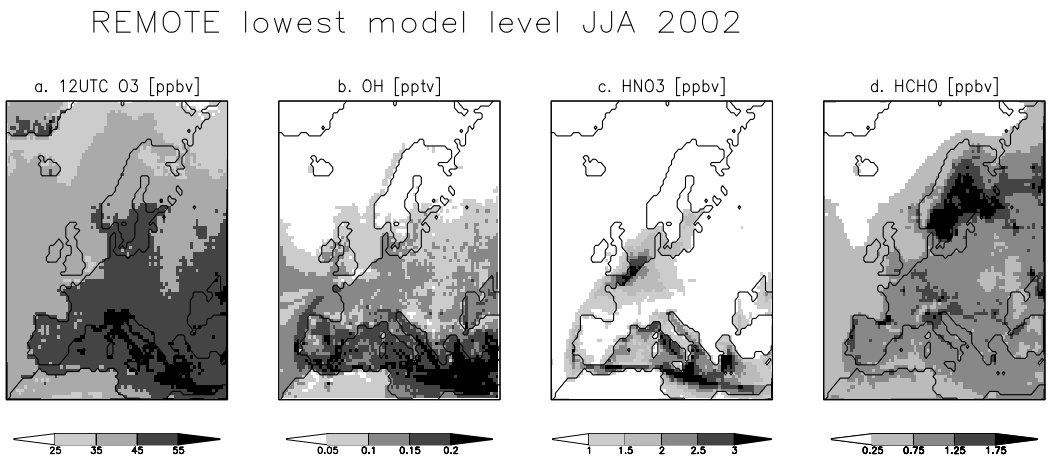

Figure 2.3: REMOTE base case, JJA 2002: Seasonal means of secondary pollutants concentration over Europe, lowest model level: (a) ozone [ppbv], (b) hydroxi radical [ppbv], (c) nitric acid [ppbv], (d) formaldehyde[ppbv].

and accumulation of secondary trace species. High air temperatures and clear sky conditions drive photo oxidation processes. High humidity promotes formation of OH. Mean monthly precipitation is below 10 mm, wet deposition is therefore negligible. Low wind velocities inhibit the horizontal advection in the Western Mediterranean (Figure 2.5). Generally, the main sulfate aerosol formation mechanism in Europe is the oxidation of SO_2 by hydrogen peroxide (H_2O_2) in cloud water. In the Mediterranean summer however, there are few clouds but high OH concentrations, resulting in the main path of sulfate aerosol production via the oxidation of SO_2 by OH in the gas phase, forming H_2SO_4 gas, which then is transformed to sulfate aerosols in the atmosphere (Bardouki et al., 2003).

There is a strong contribution of the ship emissions to the total concentration of primary and mainly secondary sulfate aerosols in the lowest model level (Figure 2.6). It accounts for almost 58% — 0.64 μg(S) m^{-3} — of the mean sulfate aerosol concentration in the lowest model level and for 54% — 4.2 mgm^{-2} — of the mean sulfate aerosol burden over the Mediterranean Sea in summer 2002. Additional sulfate aerosols are transported from the land to the sea. Sciare et al. (2003) point out that Turkey and Central Europe are the major contributors in terms of anthropogenic emissions of ${SO_4}^{2-}$ and SO^2. The contribution of land emissions is much more pronounced in the Eastern Mediterranean (Figure 2.6). The pollution from Central Europe is transported here by prevailing northwesterly winds (Figure 2.5). In the Eastern Mediterranean, pollution from land can even exceed the local ship pollution. However, even in the Eastern Mediterranean, ship tracks can be located from the $SULF_{,w}$-concentration distribution map in the lowest model level (Figure

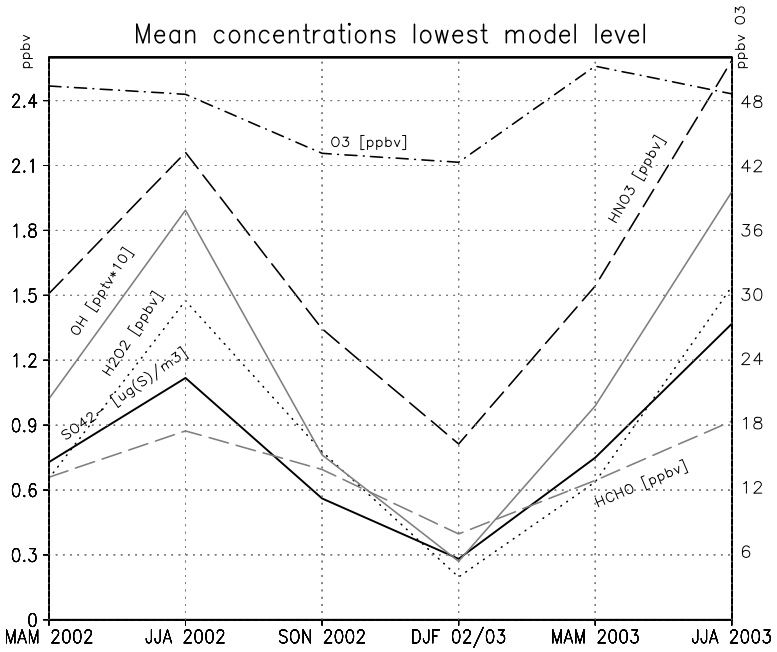

Figure 2.4: REMOTE base case, 2002-2003: Seasonal cycle of OH [pptv*10] dotted, HCHO [ppbv] grey dashed, HNO_3 [ppbv] black dashed, O_3 [ppbv] dash-dotted and SO_4^{2-} black solid, seasonal means, averaged over Mediterranean Sea, lowest model level.

2.6).

The influence of ship emissions on the total sulfate aerosol concentration decreases with increasing altitude (Figure 2.7). Averaged over the Mediterranean Sea, land emissions contribute only 42% to near surface pollution. Their contribution increases in higher atmospheric levels. 400m above the surface, it already accounts for 53% of total sulfate aerosols concentration. This can be explained with the level at which pollutants are released. Ship emissions are released in the lowest model level, while some of the land emissions are released in higher altitudes, if emitted from high chimneys. Additionally, continental pollutants are vertically mixed while horizontally transported.

2.3.2 Comparison of base case results with observations

In order to validate the model results, the calculated concentrations of sulfate aerosol and ozone were compared with available measurements. Nine EMEP stations perform continuous measurements, including SO_2, sulfate aerosol in air and in precipitation (Hjellbrekke, 2004), and ozone (Hjellbrekke and Solberg, 2004). The measurements at the Greek site Finokalia were obtained during the MINOS campaign (Mihalapous and de Reus, 2004) and were collected in summer 2001. The enhanced sulfate aerosol concentration during summer months in this region, however, can be observed in both simulated summers 2002 and 2003, which justifies the comparison between different years. Most of the EMEP

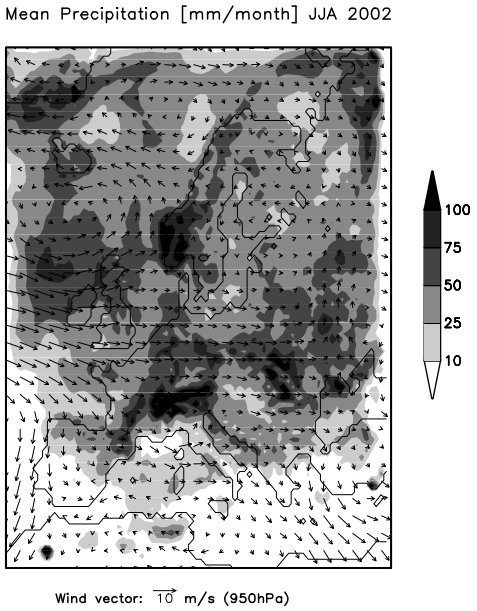

Figure 2.5: REMOTE base case, JJA 2002: Seasonal mean of precipitation [mm/month] and wind field [ms^{-1}] at 950hPa.

stations are located along the North Mediterranean Coast (Figure 2.6). In Table 1, we have summarized the seasonal mean summer sulfate concentration at the sites as simulated by REMOTE, in order to distinguish sites influenced mainly by ship emissions from those influenced mainly by land emissions. The Portuguese site and all four Spanish sites are located in areas strongly dominated by ship emissions, so does the Italian site Montelibretti. The second Italian site, Ispra, Slovakian site Iskbra and Greek site Finokalia are all dominated by land emissions. The Greek site is located in the middle of the Eastern Mediterranean Sea at the island of Crete, land emissions transported here by the northerly winds from South and Central Europe exceed local ship emissions. Finally, the Turkish site Cubuk II is also strongly influenced by land emissions, however even here, more than 450 km away from the Mediterranean coast, and over 1000 m asl, about 30% of the near surface sulfate aerosols originate from ship emissions. Compared with available observations, mean modeled sulfate concentration agrees well with measurements at sites dominated by land emissions (SI08, GR02 and TR01). Sites dominated by ship emissions are significantly underestimated by the model, possibly indicating an underestimation of ship emissions. Alternatively, the fact that surface measurements are compared with

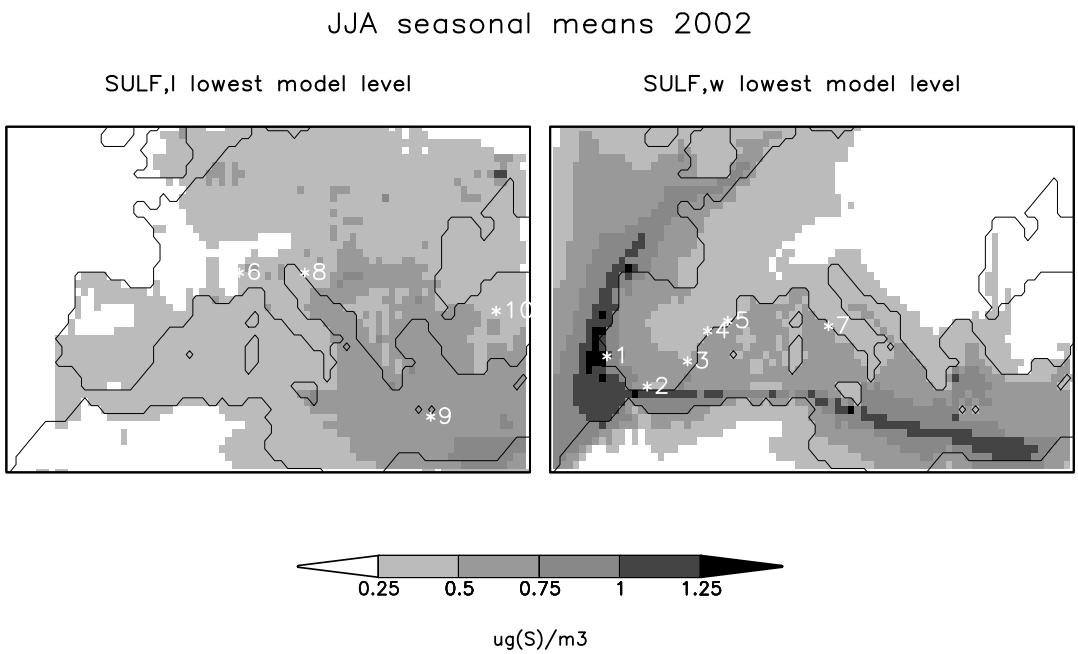

Figure 2.6: REMOTE base case, JJA 2002: Seasonal means of sulfate aerosol concentration [μg(S) m^{-3}] over Europe, lowest model level: (a) Primary and secondary sulfate originated from land emissions, (b) Primary and secondary sulfate originated from ship emissions. Locations of EMEP observational sites and the MINOS–site Finokalia. 1. PT04 Monte Velho, 2. ES07 Visnar, 3. ES12 Zarra, 4. ES14 Esl Torms, 5. ES10 Cabode Creus, 6. IT04 Ispra, 7. IT01 Montelibretti, 8. SI08 Iskbra, 9. GR02 Finokalia, 10. TR01 Cubuk II

simulated concentrations of an approximately 33 m thick layer could cause this underestimation. Another possible explanation is that the SO_2 conversion rates in the model are too low, resulting in the general tendency of the model to underestimate high end sulfate concentrations. Much better agreement with measurements is achieved with surface ozone.

Figure 2.8 shows examples of time series of model results and observations at two of the EMEP sites in the Mediterranean area — Montelibretti, a site dominated by ship emissions, and Iskbra, a site with stronger influence of land emissions. The simulated sulfate aerosol concentrations are underestimated at Montelibretti, but agree well with the observations at Iskbra. Ozone concentrations at 12 UTC are overestimated for Iskbra, while they agree well with those observed at Montelibretti.
During June 23rd to 25th a high pollution episode occurs at the Italian site Montelibretti. Peak concentration for sulfate and high ozone concentrations were observed and simulated during this period. Similar smog episodes have been observed and simulated at other sites. In summary, the overall agreement between REMOTE and observations can be regarded as satisfactory, especially when considering that point measurements are compared with grid boxes of an area of 55x55 m^2, and taking into account that the model is applied in the

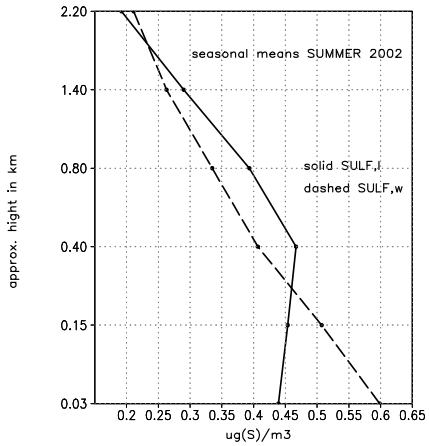

Figure 2.7: REMOTE base case, JJA 2002: Vertical distribution of seasonal mean of sulfate aerosols [μg(S) m^{-3}], averaged over Mediterranean Sea Solid: primary and secondary sulfate originated from land emissions Dashed: primary and secondary sulfate originated from ship emissions

climate mode. Unfortunately we lack observational data over water, where we simulate episodes with sulfate aerosol concentrations of up to 6μg(S) m^{-3}.

2.3.3 Sensitivity experiment — Other secondary pollutants caused by ship emissions

In order to calculate the maximum possible reduction of secondary pollutants in the Mediterranean summer atmosphere, we have switched off all ship emissions. Ship traffic in the Mediterranean Sea is responsible for 1639 Gg Yr^{-1} NO_x emissions, compared with 2352 Gg Yr^{-1} NO_x released from all other ships in European waters. NO and NO_2 are short-lived species which are not transported over long distances. Locally released NO_x is mainly responsible for the production of ozone. Switching off the release of NO_x by ships reduces surface ozone concentration by 15% from 48.6 ppbv to 41.5 ppbv in this area (Figure 2.9b, compare with basic simulation, Figure 2.3a). The formation of HNO_3 and HCHO in the experiment is reduced by 66% and 24%, respectively (Figure 2.9, d and e). OH concentration is simultaneously reduced by 42% from 0.19 pptv to 0.11 pptv (Figure 2.9c) contributing to decreased formation of H_2SO_4 and sulfate aerosol. The resulting mean sulfate aerosol concentration over the Mediterranean Sea is reduced by 46% to 0.56 μg(S) m^{-3} in the lowest model level (Figure 2.9a, compare with the base case,Figure 2.2),

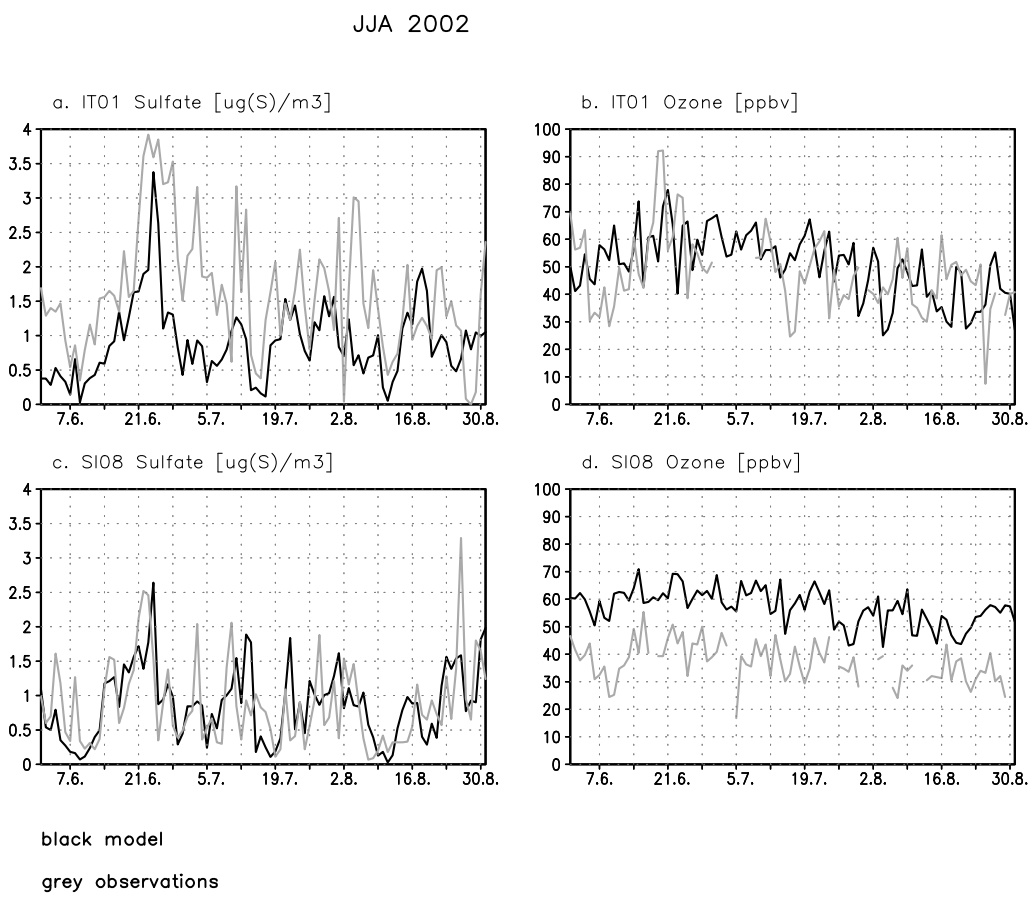

Figure 2.8: Comparison REMOTE base case (black) versus observations (grey) (Hjellbrekke, 2004), (Hjellbrekke and Solberg, 2004) daily means, summer 2002. (a) Montelibretti, Italy, sulfate aerosols [μg(S) m^{-3}], (b) Montelibretti, Italy, ozone [ppbv], (c) Iskbra, Slovenia, sulfate aerosols [μg(S) m^{-3}], (d) Iskbra, Slovenia, ozone [ppbv].

the mean sulfate aerosol column burden is reduced by 29%.

Following the usual method of simply omitting the ship emissions, e.g. Capaldo et al. (1999) and Endresen et al. (2003), results in a 29% reduction of the sulfate column burden in our study. In our base case simulation with 'land-sea-marked' emissions (3.1) we find the relative contribution of the ship emissions to be almost twice as that, 54%. The reduction of SO_x emissions does not result in a linear reduction of sulfate aerosol load, because of non-linear chemical reactions.

2.4 Direct sulfate aerosol forcing — impact of ships

The climate impact of sulfate aerosols occurs as direct and indirect radiative forcings (Haywood and Boucher, 2000). In this study, we concentrate on the TOA direct radiative

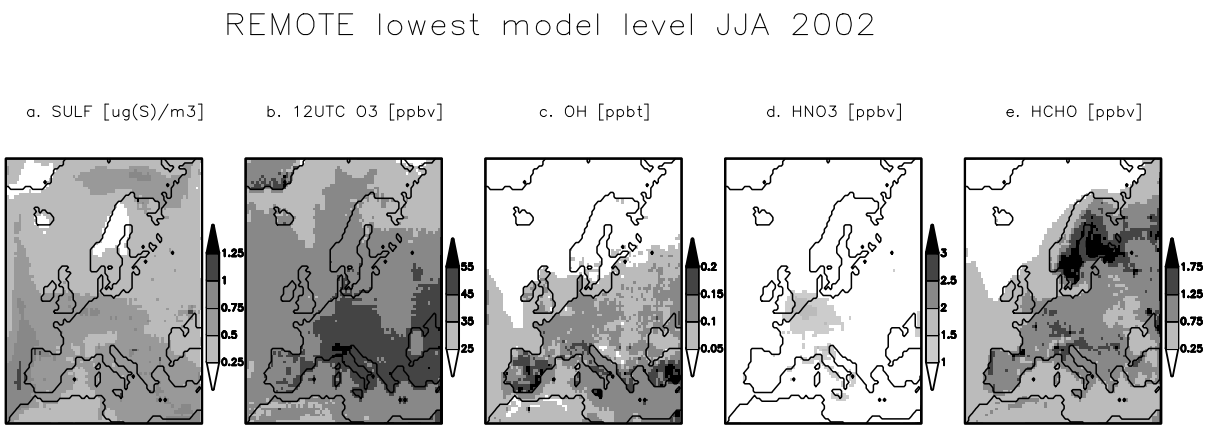

Figure 2.9: REMOTE sensitivity experiment without ship emissions, JJA 2002: Seasonal means of secondary pollutants concentration over Europe, lowest model level: (a) Sulfate aerosol [μg(S) m^{-3}], (b) Ozone [ppbv], (c) Hydroxy radical [pptv], (d) Nitric acid [ppbv], (e) Formaldehyde [ppbv].

aerosol forcing, focusing on the impact of ship emissions.
Sulfate aerosol particles scatter incoming short wave radiation, effectively raising the local planetary albedo of the clear atmosphere, thereby cooling the earth-atmosphere-system. Radiative forcing over Europe is much stronger in summer than in winter due to increased solar radiation. The combination of strong solar radiation and high atmospheric aerosol load results in strong forcing over the Mediterranean Sea during summer (Figure 2.10). In the base case, our estimated summer mean sulfate aerosol forcing averaged over Europe is -1.4 Wm^{-2}. Summer mean forcing averaged over the Mediterranean Sea is as high as -2.1 Wm^{-2}, its maximum reaching up to -3.0 Wm^{-2}, the maximum for August up to -6 Wm^{-2}. It agrees quite well with other global and regional model predictions (Feichter et al., 1997),(Langmann et al., 1998), ranging between -2 and -3 Wm^{-2} for Mediterranean summer. REMOTE underestimates sulfate aerosol concentration by the factor of 1.5 over the Mediterranean Sea. Therefore, the mean sulfate aerosol forcing is probably similarly underestimated. Andreae et al. (2002) estimated annual averaged all-sky sulfate direct radiative forcing of -4.7 Wm^{-2} over the Mediterranean Sea from measured (1996-1997) sulfate aerosol concentrations and optical properties. Since SO_x emissions from land sources have been noticeably reduced since 1997, resulting in decreased concentrations in the atmosphere, we assume that the truth lies somewhere in between.
Over 50% of the direct forcing accounts for ship emissions of SO_x (Figure 2.10, b). It

reduces dramatically if we do not consider ship emissions as in the sensitivity study (Figure 2.10d). Mean direct forcing over the Mediterranean summer atmosphere is reduced by 0.78 Wm^{-2}, which is a significant reduction of almost 38%.

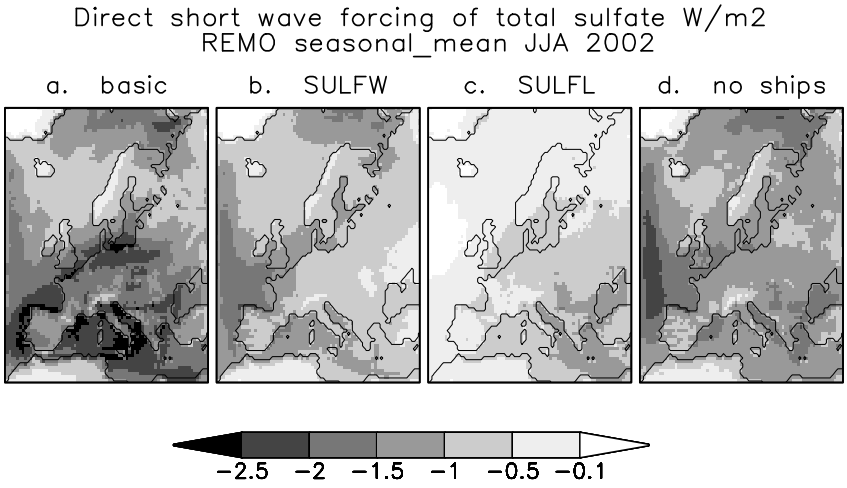

Figure 2.10: Seasonal means of direct short wave forcing of total (anthropogenic and natural) sulfate aerosol [Wm^{-2}], as determined by the radiation model: (a) REMOTE base case, DJF 2002/2003, (b) REMOTE base case, JJA 2002, (c) REMOTE sensitivity experiment without ship emissions, JJA 2002

2.5 Conclusions

In this study, we have applied the regional climate chemistry REMOTE to successfully simulate a 21 months long period, highlighting the Mediterranean pollution episode in summer 2002, and have validated sulfate aerosol and surface ozone concentrations with

observational data. Ozone agrees well with observations, sulfate is underestimated for sites with strong contribution from ship emissions, possibly indicating an underestimation of the applied ship emission inventory (1990) for the year 2002. Low vertical resolution of the model and low SO_2 conversion rates are alternative explanations. Tracing back the origin of sulfate aerosols offers the possibility to investigate the impact of land and ship SO_x emissions sources separately. Ship emissions are released only in the lowest model level and their contribution to sulfate concentration dominates in the lowest 300 m. Ship tracks can be easily distinguished from simulated sulfate concentration distribution in the lowest and second lowest model levels (ca. 30 m and 150 m altitude). Ship emissions contribute to sulfate aerosol concentration mainly in the Western Mediterranean, their contribution reaches here up to 60-85%. Averaged over the area, 0.64 μg(S)m^{-3} of sulfate aerosol near the surface originates from ship emissions, compared to 0.47 μg(S)m^{-3} from land emissions (summer mean). 54% of summer mean total column burden of sulfate aerosol accounts for ship emissions of SO_x. Consequentially, they are responsible for over 50% of direct sulfate radiative forcing. Without ship emissions, the mean summertime direct forcing over the Mediterranean is no longer outstanding and has same values as the European mean.

Ship emissions of NO_x contribute to the formation of secondary trace gases hence considerably decreasing Mediterranean air quality in summer. Most significant is the formation of nitric acid, which is reduced by 66% without ship emissions. Concentration of hydroxy radicals in the fist model level drops by 42%, formaldehyde by 24%, mean surface ozone by 15%. Secondary production of sulfate aerosols depends not only on the availability of the precursor gas SO_2, but also on that of the oxidants including OH radicals and H_2O_2. Although 54% of sulfate column burden accounts for SO_x ship emissions, it can only be reduced by 29% if all ship emissions are switched off. An up-dated ship emission inventory is needed to improve our understanding of the impact of ship emissions on summertime pollution of the lower Mediterranean troposphere. While emissions from land-based sources in Europe continue to be reduced, those at sea show a continuous increase (The European Environmental Bureau (EEB) et al., 2003). According to Swedish NGO Secretariat on Acid Rain (2003), sulfur and nitrogen oxides in ship fuel can be reduced cost-efficiently by 60-83% and by 50% respectively. The results of this study indicate that such a reduction would substantially improve air quality and reduce radiative forcing in the Mediterranean summer.

Organic aerosols, soot and dust have not been considered in this study. Secondary organic aerosol production is strongly linked with all of trace gases investigated here. Its distribution and climate forcing will be subject of future investigations. Parameterisation of aerosol size distribution, chemical composition and of aerosol-cloud interaction in REMOTE shall also improve our knowledge of the indirect aerosol forcing, so that the total climate forcing of sulfate and organic aerosols can then be investigated.

Acknowledgements

We thank Martin Schultz and Ulrike Niemeier for providing the MOZART data, Anne-G. Hjellbrekke for providing the EMEP observation data, Marian de Reus for providing the MINOS observation data, Melissa Pfeffer and Martin Schultz for reviewing the manuscript

internally. This research was partly financially supported by EU project CARBOSOL.

Chapter 3

Direct short wave radiative forcing of sulfate aerosol over Europe from 1900 to 2000

[1] **Abstract**

Based on historical simulations of the atmospheric distribution of sulfate aerosol over Europe, we have estimated the evolution of the direct short wave radiative forcing due to sulfate aerosol from 1900 to the present day. Following the trend of atmospheric sulfate burden, the radiative forcing reaches its peak in the 1980's. Since then, environmental policies regulating SO_x emissions successfully reduced the atmospheric load. On average, the forcing of the year 2000, representing present day, equals that of the 1950's. Spatially, the forcing maxima experienced a shift from the northwest to the southeast during the century. Forcing is strongest during summertime, with a seasonal mean of –2.7 Wm^{-2} in the 1980's and –1.2 Wm^{-2} in summer 2000. The mean forcing efficiency is slightly reduced from –246 W(g sulfate)$^{-1}$ in the 1900's to –230 W(g sulfate)$^{-1}$ in the year 2000, it declines with changed geographical distribution of sulfur emissions.

[1] to be submitted to *JGR* as: Marmer, E., Langmann B., Fragerli, H., Vestreng V., Direct short wave radiative forcing of sulfate aerosol over Europe from 1900 to 2000, 2006.

3.1 Introduction

Anthropogenic emissions have caused serious environmental problems in Europe since the beginning of industrialization, contributing to soil, water and air pollution. Air pollution affects climate through absorbing and scattering aerosol particles, which can warm or cool the Earth-atmosphere system. Emissions of SO_x and black carbon are particularly relevant for the climate.
SO_x, emitted mostly as SO_2 gas, is converted in the atmosphere via gaseous and aqueous chemical reaction to sulfate aerosol. Sulfate aerosol has an impact on climate via direct and indirect radiative forcing. For sulfate aerosol, the direct effect results from scattering of incoming solar radiation back to space. The indirect effect results from the ability of the sulfate aerosol particles to act as cloud condensation nuclei, resulting in more but smaller cloud droplets, increasing the cloud albedo (Twomey, 1974). On the other hand, smaller cloud droplets can suppress precipitation, prolonging the life time of the cloud and the aerosol (Albrecht, 1989). The combination of these effects and their feedbacks is up to now poorly understood (IPCC, 2001).
Additional uncertainties exist about the direct, semi-direct and indirect effects of black carbon. Black carbon strongly absorbs the solar radiation and warms the aerosol layer. It can trap more energy than is lost by scattering to space to overall warm the Earth-atmosphere system. Absorption of solar radiation by black carbon particles in clouds can evaporate cloud droplets reducing cloud cover (Ackerman et al., 2000). Further, black carbon particles in cloud droplets can reduce the cloud albedo (Krüger and Grassl, 2002) and can act as ice nuclei (DeMott et al., 1999).
Considering the climate impact of both sulfate and black carbon aerosols presents yet another problem: for newly released particles their climate impact can be treated individually, whereas aged particles are internally mixed. Internally mixed particles have different optical and hygroscopic properties depending on their age and chemical composition (Lesins et al., 2002). Haywood et al. (1997), Myhre et al. (1998) and Lesins et al. (2002) showed that an internal mixture of sulfate and black carbon results in substantially different forcing than an external mixture.
In this study we investigate the historical evolution of the aerosol radiative forcing over Europe during the 20th century. We look at the direct forcing only, because it is the best understood aerosol effect. The study is further limited to sulfate aerosol, since a consistent historical emission inventory of black carbon in Europe in suitable resolution is not yet available.
Myhre et al. (2001) estimated the averaged global radiative forcing evolution from 1750 to 2000, utilizing a radiation transfer model. All known radiative forcings – greenhouse gases, ozone, anthropogenic and natural aerosols (including sulfate and black carbon), and solar irradiance radiation – were considered. The direct aerosol forcing was computed assuming internal and external aerosol mixtures. The spatial distribution of different radiative forcings was not computed. This study points out the increasing importance of the anthropogenic aerosol forcing for the past 100 years. Uncertainties are large for the radiative forcings by anthropogenic aerosols because of the uncertainties in emissions and calculations of the forcings itself.

Boucher and Pham (2002) computed the direct and indirect sulfate aerosol forcing over the period 1850 to 1990 applying a global GCM. They also focused on sulfate aerosol only, because more information is available for sulfur sources than for other aerosol species. They found that the global direct sulfate forcing has increased from near zero (1850) to –0.42 Wm^{-2} in 1990, with nearly constant forcing efficiency of –150 W(g sulfate)$^{-1}$ (ratio of the radiative forcing to the anthropogenic sulfate burden). The global forcing was found to be fairly constant between 1980 and 1990 due to emissions reduction in the US and Europe, with a spacial shift from the US, Europe, Russia and the North Atlantic to Southeast Asia and the Indian and Pacific Oceans.
Another study on the trend in tropospheric aerosol loads and the direct radiative forcing was carried out by Tegen et al. (2000). The global trend of the atmospheric load and forcing of sulfate and carbonaceous aerosols from fossil fuel burning as well as soil, dust and sea salt from 1950 to 1990 was constructed. Globally, a range of top-of-atmosphere direct forcing of –0.5 to +0.1 $Wm^{-2}$was found due to the uncertainty in the contribution of the black carbon aerosol.
For our study we have utilized a regional model, which provides a better resolution than the earlier performed global simulations, allowing us to have a closer look at different regions in Europe. In order to better demonstrate the regional differences, we have calculated sulfate direct forcing for five selected areas in Europe, representing different geographical and atmospherical conditions, and discuss the different trends for each of these areas. The results of the present study serve as a baseline for future investigations on aerosol climate impact evolution over Europe, which should include black carbon.

3.2 Model set-up

3.2.1 Emissions

In this section we describe the set-up of historical emissions for SO_x, but also for NO_x, NH_3, CO and VOC, which serve as input for the model simulations. Anthropogenic emission input data of SO_x, NO_x, NH_3, CO and VOC from 1980 to 2003 are based upon emissions reported per sector and grid officially reported to the Convention on Long-Range Trans-boundary Air Pollution (e.g. Vestreng et al., 2004).
Prior to 1980, historic emissions estimates by (van Aardenne et al., 2001) for CO, NH_3 and VOC were available globally per sector on a 1 × 1 degree resolution. The EDGAR-HYDE sectors were translated to Selected Nomenclature for Air Pollution sectors (SNAP)(UNECE/EMEP, 2002). The datasets were then converted to emissions per country and SNAP sector. Scaling factors per country and sector were deduced by
$f_{Year}(\text{country, sector}) = \frac{emission_{Year}(country,sector)}{emission_{1980}(country,sector)}$
and used to scale the EMEP 1980 emissions backwards in time. In this way, the finer resolution (50 × 50 km^2) of the EMEP data could be kept and the evolution of the historic emissions included. In the data from van Aardenne et al. (2001), spatial distribution over the years are only different when the distribution between the sectors change. Thus, we loose no information when applying only the scaling factors as the sectorial information

is kept.
For SO_x and NO_x we used the emissions by Mylona (1996) and Vestreng and Semb (2006), respectively, available on the (50×50 km^2) resolution. Emission scaling factors were defined in the same way as for NH_3, VOC and CO. The historical emissions for NO_x and SO_x were available from 1880-1985, for the countries with country borders as they were historically. For instance, emissions are not availabl separately for the countries within the Former Soviet Union, and emissions from Austria did include emissions from the whole Austrian Empire before 1920. Thus, we have made the following assumptions: The countries in the Former Soviet Union are scaled with the same factors from 1920 to 1980. East and West Germany are scaled separately back to 1950, but prior to this as the sum. The areas corresponding to Czech Rebublic and Slovakia are scaled with emissions for Former Czechoslovakia back to 1920. In the same period, Slovenia, Croatia, Bosnia and Herzegovina, Serbia and Montenegro and The Former Yugoslav Republic of Macedonia are scaled using the historic emissions of Former Yugoslavia.
For the years prior to 1920, the changes of borders have been extensive and more crude assumption had to be made. Thus, the uncertainties related to spatial distribution in this period are larger. Austria was part of the Austrian Empire, including Czech Republic and Slovenia. For e.g. 1910, Austria is scaled with
$\frac{Austrianemissions(1920)}{Austrianemissions(1980)} * \frac{AustrianEmpireemissions(1910)}{AustrianEmpireemissions(1920)}$,
where the Austrian Empire emissions for 1920 is estimated as the sum of emissions from Austria plus X*Former Czechoslovakia and Y*Former Yugoslavia. X has been defined as Czech Republic/(Czech Republic+Slovakia) for 1980, Y as Slovenia/(Slovenia, Croatia, Bosnia and Herzegovina, Serbia and Montenegro and The Former Yugoslav Republic of Macedonia) for 1980. Scaling factors for the area corresponding to Slovenia is the same as used for all the Former Yugoslavia. The same procedure has been followed to define scaling factors for Hungary prior to 1920, as The Hungarian Kingdom included Hungary, Slovakia and Bosnia and Herzegovina. Hungary is scaled as
$\frac{Hungarianemissions(1920)}{Austrianemissions(1980)} * \frac{HungarianKingdomemissions(1910)}{HungarianEmpireemission(1920)}$,
where the Hungarian Empire emissions for 1920 is estimated as the sum of emissions from Hungary plus X*Former Czechoslovakia and Y*Former Yugoslavia. X has been defined as Slovakia/(Czech Republic+Slovakia) for 1980, Y as (Bosnia and Herzegovina)/(Slovenia, Croatia, Bosnia and Herzegovina, Serbia and Montenegro and The Former Yugoslav Republic of Macedonia) for 1980. Bosnia and Herzegovina scaled equally to other countries in the Former Yugoslavia. Before 1920, Russia included Poland, and United Kingdom included Irelans. Similar procedures were followed for these countries.
The heights of the stacks have changed significantly during the last century, which we have taken into account by defining a 'tall stack' (1955-present) and a 'low stack' (previous to 1955) period. In the model calculations, the effective emission heights of emissions from power plants and industry are moved one model layer closer to the ground in the low-stack period than in the 'tall-stack' period. In the present-day calculations, most emissions from powerplants are released to an effective emission height of approximately 400 meters. In the low-stack period, the effective emission heights are around 200 meters. Total releases of SO_x, NO_x, NMVOC and CO from ship traffic in the Atlantic Ocean, the North Sea, the Baltic Sea, the Black Sea and the Mediterranean are used as estimated

by Lloyd's Register of Shipping, London (1995, 1998, 1999). These estimates are of the same magnitude as those derived by ENTEC for 2000, thus we assume that they are valid for 2000. Ship emissions have become increasingly important, e.g. Endresen et al. (2003) reports a 1.6% per year increase in fuel consumption from shipping between 1996 and 2000. In the model calculations we have assumed a 2.5% increase per year in the period 1980-2000.
Volcanic SO_x emissions from Mt. Etna are assumed constant in time and released in the appropriate model level.

3.2.2 Unified EMEP Model

The Eulerian EMEP model (Simpson et al., 2003a) was utilized to determine the historical sulfate aerosol distribution. It is a multi-layer atmospheric dispersion model designed for simulating the long-range transport of air pollution over several years. The model domain is centred over Europe and also includes most of the North Atlantic and the polar region. The model has 20 vertical layers in σ-coordinates below 100hPa. It is primarily intended for use with a horizontal resolution of ca. $50\times50\text{km}^2$ (at 60 degrees N) in the EMEP polar stereographic grid. The chemical scheme uses about 140 reactions between 70 species. The dry deposition module makes use of a stomatal conductance algorithm which was originally developed for calculation of ozone fluxes, but which is now applied to all pollutants where stomatal control is important (Simpson et al., 2003b; Tuovinen et al., 2004, e.g.). Dry deposition of aerosol particles depends on their size, with the model version used here distinguishing between fine and coarse aerosols. Details of the formulation are given in Simpson et al. (2003a). Parameterisation of the wet deposition processes in the EMEP model includes both in-cloud and sub-cloud scavenging of gases and particles, using scavenging coefficients.
The EMEP Unified model use meteorological data from PARLAM Benedictow (2002), a dedicated version of the operational HIRLAM model (High Resolution Limited Area Model) maintained and verified at Norwegian Meteorological Institute. The numerical solution of the advection term is based upon the fourth order Bott scheme (Bott, 1989a,b). The lateral boundary conditions for most species are based on measurements as described in Simpson et al. (2003a) and Fagerli et al. (2004). Furthermore, a scaling factor has been applied to account for the change in the concentrations at the boundary during the time period 1900-2000. This factor has been defined based on the EPA emissions (EPA, 2000, and updates on their web-page, www.epa.gov) for SO_x and NO_x emissions for the 1980-2000 period. The trends in ammonium aerosol were set by weighting the trend of SO_x emissions with 2/3 and NO_x emissions with 1/3, assuming that the production of ammonium nitrate and ammonium sulfate determines the trend. For the period prior to 1980, we have used the winter trends of sulfate and nitrate from an ice core at Col du Dome (4250 meters above sea level, French Alps). In the winter time, Col du Dome is above the boundary layer most of the time. Most of the air pollution deposited at this sites originates from sources outside the western boundary of the EMEP domain (Fagerli, 2006), thus the trend extracted from the ice core is a good indicator of the air pollution

arriving from North America. For ammonium, we used the trends of NH_3 emissions from United States derived from van Aardenne et al. (2001). Evaluations of the EMEP model using all present-day EMEP measurement data are available elsewhere (e.g. Fagerli et al., 2003, 2006; Simpson et al., 2006; Jonson et al., 2006) and show that the model results agree well with the measurements. For this study, the EMEP model is run for every tenth year for the period 1900-1980 plus 1985, 1990, 1995 and 2000 using appropriate boundary conditions and emissions. The meteorological year is 1997 for all the model runs. This was done because no set of meteorological data back to 1900 was available. Consequently, the inter-annual variability which has an important influence on sulfate aerosol distribution and its forcing could not be considered.

3.2.3 Radiation Transfer Model

The constructed trend of sulfate aerosol burden presented above was used as input for the Off-line Radiation Transfer Model (ORTM). A detailed model description can be found in Langmann et al. (1998). ORTM determines the direct and indirect short wave forcing of sulfate aerosol based on the variable sulfate mass distribution and meteorological input data. The delta-Eddington approximation includes single as well as multiple scattering. Only the short wave part of the solar spectrum, 0.2–5 μm, subdivided into 18 wavelength intervals, is considered, because sulfate aerosol has a negligible radiative effect in the infrared. Optical properties of dry sulfate aerosol are determined from Mie theory calculations, assuming a zero-order logarithmic size distribution n(r) (Lenoble and Brogniez, 1984), with a mean particle radius r_m of 0.05 μm and a geometric standard deviation σ of 1.8. The particle density was set to 1.6 gcm^{-3}, which is equivalent to a mean particle composition of 75% H_2SO_4 and 25% H_2O. The modification of aerosol specific extinction due to the relative humidity of the ambient air (RH) is considered using a simple approximation adapted from the data given by Nemesure et al. (1995). For relative humidities (RH) below 80%, the specific extinction is enhanced by a factor of RH*0.04, assuming a minimum relative humidity of 25%. For relative humidity exceeding 80%, the specific extinction increases exponentially with RH. The factor 9.9 is reached for RH=100%. The single scattering albedo and the asymmetry factor are assumed to be independent of RH. This approach might result in a small overestimation of the short-wave radiative forcing of sulfate aerosol, because with increasing relative humidity forward scattering is increased and backscattering in space direction reduced (asymmetry factor increased).

3.3 Historical trend of the European atmospheric load of sulfate aerosol

The atmospheric load of sulfate over Europe increased from 1900 to 1980 due to expanding industrialization since the early 20th century and uncontrolled emissions of SO_x (sulfur dioxide and sulfate). The sulfate load more then doubled during the first half of the century from 1.4 mg(m^{-2}) sulfate in the 1900's to 3.1 mg(m^{-2}) in the 1950's, with a

very rapid growth in the following 20 years, when it again more then doubled reaching 6.7 mg(m^{-2}) 1970's. (Figure 3.1). The maximum annual mean of the total column burden was reached in the 1980's, with 7.5 mg(m^{-2}) sulfate, more than 5 times higher then at the beginning of the century. The awareness of the health risks and environmental impacts of the atmospheric sulfate aerosol pollution resulted in emission control in Western Europe in the 1980's, leading to a constant and significant reduction of anthropogenic SO_x emissions (Mylona, 1996). Eastern Europe followed suit in the 1990's. From the 1980's until the present, the sulfate load has been decreasing. The mean load in the year 2000 was 3.3 mg(m^{-2}), slightly higher than in the 1950's.

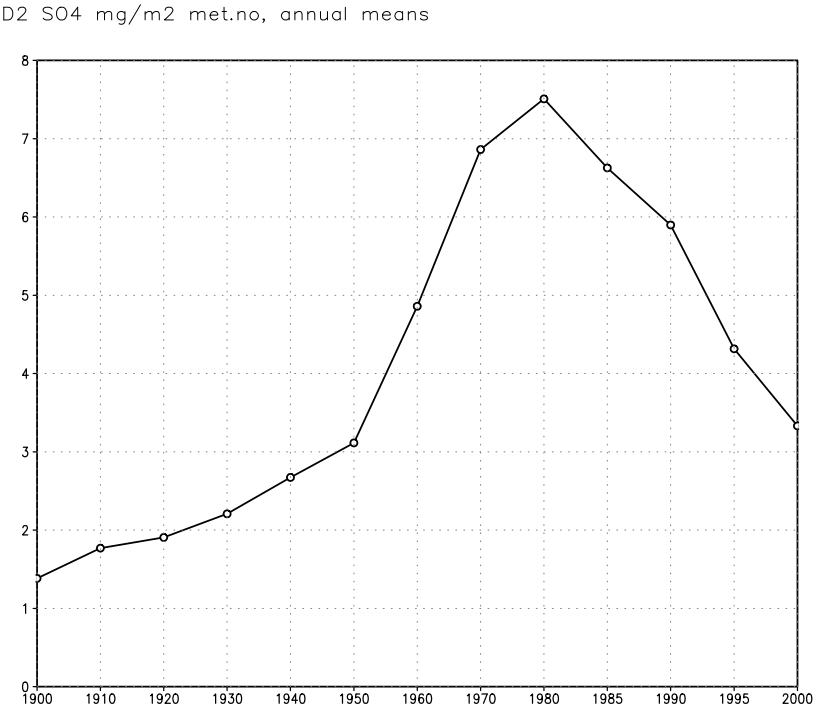

Figure 3.1: Total atmospheric sulfate load [mg(m^{-2})] over Europe, annual means, 1900-2000

3.4 Historical trend of the European direct radiative forcing

The temporal pattern of the direct aerosol forcing directly reflects the pattern of sulfate aerosol burden. The forcing is negative, because sulfate aerosol particles scatter incoming short wave radiation. The annual negative maximum of the forcing is seen in July, while the minimum is found in December (Figure 3.2). During winter months, solar radiation is very weak in high latitudes and the aerosol forcing is almost negligible. Like the atmospheric sulfate load, the direct radiative forcing increased from 1900 to 1980, it more

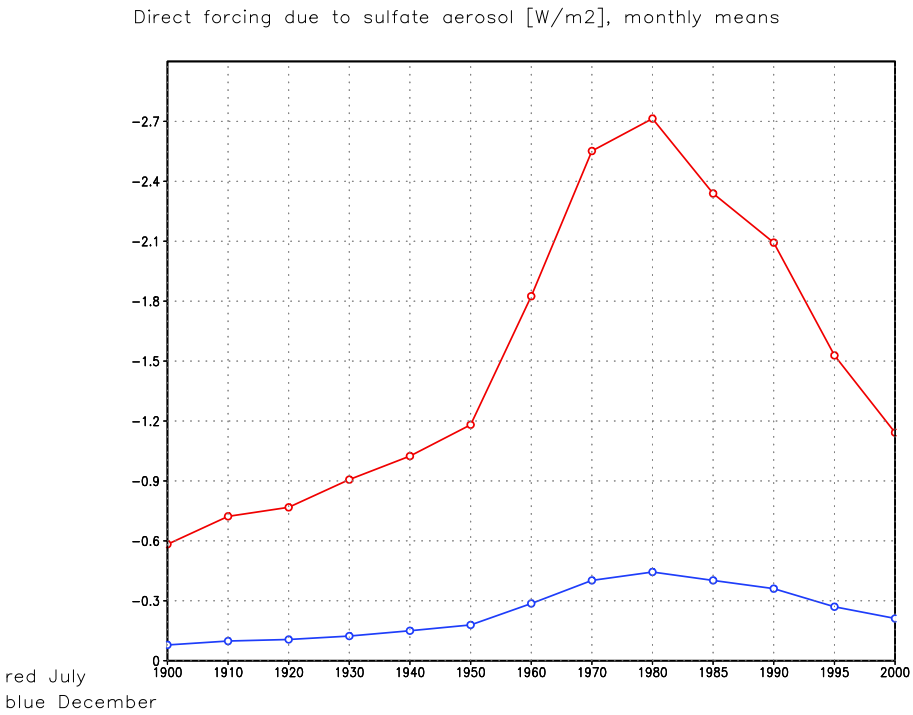

Figure 3.2: Direct short wave radiative forcing due to sulfate aerosol [Wm^{-2}] over Europe, 1900-2000, monthly means. Blue: December, red: July

then doubled between the 1950's and the 1970's. After 1980 the direct forcing steadily decreased. The monthly mean of the sulfate direct short wave forcing over Europe was –0.08 Wm^{-2} in December 1900 and –0.4 Wm^{-2} in December 1980, from when it constantly decreased to –0.2 Wm^{-2} in December 2000, again comparable to December 1950. During summer, enhanced solar radiation results in a stronger forcing. The forcing is 5 to 7 times stronger in July than in December. The historical trend is much more pronounced in summer: from –0.6 Wm^{-2} in July 1900 the forcing increased to –2.7 Wm^{-2} in July 1980, and then it steadily decreased. In July 2000 the direct sulfate forcing was reduced to –1.1 Wm^{-2}, which is again comparable to the value in July 1950.

3.5 Regional patterns of the historical trend

In order to consider the regional aspects of the historical trend of the direct short wave forcing of sulfate aerosol, we have analyzed the spatial evolution. The spatial evolution of the atmospheric load and the radiative forcing is discussed separately for winter (December, January, February) and for summer (June, July, August).

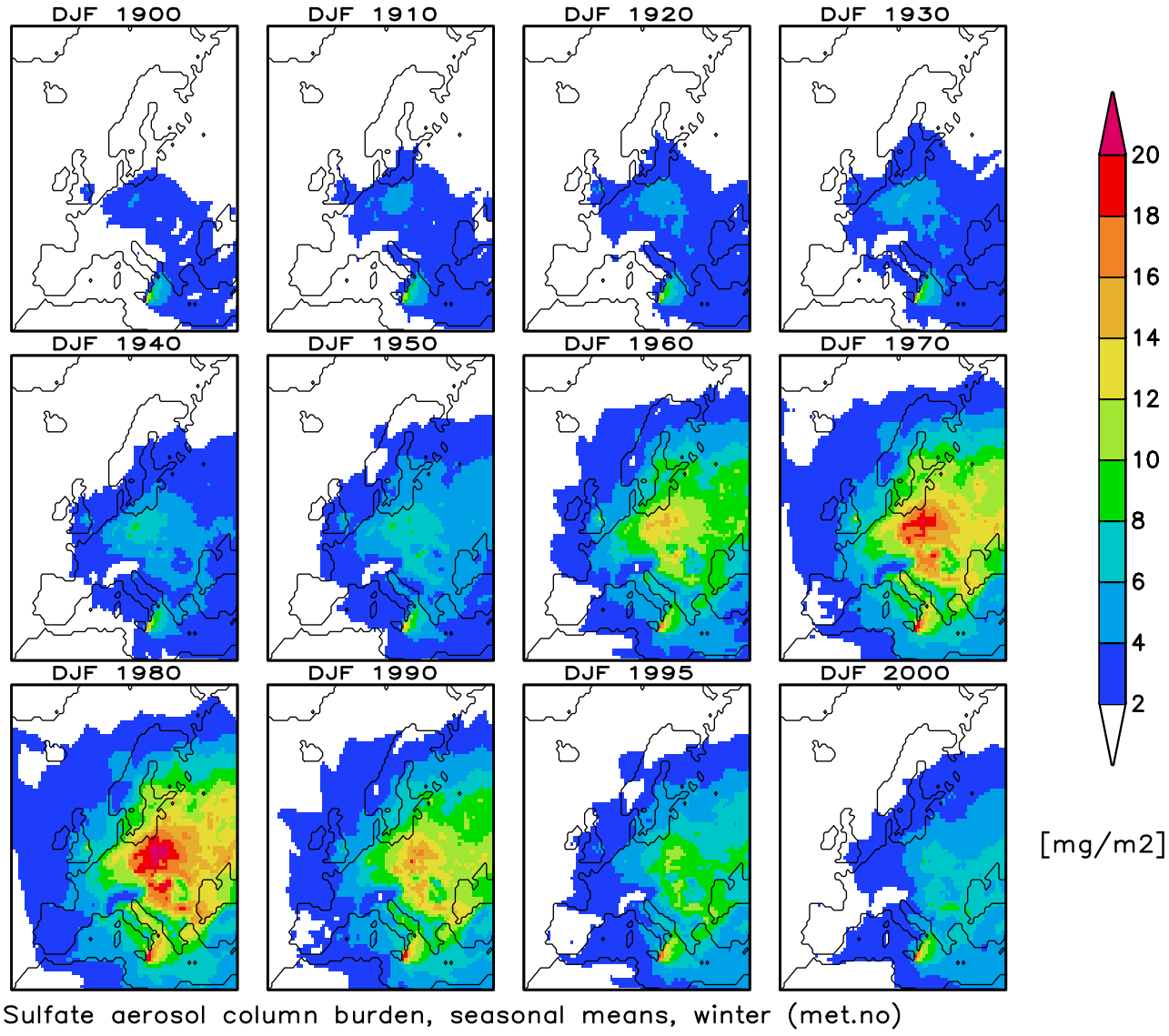

Figure 3.3: Wintertime horizontal distribution of the total atmospheric sulfate load, [mg(m^{-2})], seasonal means, 1900-2000

3.5.1 Winter

During winter, photochemical processes responsible for the production of secondary pollutants are limited due to weak solar radiation intensity.
In winter 1900, the highest atmospheric load can be found over central and south-eastern Europe, mainly over Germany, with a seasonal mean over Germany of 5 mg(m^{-2}) sulfate, compared with the mean European value of 1 mg(m^{-2}) (Figure 3.3). A second maximum is located over the Mediterranean Sea, which originates from the volcanic degassing of

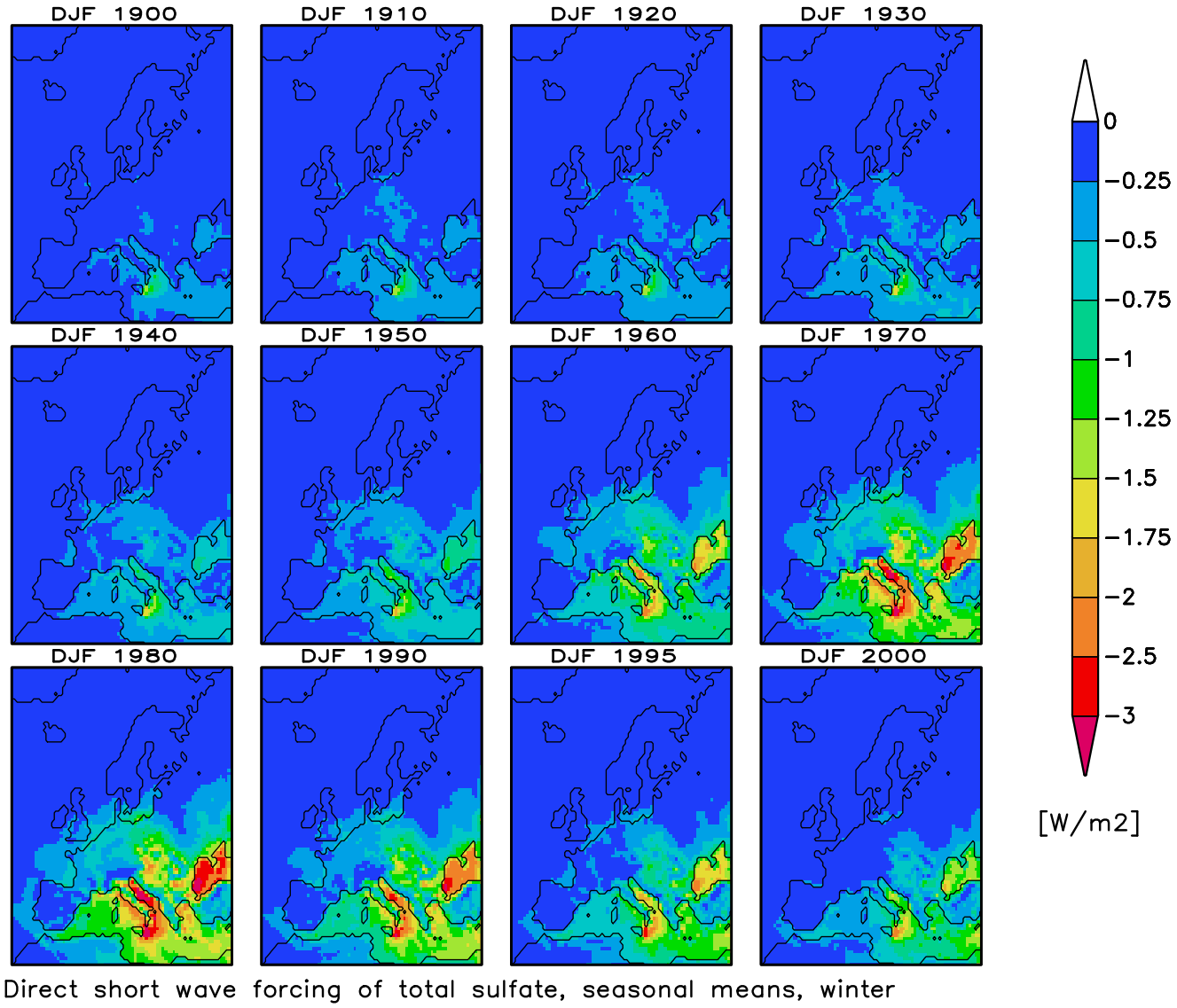

Figure 3.4: Wintertime direct radiative forcing due to sulfate aerosol, [Wm^{-2}], seasonal means, 1900-2000

Mt. Etna — a point source producing about 13 mg(m^{-2}) sulfate burden close to the source. The central European pollution maximum intensified and expanded northwards, eastwards and southwards during the century. In the 1950's the maximum reached 7 mg(m^{-2}), in the 1980's over 18 mg(m^{-2}). The wintertime pollution over eastern Europe is mainly due to domestic heating with brown coal. The Mediterranean plume increased after the 1960's due to additional anthropogenic sources, including industry and traffic. During the 1980's, the European continent excluding northern Scandinavia and the Iberian Peninsula was very polluted during winter, with sulfate aerosol loads exceeding 14

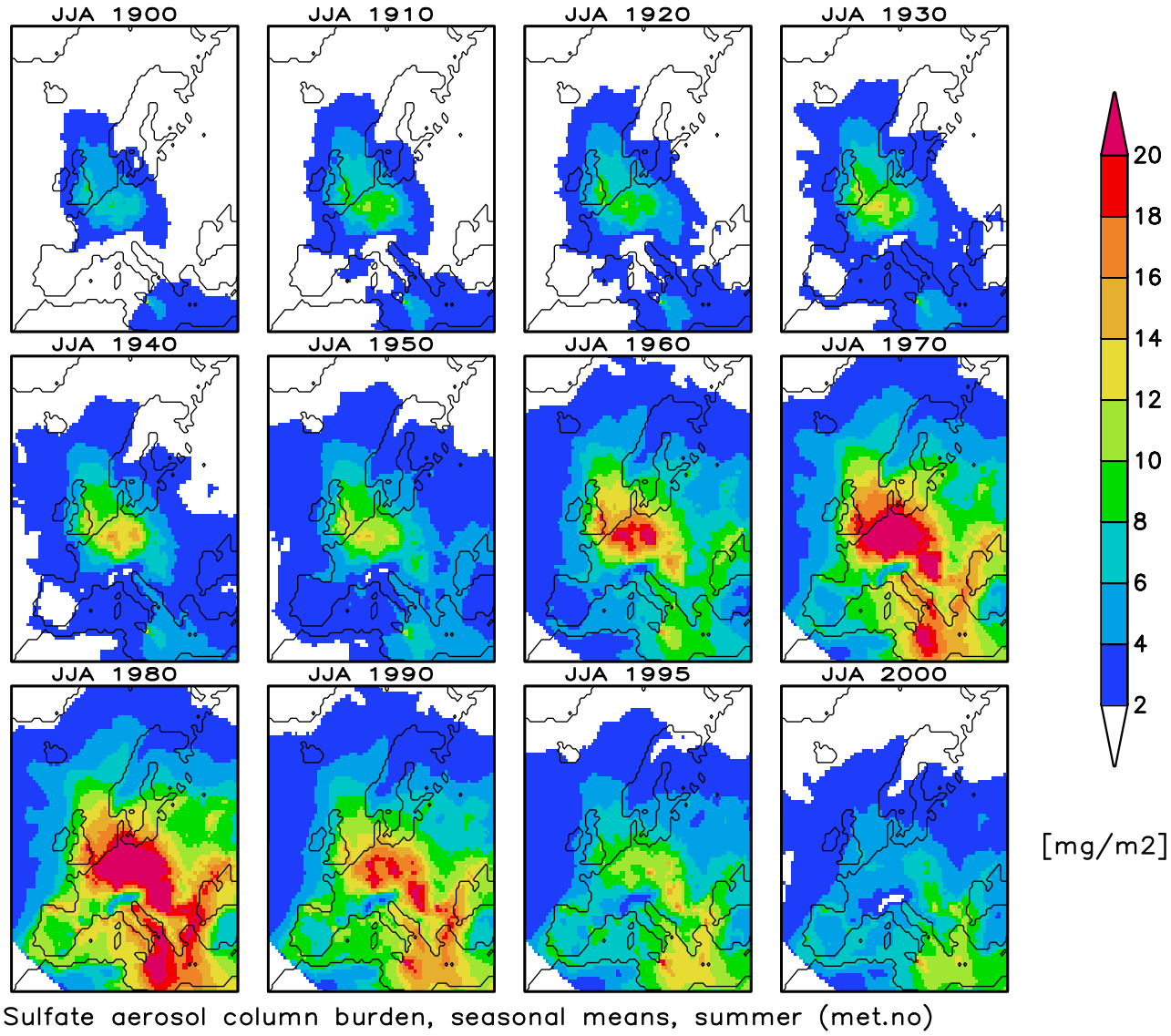

Figure 3.5: Summertime horizontal distribution of the total atmospheric sulfate load, [mg(m^{-2})], seasonal means, 1900-2000

mg(m^{-2}) over most of the continent. The pollution maximum was shifted from Germany towards the East: Poland, Western Soviet Union, Czechoslovakia, Yugoslavia, Hungary and Bulgaria. From the 1980's until the year 2000, the sulfate pollution was significantly reduced, with mean values of 3 mg(m^{-2}) over western Europe, and 7 mg(m^{-2}) over eastern and southern Europe and the eastern Mediterranean Sea. The mean European atmospheric load in winter 2000 is close to that of the 1950's, but the regional distribution is different. In winter of the 1950's the pollution maximum was located over Germany and Poland, whereas it was shifted south eastwards towards the Black Sea during winter

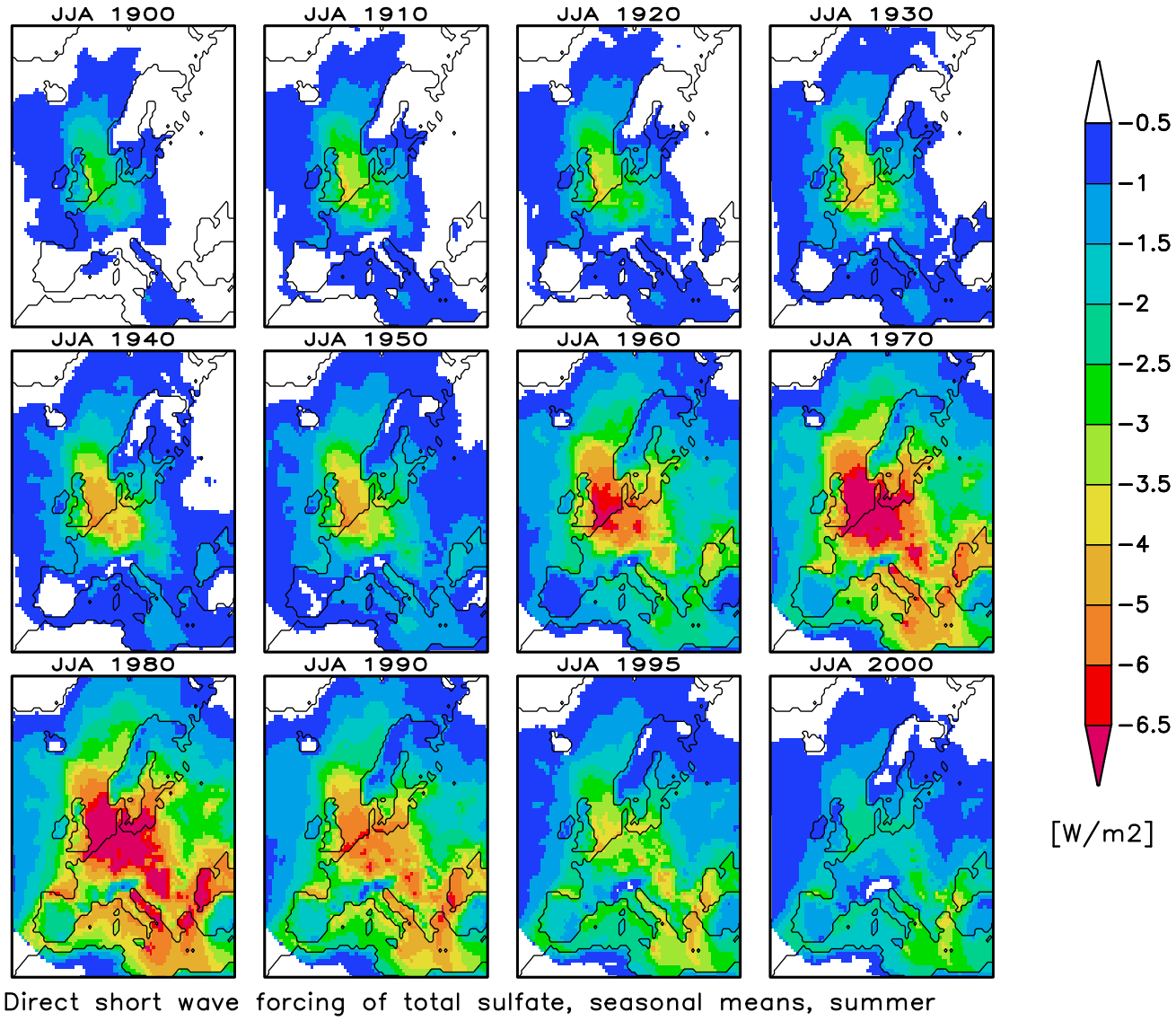

Figure 3.6: Summertime direct radiative forcing due to sulfate aerosol, [Wm^{-2}], seasonal means, 1900-2000

2000.

The spatial evolution of the wintertime direct sulfate forcing does not follow that of the atmospheric load (Figure 3.4). Because of weak radiation in the higher latitudes, the forcing is almost negligible in these regions. The forcing is concentrated in the lower latitudes, over areas with high atmospheric aerosol load, predominantly over the Black Sea and the Mediterranean Sea. From seasonal mean of –0.3 Wm^{-2} over these areas in 1900, it reached –1.8 Wm^{-2} over the Mediterranean Sea and –2.5 Wm^{-2} over the Black Sea in 1980. The mean December forcing in 2000 is slightly higher then in the 1950's, with

a similar spatial pattern — it is concentrated in the lower latitudes with the strongest forcing observed over the Mediterranean Sea and the Black Sea. While some forcing is detectable over central Europe in winter in the 1950's, it is negligible in winter 2000. This is clearly due to reduced atmospheric load over western and central Europe in winter 2000 compared to the 1950's.

3.5.2 Summer

During the summertime, photochemical processes responsible for the production of sulfate aerosol are enhanced due to strong solar radiation. In southern Europe, wet deposition is strongly limited by summertime aridity. These meteorological conditions cause pollution enhancement. Only in eastern Europe the summertime pollution is reduced, because domestic there heating is one of the main pollution sources. The spatial evolution of direct radiative forcing due to sulfate aerosol in summer is very similar to the spatial evolution of the sulfate atmospheric load (Figure 3.5 and Figure 3.6). In summer 1900, two pollution maxima can be seen – one over northwestern Europe (Great Britain, Netherlands, Belgium, Western Germany) and the North Sea and a second over the Mediterranean Sea. The northwestern plume intensified until the 1980's: The seasonal summertime mean increased from 6 mg(m^{-2}) in 1900's to over 24 mg(m^{-2}) in the 1980's; it expanded south eastwards towards the Black Sea (Figure 3.5). The Black Sea was relatively unpolluted during summer in the first half of the century. The pollution enhanced rapidly from 3 mg(m^{-2}) in the 1950's to 12 mg(m^{-2}) in the 1980's. The Mediterranean pollution maximum expanded from the 1950's through the 1980's when the summertime mean value exceeded 22 mg(m^{-2}). From the 1980's the summertime pollution over Europe began to decrease: The decrease of the Mediterranean plume is much slower than that of the plume over northwestern Europe. From 1995 on, the Mediterranean Sea is the most polluted area in summertime Europe. The main contributor to the summertime Mediterranean pollution are ship emissions. 54% of the total sulfate aerosol column burden over the Mediterranean in summer originates from ship emissions, contributing more than 50% of the direct radiative forcing (Marmer and Langmann, 2005).
The spatial pattern of the aerosol burden in summer is very well reflected in the spatial evolution of the direct sulfate aerosol forcing (Figure 3.6). The forcing over the North Sea and western Europe enhanced steadily since the 1900's. Until the 1970's, the forcing was strongest over northwestern Europe with mean summer values exceeding –6.5 Wm^{-2}. Afterwards the forcing over the Mediterranean became dominant with values of up to –6 Wm^{-2}. The forcing over the Black Sea was very high from 1970 until 1990. By the year 2000, the summer mean direct forcing over northwestern Europe was –1.5 to –2 Wm^{-2}, while over the central Mediterranean Sea, particularly over the Aegean Sea, it reached –3.5 Wm^{-2}. While the mean forcing in July 2000 has a similar value as July 1950, its maxima shifted from the North Sea to the Mediterranean Sea. In July 2000, the forcing over the North Sea was –1.5 Wm^{-2}, compared to –5 Wm^{-2} in the 1950's.

3.5.3 Forcing efficiency

The concept of 'forcing efficiency', defined as the ratio between the direct radiative forcing and the column burden was introduced by Boucher and Theodore (1995). We found the modern European mean forcing efficiency to be –230 W(g sulfate)$^{-1}$. It is well within the range of mean global sulfate forcing efficiencies from different simulations and methods of –130 to –370 W(g sulfate)$^{-1}$ (Seinfeld, 2002). According to our findings, the forcing efficiency depends strongly on the season, the latitude and the surface albedo. In our model, the mean forcing efficiency is –78 W(g sulfate)$^{-1}$ in December and –335 W(g sulfate)$^{-1}$ in July, averaged from 1900–2000. These results qualitatively agree with the study of Boucher and Theodore (1995), with forcing efficiency of –62 W(g sulfate)$^{-1}$ for Central Europe in January, and of –193 W(g sulfate)$^{-1}$ for July. Boucher and Theodore (1995) also found a pronounced negative correlation between the forcing efficiency and the cloud cover fraction. Climatological dependencies of the forcing efficiency could not be analyzed in this study, because the same meteorological year was used for all simulations. Additionally, the forcing efficiency depends the influence of the relative humidity on the aerosol optical properties. The forcing efficiency is not a temporally constant value. In December, the forcing efficiency in 2000 with –83 W(g sulfate)$^{-1}$is higher than in the 1900's with –76 W(g sulfate)$^{-1}$(Figure 3.7), because of the shift of sulfate aerosol burden maxima from higher to lower latitudes. The December forcing efficiency has a minimum of –69 W(g sulfate)$^{-1}$ in the 1960's. This is because the aerosol burden in the higher latitudes, which results in no or very low forcing during winter, initially increased faster then in the low latitudes. This trend was reversed since the 1960's. In July, the forcing efficiency is significantly reduced from –363 in the 1900's to –305 W(g sulfate)$^{-1}$ in 2000. This reduction is caused by the shift of the pollution maxima from North to South. During the summertime, there are longer hours of daily solar radiation in the North, resulting in higher forcing efficiency. The annual mean forcing efficiency also slightly reduced from –246 to –230 W(g sulfate)$^{-1}$. The global mean historical forcing efficiency remained nearly constant in the work of Boucher and Pham (2002). Probably, increased and decreased forcing tendencies compensate on the global mean.

3.5.4 Direct forcing at some selected areas

Five different areas were selected to further illustrate different regional patterns of the direct radiative sulfate forcing: the English Channel, the Black Sea, Denmark, the Island of Sicily and Sonnblick, an Alpine mountain site. Surface albedo is lower over water than over land, resulting in stronger forcing efficiency over maritime areas. The present day forcing efficiency over the Black Sea is –385 W(g sulfate)$^{-1}$ in July and –190 W(g sulfate)$^{-1}$ in December, and over the English Channel –440 W(g sulfate)$^{-1}$ in July (Table 3.1).

These values are much higher than the European mean. In winter, the English Channel receives less solar radiation than the Black Sea, resulting in lower efficiency of –70 W(g sulfate)$^{-1}$ in December. Seasonality is also very pronounced over Denmark, our most northern area, with strong forcing efficiency in July and weak in December. On the contrary, our most southern area, the Island of Sicily, shows almost the same forcing

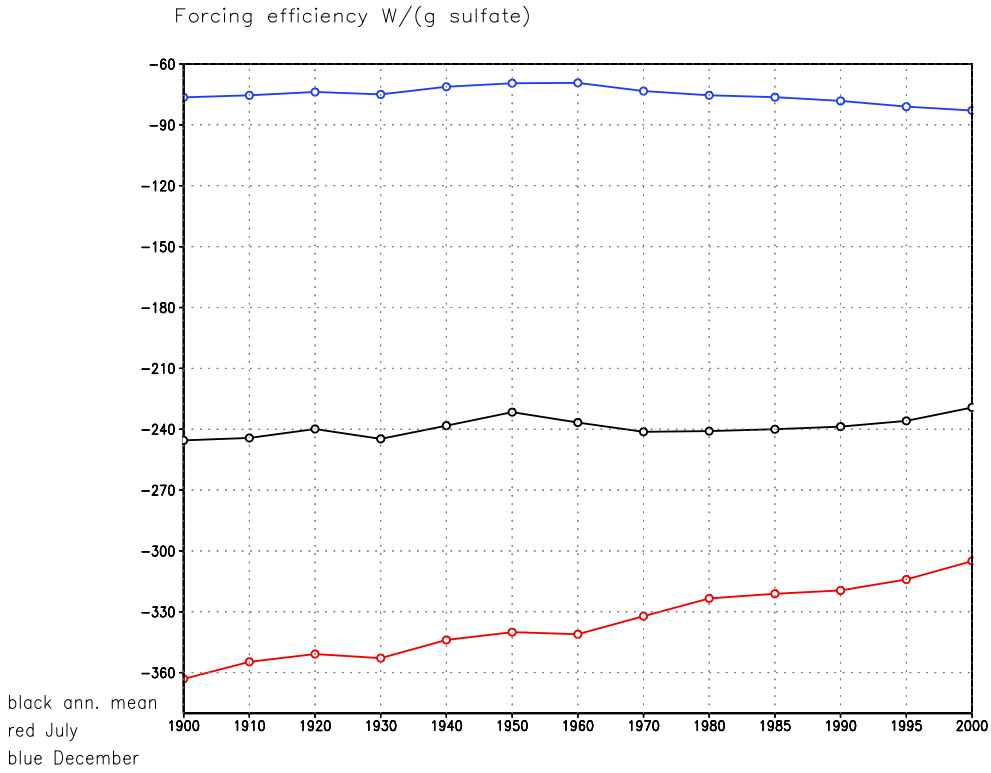

Figure 3.7: Historical trend in the forcing efficiency of sulfate aerosol over Europe, [W(g sulfate)$^{-1}$], 1900-2000. black: yearly mean, blue: monthly mean December, red: monthly mean July

efficiency values for July (–190 W(g sulfate)$^{-1}$) and December (–157 W(g sulfate)$^{-1}$). Relative to the European mean, the efficiency is low in summer, because of shorter days in the South than in the North, and high in winter, for the opposite reason. The surface albedo is high at the snow covered mountains and the additional scattering by aerosols does not result in a significant forcing efficiency over Sonnblick (3106 m asl; 3500 m asl in the model) in December. The atmospheric burden of sulfate aerosol is the lowest at this elevated site – this site represents free tropospheric conditions. Nevertheless, the direct forcing shows a pronounced historical trend, indicating that the sulfate aerosol pollution from nortwestern Europe has reached this remote elevated region. The July forcing has a maximum in the 1985, and by the year 2000, this forcing is smaller than at the beginning of the century (Figure 3.8). The forcing over the English Channel, which is located close to strong sulfur emission sources, reaches –5.2 Wm^{-2} in the 1970's, by the year 2000 it also reduced close to the values of the 1900's. Similar trend can be found over Denmark. Comparing the trends over Sonnblick, Denmark and the English Channel to that over the Black Sea, reveals the shift of the forcing maxima from northwestern to southeastern Europe (section 3.5.3). The modern forcing over the Black Sea with –2.5 Wm^{-2} in July is 10 times stronger than at the beginning of the last century; the modern forcing in December is 5 times stronger than in the 1900's. The modern forcing over the Black Sea

Area	Forcing efficiency [W(g sulfate)$^{-1}$]	
	July 2000	December 2000
English Channel	–440	–70
Black Sea	–385	–190
Denmark	– 360	– 72
Sonnblick	– 212	– 33
Island of Sicily	–190	–157
European mean	-338	–78

Table 3.1: Forcings efficiencies for the selected areas in July and in December 2000

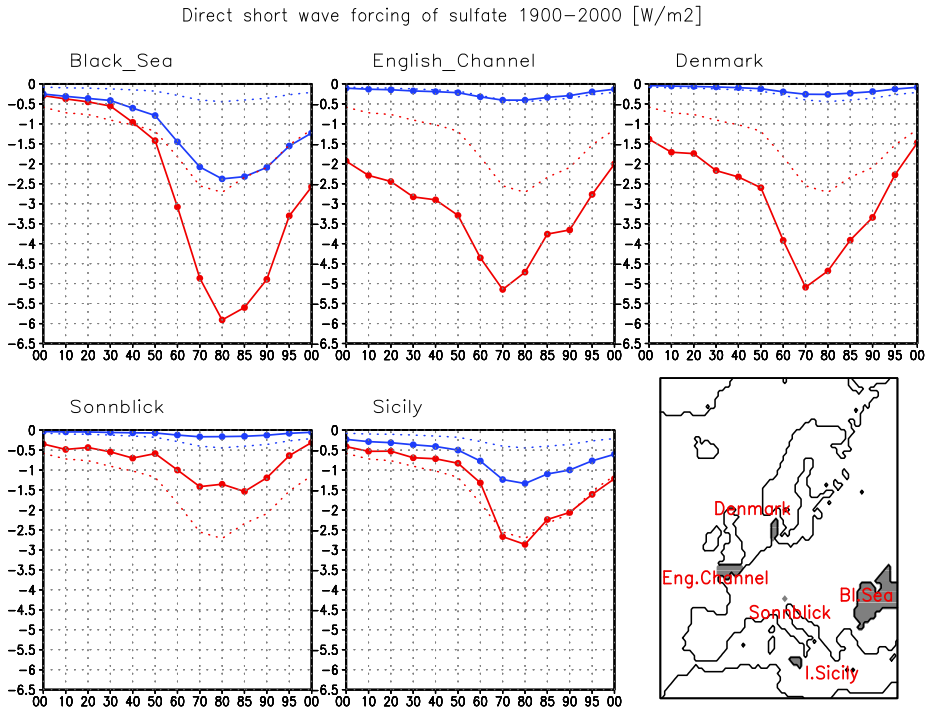

Figure 3.8: Historical trend of the direct sulfate forcing at the selected areas for July (red) and December (blue). Dotted lines show the trend of the European mean forcing in July (red) and December (blue). Map of the selected areas.

is similar to that in the 1960's, its reduction in the past 30 years less efficient than of the Eropean mean forcing. The forcing over Sicily shows the same trend as over the Black Sea, but the absolute values are much lower.

3.6 Summary and conclusions

We have provided an estimate of the historical evolution of the direct radiative forcing of sulfate aerosol over Europe, emphasizing on regional characteristics. The mean direct forcing has increased since the 1900's reaching it's peak in the 1980's and then returning in present times to approximately the values of the 1950's. Despite the different distribution of the atmospheric load in December 1950 and 2000, the winter forcing distribution remains very similar, with maxima over the Black and the Mediterranean Seas. We found pronounced shift of the summer forcing maxima from northwestern to southeastern Europe. We can clearly observe that emission reductions, introduced in the 1980's, have led to a significant reduction in the atmospheric load and the direct forcing over Europe. The regional direct aerosol forcing depends not only on the sulfate load, but also on the latitude, the season, the cloud cover and the surface albedo.
An uncertainty that needs to be carefully considered is the assumption of the same meteorological year (1997) for all simulations. Meteorological conditions play a very important role in aerosol production, transport and deposition (Marmer et al., 2006) and can result in inter-annual concentration variabilities of up to 30% (Putaud et al., 2004). Furthermore, meteorology has an important impact on the forcing itself, via changes in surface albedo due to snow cover, changes in cloud cover and relative humidity of the ambient air. The aerosol forcing thus depends not only on the emissions strength, but also on inter-annual meteorological variability, which was not considered. Additional uncertainty is caused by the treatment of RH in the radiation model.In ORTM, size-dependent Mie calculations have been applied for dry aerosol particle size. The specific extinction obtained for a dry particle was then multiplied with a RH dependent growth factor. This approach may underestimate the direct radiative forcing for high relative himidities.
With black carbon to be included in future work, we expect different historical evolution of the aerosol forcing distribution and strength. Black carbon is highly absorbing and so its radiative forcing is positive in sign. Thus, the forcings might partially offset each other. The non-linearity of the aerosol burden response associated with emission changes as suggested by (Stier, 2004) can additionally affect the historical aerosol burden and the corresponding direct forcing when black carbon is included. On seasonal and regional scales the sign of the total forcing might vary substantially. Historical gridded emission inventory of carboneous aerosols for Europe need to be established in order to complete the model simulations of the direct aerosol forcing evolution.

Acknowledgements
We thank Stefan Kinne and Melissa Pfeffer for reviewing the manuscript internally. This research was financially supported by EU project CARBOSOL.

Chapter 4

Inter-annual variability of aerosol distribution and direct radiative forcing over Europe

[1] **Abstract**

Aerosol distribution over Europe and its direct radiative forcing have been simulated with a regional atmosphere-chemistry model and an off-line radiation transfer model. Primary and secondary organic and inorganic aerosols have been considered. The simulation was conducted for two different meteorological years 2002 and 2003 to analyze the spatial and temporal variability of the aerosol distribution and the direct forcing. Meteorological conditions play a major role in spatial and temporal variability in the European aerosol burden distribution. Regionally, year to year variability of monthly mean aerosol burden can reach up to 100 % due to different weather conditions. The mixing state of aerosols, externally or internally, is shown to influence the strength, regional distribution and sign of radiative forcing, thereby regulating the forcing efficiency. Comparisons with measurements indicate the importance of biomass burning emissions, which are not considered in the model simulations presented here. Due to lack of these emission sources and due to additional unknown formation processes of secondary organic aerosol, the carbonaceous aerosols are underestimated by a factor of 2-5 for black carbon and 10 for the organic carbon, respectively. Modeled sulfate aerosol is well represented. Sensitivity studies show a mean European direct forcing of –0.3 Wm^{-2} in winter and –2.5 Wm^{-2} in summer, regionally ranging from –5 to + 4 Wm^{-2}.

[1] to be submitted to *JGR* as: Marmer, E., Langmann B., Hungershöfer, K., Trautmann, T. Inter-annual variability of aerosol distribution and direct radiative forcing over Europe, 2006.

4.1 Introduction

Determining the aerosol impact on climate presents a great challenge for climate research. This requires a detailed knowledge of the strength and regional distribution of the emission sources of primary aerosol particles and of the precursor gases involved in formation of secondary aerosol particles. Fossil fuel combustion is thought to be the major contributor to anthropogenic emissions in Europe for sulfur dioxide (SO_2), precursor of sulfate aerosol, black and primary organic carbon. The source-apportionment analysis of continuous aerosol samples at five European sites indicates that biomass burning contributes an important part to primary carbonaceous aerosol concentration (Gelencsér et al., 2006).
Geographically localized sources and sinks and relatively short atmospheric lifetimes cause extreme spatial and temporal inhomogeneity of aerosol distribution and chemical composition (Haywood and Boucher, 2000). Continuous aerosol measurements all over Europe (1991-2001) revealed significant inter-annual concentration variabilities of up to 30% (Putaud et al., 2004). Hongisto et al. (2003) applied a regional transport-chemistry model over Europe (1993-1998) and showed that the regional inter-annual variability of sulfur deposition strongly depends on the prevailing meteorological conditions. Hence, accurate modeling of meteorological conditions is necessary for the accurate prediction of the spatial and temporal variability of aerosol distribution.
The direct aerosol forcing results from the ability of aerosol particles to scatter and/or absorb solar radiation. The sensitivity of the modeled European climate to a change in its aerosol direct forcing due to different aerosol distributions was investigated by Hohenegger and Vidale (2005), emphasizing the importance of the accuracy of the predicted aerosol distribution. Regional and temporal distribution of this forcing also depends on meteorological conditions. Partially absorbing aerosol may exert a local negative forcing over regions with low surface albedo and a positive forcing over regions with high surface albedo (e.g. Haywood and Shine, 1995; Chylek and Wong, 1995). Similar results are found if partially absorbing aerosol resides above clouds with high albedo (Haywood et al., 1997). The variability of the aerosol direct forcing intensity and sign further depends on the aerosol chemical composition.
The radiative forcing of externally mixed aerosol is determined by adding up the forcings exerted by individual aerosol compounds. This assumption is acceptable for newly released aerosols, but aged particles are found to be mixed internally (e.g. Murphy and Thomson, 1997; Middlebrook et al., 1998). Considering the internal mixing of sulfate and black carbon aerosols can substantially alter forcing estimates (e.g. Haywood et al., 1997; Myhre et al., 1998; Lesins et al., 2002). Lesins et al. (2002) showed that for specific internal mixing assumptions nearly all of the cooling effect predicted for the external mixture is set off by the black carbon absorption enhancement.
Relatively few studies have investigated the direct radiative forcing resulting from organic aerosol (Kanakidou et al. (2004) and references therein). Only in Chung and Seinfeld (2002) has secondary organic aerosol formation been treated explicitly. A considerable fraction of total carbonaceous aerosol is thought to be secondary (30 to 80 %, (Gelencsér et al., 2006)), therefore its contribution to aerosol pollution and forcing should be considered.

All forcing estimates described above utilized global climate models, whose coarse resolution leads to the smoothing of local inhomogeneities of the aerosol distribution. To improve on this, we have utilized a regional atmosphere-chemistry model over Europe to simulate aerosol mass distribution for the years 2002 and 2003. Sulfate, black carbon and primary and secondary organic carbon aerosols have been included. The very different meteorological conditions for these years allow us to investigate their impact on aerosol column burden, including the impact on secondary particle formation. Evaluation of the modeled results with available measurements and source-apportionment analysis of aerosol samples allows us to estimate the accuracy of predicted aerosol concentration distribution and to investigate the reasons for model deficiencies. We have also utilized an off-line radiation transfer model to determine the direct aerosol forcing assuming both externally and internally mixed aerosols. The dependency of this forcing on aerosol burden distribution and meteorological conditions is further analyzed. Finally, we have performed a sensitivity experiment determining the direct forcing of the aerosol burden scaled to measurements. The experiment result is considered to be a high-end estimate of the European aerosol forcing.

4.2 Experimental set-up

4.2.1 Atmosphere-chemistry model

The regional atmosphere-chemistry model REMOTE (REgional Model with Tracer Extension, (Langmann, 2000)) determines the physical and chemical state of the model atmosphere at every time step. A terrain following, hybrid pressure-sigma coordinate is used in the vertical with 19 vertical layers of unequal thickness between the ground and the 10 hPa pressure level. The horizontal resolution for the presented investigations is 0.5° on a spherical rotated grid. The dynamical part of the model is based on the global ECHAM 4 model (Roeckner, 1996), (Jacob, 2001). The prognostic equations for surface pressure, temperature, specific humidity, cloud water, horizontal wind components and trace species mass mixing ratios are written on an Arakawa-C-Grid (Mesinger and Arakawa, 1976). In the current model set-up, 63 chemical species are included. The species transport is determined by horizontal and vertical advection according to the algorithm of Smolarkiewitz (1983), convective up- and downdraft by a modified scheme of Tiedtke (1989) and vertical diffusion after Mellor and Yamada (1974). Dry deposition velocities are computed as in Wesley (1989) dependent on the friction velocities and stability of the lowest model layer. Wet deposition is computed according to Walcek et al. (1986) by integrating the product of the grid-averaged precipitation rate and the mean cloud water concentration. The gas-phase chemistry package RADM II (Stockwell et al., 1990) is implemented with a quasi-steady-state approximation (QSSA) solver (Hesstvedt et al., 1978). 43 longer-living prognostic species and 20 short living diagnostic molecules react in the gas phase. The photochemical gas phase mechanism consists of 158 reactions. Clear sky photolysis rates are calculated by a climatological pre-processor model (Madronich, 1987). The presence of clouds modifies photolysis rates as described by Chang et al. (1987).

At the first time step, REMOTE was initialized using meteorological analysis data of the European Center for Medium Range Weather Forecast (ECMWF), which were updated at the lateral boundaries every 6h. Chemical initial and boundary concentrations were prescribed by the model results of the global chemistry transport model MOZART Horowitz et al. (2003) for 14 species including PAN, HNO_3, H_2O_2, CO, NO, NO_2, O_3 and 7 hydrocarbons. Concentrations of the other species are derived from available measurements (Chang et al. (1987) and references therein) and are held constant at the lateral model boundaries throughout the simulation.

Emissions

Temporally variable emissions of SO_x, NO_x, NH_3, CO, VOC for the year 2001 and $PM_{2.5}$ emissions for the year 2000 were included in the 2002-2003 simulation. The emissions were provided by the Norwegian Meteorological Institute (Vestreng, 2003; Vestreng et al., 2004), with monthly emission factors for each country and emission sector. Chemical speciation of $PM_{2.5}$ emissions into primary organic carbon (POC) and black carbon (BC) is based on Andersson-Skøld and Simpson (2001). Recently, a new emission inventory for POC and BC became available from IIASA (Bond et al., 2004). Test simulations with prescribed IIASA emissions did not result in significantly different atmospheric concentration of carbonaceous aerosols. Anthropogenic VOC emissions are distributed in 12 different classes of volatile organic compounds (VOC) according to Memmesheimer et al. (1991). Biogenic VOC emissions are calculated in REMOTE as a function of temperature, solar radiation and land-use, based on the approach of Guenther et al. (1991, 1993). We assume that 96% of the total SO_x is emitted as SO_2 and 4% as $SO_4{}^{2-}$. SO_x is emitted from natural and anthropogenic sources with DMS treated as SO_x. Natural sources of NO_x are not considered. SO_x and NO_x emissions from point sources are distributed vertically between the seven lowest model levels following Memmesheimer et al. (1991).

Secondary organic aerosol production

In REMOTE, we consider secondary organic aerosol (SOA) production according to the approach of Schell (2000). In this Secondary ORGanic Aerosol Model (SORGAM), gas/particle partitioning of interacting low vapor pressure products is treated as an absorption process into the organic mass of aerosol particles. The precursor gases, or volatile organic compounds (VOC), are of anthropogenic and biogenic origin (Section 4.2.1). OH, NO_3 and O_3 oxidize these volatile gases to form semi-volatile compounds. Little is known about detailed chemical degradation pathways of organic compounds leading to low-volatile products, which then partition between the gas phase and the particle phase to form SOA. In SORGAM, these processes are parameterized through measured and estimated stoichiometric coefficients that relate the reactive organic gases with semi-volatile organic products. We consider products of aromates, higher alkanes and higher alkenes. Isoprene is also thought to contribute to SOA formation under certain atmospheric conditions (Limbeck et al., 2003) and Claeys et al. (2004). We have not included products of isoprene, however, because very low aerosol yield of the isoprene products require very high isoprene concentrations in order to generate substantial amount of secondary aerosol.

4.2.2 Radiation transfer model ORTM

The direct radiative shortwave aerosol forcing was calculated using the Off-line Radiation Transfer Model (ORTM) described by Langmann et al. (1998). The direct shortwave radiative aerosol forcing is calculated based on the variable aerosol mass distribution and meteorological input data. The delta-Eddington approximation includes single as well as multiple scattering. Only the shortwave part of the solar spectrum 0.2–5 μm, subdivided into 18 wavelength intervals, is considered, because aerosols considered here have a negligible radiative effect in the infrared. Optical properties of the dry sulfate aerosol are determined from Mie theory calculations. The modification of aerosol specific extinction due to relative humidity of the ambient air is considered using a simple approximation adapted from the data given by Nemesure et al. (1995). For relative humidities (RH) below 80 %, the specific extinction is enhanced by a factor of RH*0.04, assuming a minimum RH of 25 %. For RH exceeding 80 %, the specific extinction increases exponentially with RH. The factor 9.9 is reached for RH = 100 %. Exponential growth is assumed for hygroscopic aerosols (sulfate and organic carbon in case of external mixing as well as for internally mixed aerosols). Black carbon, if externally mixed, is assumed to be mostly hydrophobic and its specific extinction increases only linearly with RH. Single scattering albedo and the asymmetry factor are assumed to be independent of RH. This approach might result in a small overestimation of the shortwave radiative forcing of scattering aerosols, because with increasing relative humidity forward scattering is increased and backscattering in space direction reduced (asymmetry factor increased).

4.2.3 Aerosol optical properties

The ORTM has been extended for this work to include OC and BC aerosol in addition to sulfate. The broadband aerosol optical properties for the externally mixed aerosols were determined in two steps: First, the spectral optical properties in the wavelength region between 0.2 μm and 5 μm were calculated based on Mie theory. In a second step, these spectral quantities were weighted by the extraterrestrial solar flux (Wehrli, 1985), and averaged over the applied wavelength intervals of the ORTM. REMOTE determines aerosol mass, and does not provide information about particle size distributions or particle densities, so we had to make assumptions about these properties for the Mie calculations. In Table 4.1, assumptions made by different authors, demonstrating substantial differencies, are presented. In this study, a log-normal size distribution with a geometric mean radius of 0.05 μm for sulfate and OC, a geometric standard deviation σ_g of 1.8 for sulfate and 2 for OC, and a particle density of 1600 kg(m^{-3}) and 1200 kg(m^{-3}), respectively have been assumed. The geometric mean radius for BC particles is assumed to be 0.0118 μm with a σ_g of 2.0 and a particle density of 1800 kg(m^{-3}).
In case of an internal mixture of sulfate, black and organic carbon a monomodal log-normal size distribution with a geometric mean radius of 0.05 μm and a geometric standard deviation σ_g of 2.0 was assumed. The chemical composition of the internally mixed aerosol for every grid box was determined from the volume of sulfate, BC and OC in 10 % intervals. An effective refractive index for the mixture was retrieved from the refractive indices of the single components with the volume-weighted mixture approach. Similarly,

a mean particle density was determined. Optical properties as a function of wavelength for external and internal mixture are presented in Figure 4.1.

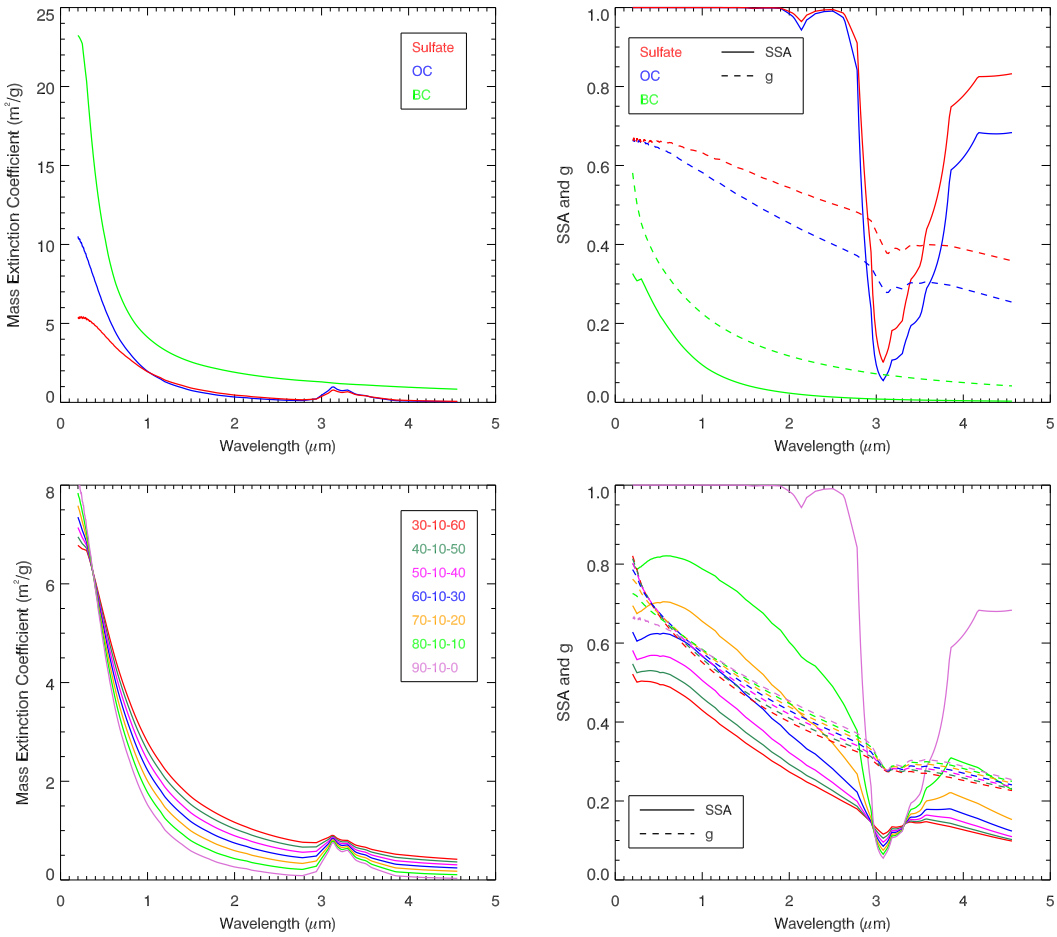

Figure 4.1: Mass extinction coefficient (left) and single scattering albedo (SSA) and asymmetry factor (g) (right) as a function of the wavelength for externally mixed (top) and internally mixed aerosols (bottom). Examples for eight different internal mixtures with mass contributions of sulfate-OC-BC [%] for the internally mixed aerosols are shown (bottom). The scales of the mass extinction coefficient (left) are different for externally (top) and internally (bottom) mixed aerosols.

Author	Aerosol	r_{gN} [μm]	σ_g	density [kg(m^{-3})]	refractive indices at 0.55 μm
Langmann et al. (1998)	Sulfate	0.05	1.8	1600	$1.43 - i\,2.0*10^{-8}$
Hess et al. (1998)	Sulfate	0.1	2.0	1760	$1.53 - i\,6.0*10^{-3}$
Koepke et al. (1994)	Sulfate	0.07	2.03	1700	$1.43 - i\,1.0*10^{-8}$
Penner et al. (1998)	Sulfate	0.05	2.0	1200	$1.53 - i\,1.0*10^{-7}$
Penner et al. (1998)	BC	0.0118	2.0	1800	$1.75 - i\,4.4*10^{-1}$
Hess et al. (1998)	BC	0.01	2.0	1000	$1.75 - i\,4.4*10^{-1}$
Cooke et al. (1999)	OC	0.02	2.0	1800	
this study	Sulfate	0.05	1.8	1600	$1.43 - i\,2.0*10^{-8}$
this study	BC	0.0118	2.0	1800	$1.75 - i\,4.4*10^{-1}$
this study	OC	0.05	2.0	1200	$1.53 - i\,1.0*10^{-7}$

Table 4.1: Aerosol physical and optical properties as found in literature

4.3 Aerosol concentration distribution: Model results and observations

4.3.1 Sulfate aerosol

Of 16,028 Gg(SO_x)yr^{-1} emitted in Europe, only 4% is assumed to be emitted as primary sulfate aerosol. The larger part is emitted as sulfur dioxide and then converted in the atmosphere into sulfate aerosol via gaseous and aqueous phase chemical reactions. SO_x emissions over land vary substantially with time mainly to domestic heating in winter (Figure 4.2). The atmospheric column burden of sulfate aerosol shows a pronounced spatial, seasonal and inter-annual variability (Figure 4.3). During winter, a concentration maximum is found over central Europe; during summer, the maximum is found over the Mediterranean Sea. The summer maximum of 8-10 mg(m^{-2}) is higher than the winter maximum of 5-6 mg(m^{-2}). The sulfate aerosol burden over south-central Europe is higher in spring and summer 2003 compared to 2002; the opposite is true over northern Europe. The simulated vertical distribution of sulfate aerosol shows the strongest decrease with height in winter (Figure 4.4). In spring 2002, the decrease with height is steeper than in 2003. The summer/winter concentration ratio is 1.5 at the lowest model level and 3.7 at about 3 km height.
The model was validated against observations from Co-operative Programme for Monitoring and Evaluation of the Long-Range Transmissions of Air Pollutants in Europe (EMEP) (Hjellbrekke, 2004) (Figure 4.5). There is a large scatter for all seasons. The best agreement is found for spring and fall 2002. In summer, the lower end values (<0.6 μg(S)m^{-3}) are well represented by the model, while the higher values are underestimated. The largest scatter was found in winter. It must be kept in mind that it is difficult to compare point measurements with model of 0.5 °resolution.
Aerosol measurements obtained during the EU-Project CARBOSOL (Gelencsér et al., 2006) at five sites: Sonnblick, Puy De Dome, Schauinsland, Aveiro and K-Puszta, were

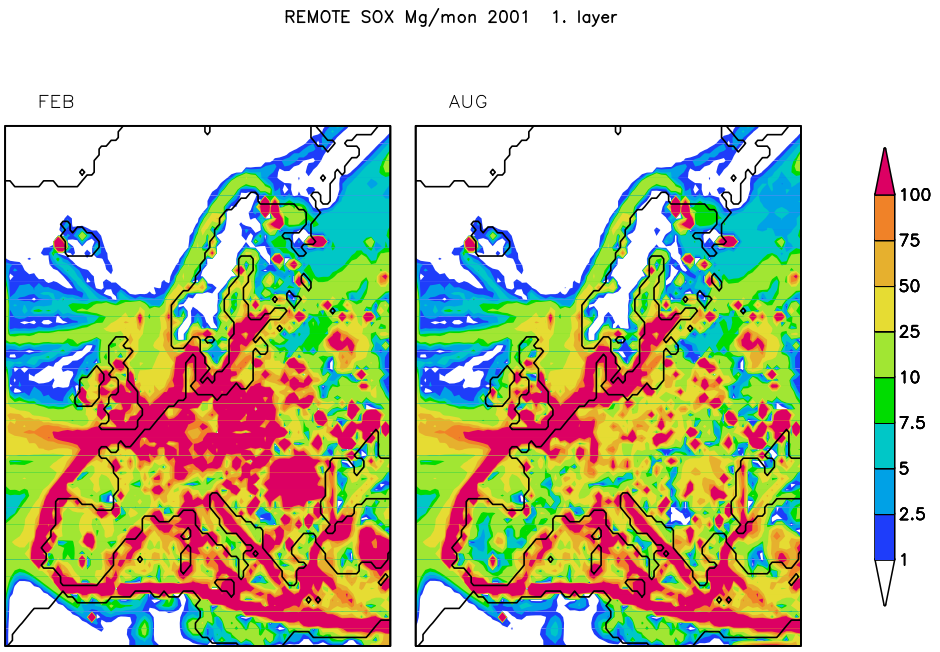

Figure 4.2: Monthly mean SO_x emissions into the lowest model level [Mg(mon^{-1})] for February and August.

also compared with the model results (Figure 4.6). The detailed description of the sampling sites, sampling and analyses can be found in Pio et al. (2006). Here, we have chosen a higher model level for the three elevated sites, to compare modeled and observed aerosol concentrations at the free troposphere. We have simulated the years 2002 and 2003, while the observations were obtained for the years 2003 and 2004, so we compare the observed and modeled concentrations for the year 2003. In both, the modeled and observed concentrations, inter-annual variability can be observed at all sites. The annual variability of sulfate aerosol concentration is very well captured by REMOTE. At the southwestern (Aveiro) and the three central European sites maxima during the summer and minima during the winter are visible in the modeled and observed data sets. The annual variability is reversed at the southeastern European site K-Puszta, where the concentration increases during wintertime. High SO_x emissions from domestic heating result in enhanced wintertime sulfate aerosol pollution. At K-Puszta, REMOTE can reproduce the concentration increase during winter but does not capture the very high value of 4.5 μg(S)m^{-3} in February 2003.

4.3.2 Carbonaceous aerosols

In our simulations, the $PM_{2.5}$ emissions were artificially specified as black (BC) and primary organic carbon (POC) (Andersson-Skøld and Simpson, 2001) (Figure 4.7). Generally, $PM_{2.5}$ represents 80-90% of PM_{10}; PM_{10} represents 80% of the total particulate matter. In the model, these aerosols are transported in the atmosphere and removed by

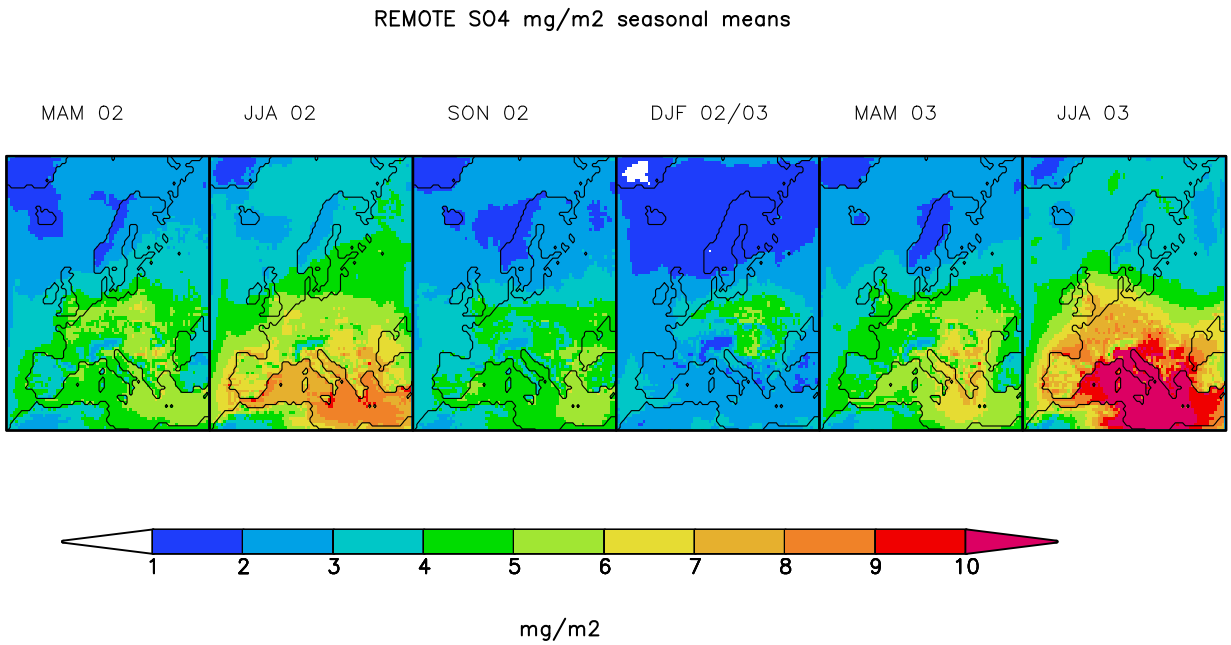

Figure 4.3: Modeled seasonal means of sulfate column burden [mg(m^{-2})] for March-April-May (MAM), June-July-August (JJA), September-October-November (SON) and December-January-February (DJF), 2002–2003.

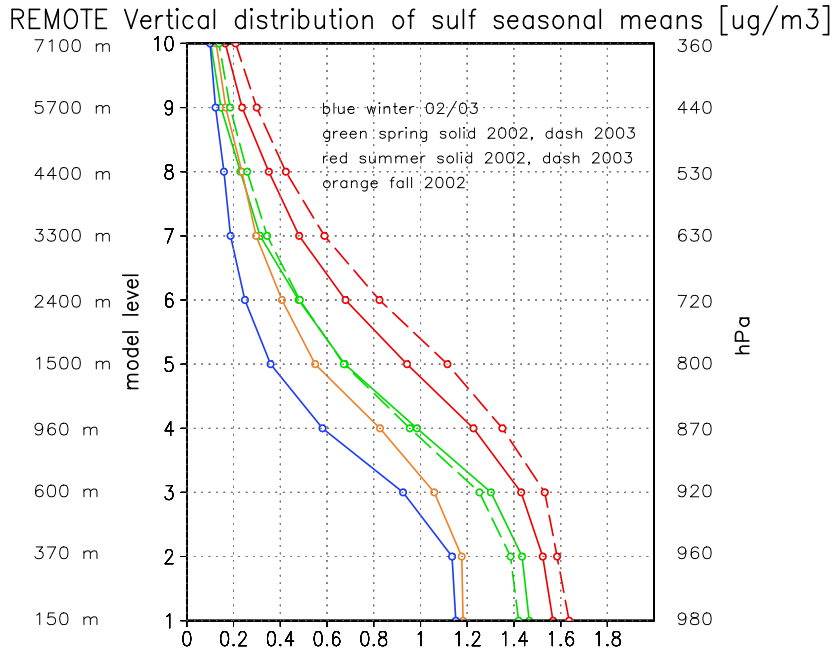

Figure 4.4: Modeled seasonal mean sulfate concentration [μg(m^{-3})], vertical profiles.

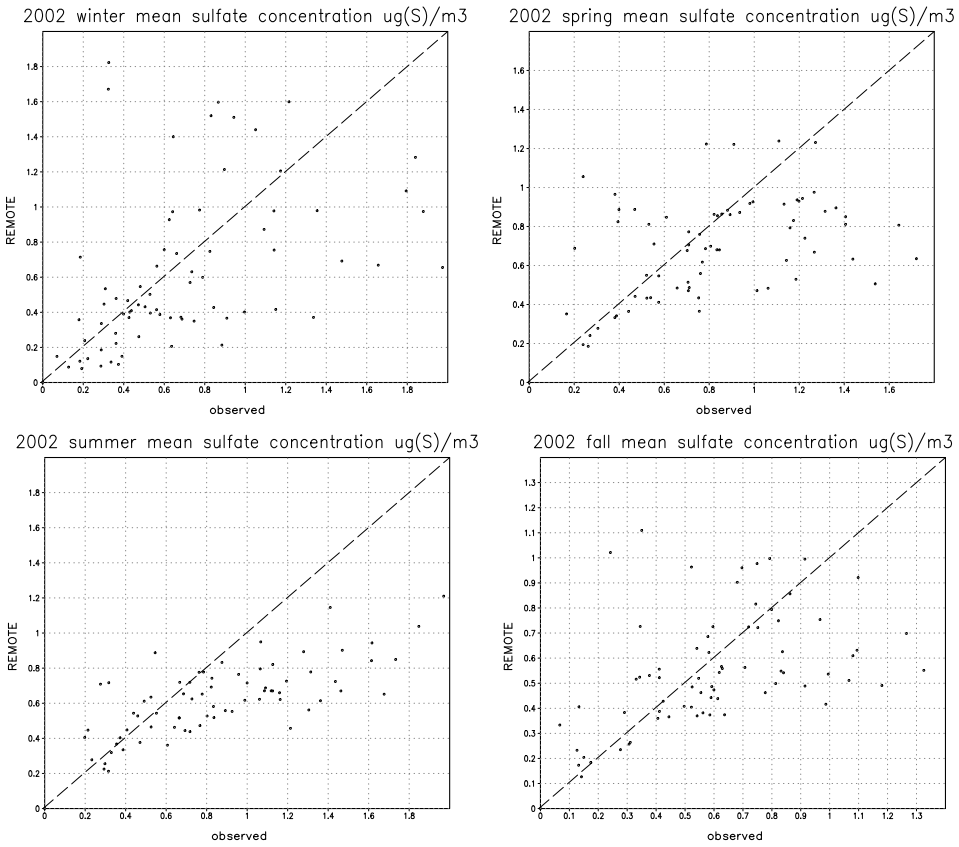

Figure 4.5: Observed versus modeled surface sulfate concentration [μg(S)m^{-3}] at 74 EMEP sites (Hjellbrekke, 2004).

dry and wet deposition. Unlike sulfate aerosol, they are not subject to chemical reactions. Contribution of BC and POC to the total aerosol load is similar to each other (Figure 4.8) and an order of magnitude lower than that of sulfate (Figure 4.3). The geographical distribution of primary carbonaceous particles is also similar to each other. High pollution levels are found close to strong emission sources. The seasonal variation of BC and POC is not as pronounced as that of sulfate aerosol. In spring and summer, the atmospheric load increases over Southern Europe. A pollution maximum was simulated over eastern Europe in winter. Pollution is slightly higher in spring 2003 than in 2002. The most significant feature in Figure 4.8 is the extremely enhanced pollution over western, central and southern Europe in summer 2003 (excluding the Iberian Peninsula). Maximum surface concentration of carbonaceous aerosols is found during winter (Figure 4.9), as opposite to that of sulfate. The vertical lapse rate of primary carbonaceous aerosols is steeper than that of sulfate for all seasons.

An important contribution to the total organic carbon (TOC) is provided by secondary organic aerosol (SOA) production. In the model, SOA is formed in the atmosphere when gas-phase organic species undergo oxidation, leading to products of sufficiently low vapor pressure that can partition between the gas and aerosol phase. Biogenic VOC emissions

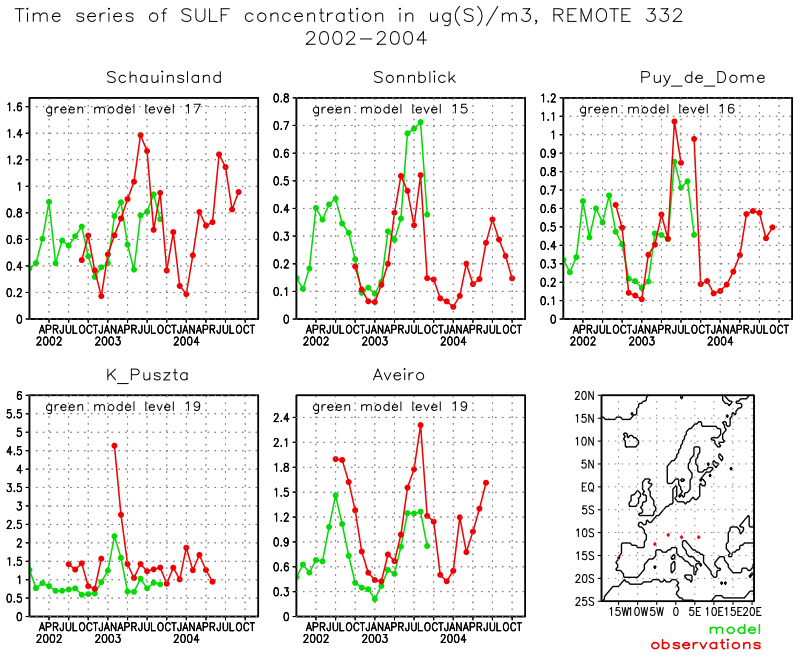

Figure 4.6: Observed (red) versus modeled (green) monthly mean time series of sulfate concentration [μg(S)m^{-3}] at five CARBOSOL sites. Map of the observational sites, from left to right: Aveiro, Puy de Dome, Schauinsland, Sonnblick, K-Puszta

are important precursor gases for SOA production. They are emitted by coniferous forests mainly in summer. In Scandinavia, SOA production during summertime is the dominant source of organic material, contributing more than 70 % to the organic aerosol burden. In central and southern Europe, anthropogenic sources additionally contribute to SOA production. Here, the seasonal variability of SOA burden is also very pronounced, with its maximum in summer (30-50 % of TOC burden) and low production during winter (5-15 %) (Figure 4.10). SOA is largely formed in the upper troposphere, its contribution to the surface concentration is much less than its contribution to the total column burden. At the surface, SOA contributes only 1-10 % to the total organic carbon over most of Europe in winter and 10-40 % in summer. Only over Scandinavia, SOA presents almost 70 % of total organic matter even in the lowest model level (Figure 4.11). Simulated concentrations of BC at the CARBOSOL sites were compared with measurements (Figure 4.12). Total organic carbon was compared with simulated total and primary organic carbon in Figure 4.13, where the modeled values were multiplied by a factor of 10. The model clearly underpredicts both carbonaceous species. Reasons for this underestimation can be sought in the source-apportionment analysis of the CARBOSOL samples (Gelencsér et al., 2006). The sampled species were specified as emitted from fossil fuel combustion and from biomass burning. Keeping in mind that biomass burning emissions are not included in our emission inventory, we have compared the modeled BC and POC with sampled BC and POC appointed to fossil fuel combustion and find a much better agreement (Table 4.2). Good agreement between modeled and sampled fossil fuel BC was found

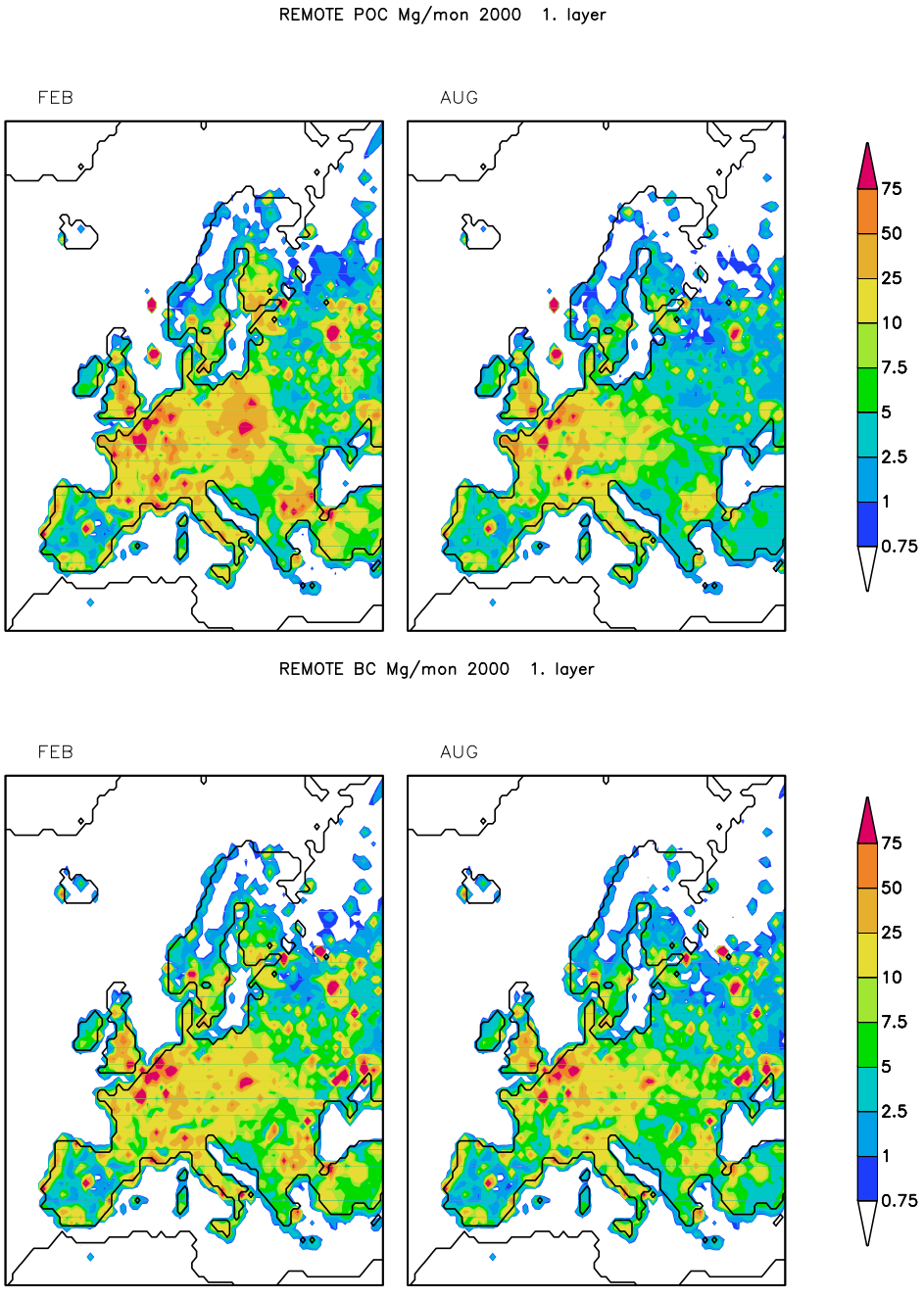

Figure 4.7: Monthly mean of POC (top) and BC (bottom) emissions into the lowest level [Mg(mon^{-1})] for February and August.

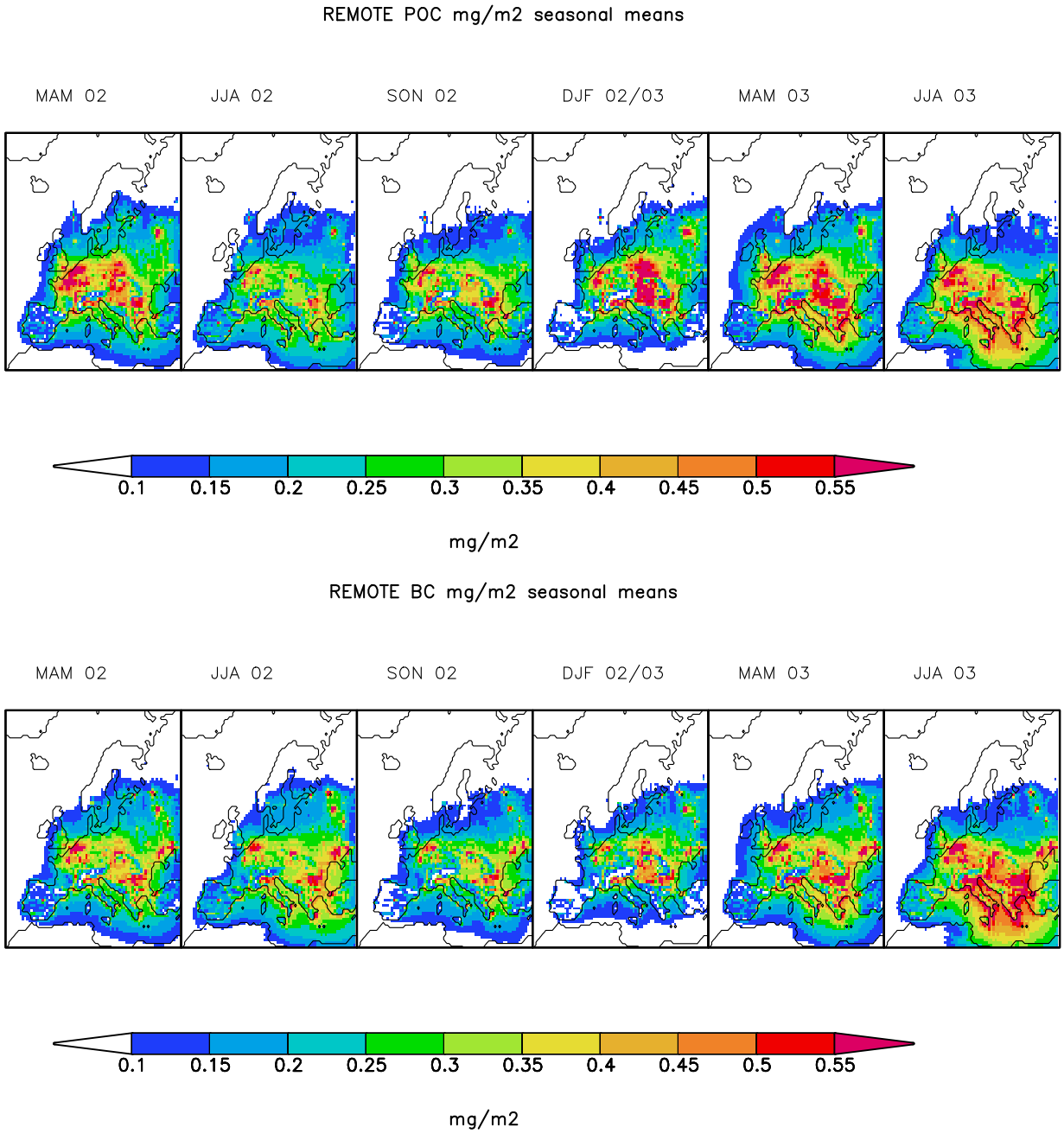

Figure 4.8: Modeled seasonal means of POC (top) and BC (bottom) column burden [mg(m^{-2})] for March-April-May (MAM), June-July-August (JJA), September-October-November (SON) and December-January-February (DJF), 2002–2003.

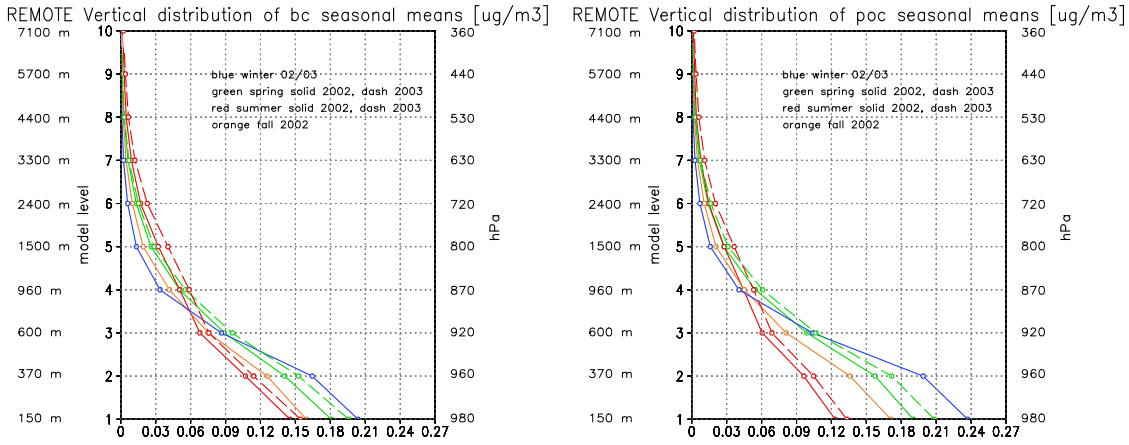

Figure 4.9: Modeled seasonal means of BC (left) and POC (right) concentration [μg(m^{-3})], vertical profiles.

CARBOSOL site	BC_{ff}[1]	BC modeled	BC_{ff}[1]	BC modeled	
	winter	winter 02/03	summer	summer 02	summer 03
Aveiro	0.674	0.249	0.478	0.232	0.235
K-Puszta	1.250	0.841	0.364	0.307	0.348
Schauinsland	0.219	0.219	0.197	0.185	0.259
Puy de Dome	0.171	0.092	0.185	0.108	0.124
Sonnblick	0.015	0.061	0.105	0.122	0.165
	POC_{ff}[1]	POC modeled	POC_{ff}[1]	POC modeled	
Aveiro	0.391	0.170	0.277	0.130	0.132
K-Puszta	0.726	0.787	0.211	0.210	0.245
Schauinsland	0.127	0.184	0.114	0.148	0.195
Puy de Dome	0.099	0.027	0.107	0.060	0.077
Sonnblick	0.009	0.019	0.061	0.036	0.062

[1] from fossil fuel combustion (Gelencsér et al., 2006)

Table 4.2: Seasonal mean BC and POC from fossil fuel combustion (Gelencsér et al., 2006) compared with modeled BC and POC at CARBOSOL sites, values given in μg(C)m^{-3}.

for Schauinsland and K-Puszta. At Sonnblick, the modeled concentration during winter is overestimated by a factor of 4, probably because of this high site's elevation. The site may represent the free troposphere during winter time inversion conditions, which could not be captured by the model. The BC concentration at Puy de Dome is underestimated by a factor of 2, and at Aveiro by a factor of 3 in winter, and a factor of 2 in summer. 61 % of measured BC in winter and 14 % in summer in Aveiro is found to originate from biomass burning; for other sites this contribution varies from 13 to 30 % (Gelencsér et al., 2006). Our not considering biomass burning emissions in the emission inventory explains the underestimation of BC by REMOTE. For OC, the analysis goes even further, trying to identify primary and secondary organic aerosols. Modeled POC concentrations agree well with the POC amounts apportioned to the fossil fuel combustion at Schauinsland and K-Puszta. At Sonnblick, the POC concentration is again overestimated by a factor of 2 in winter. At Puy de Dome, it is underestimated by a factor of 4 in winter and a

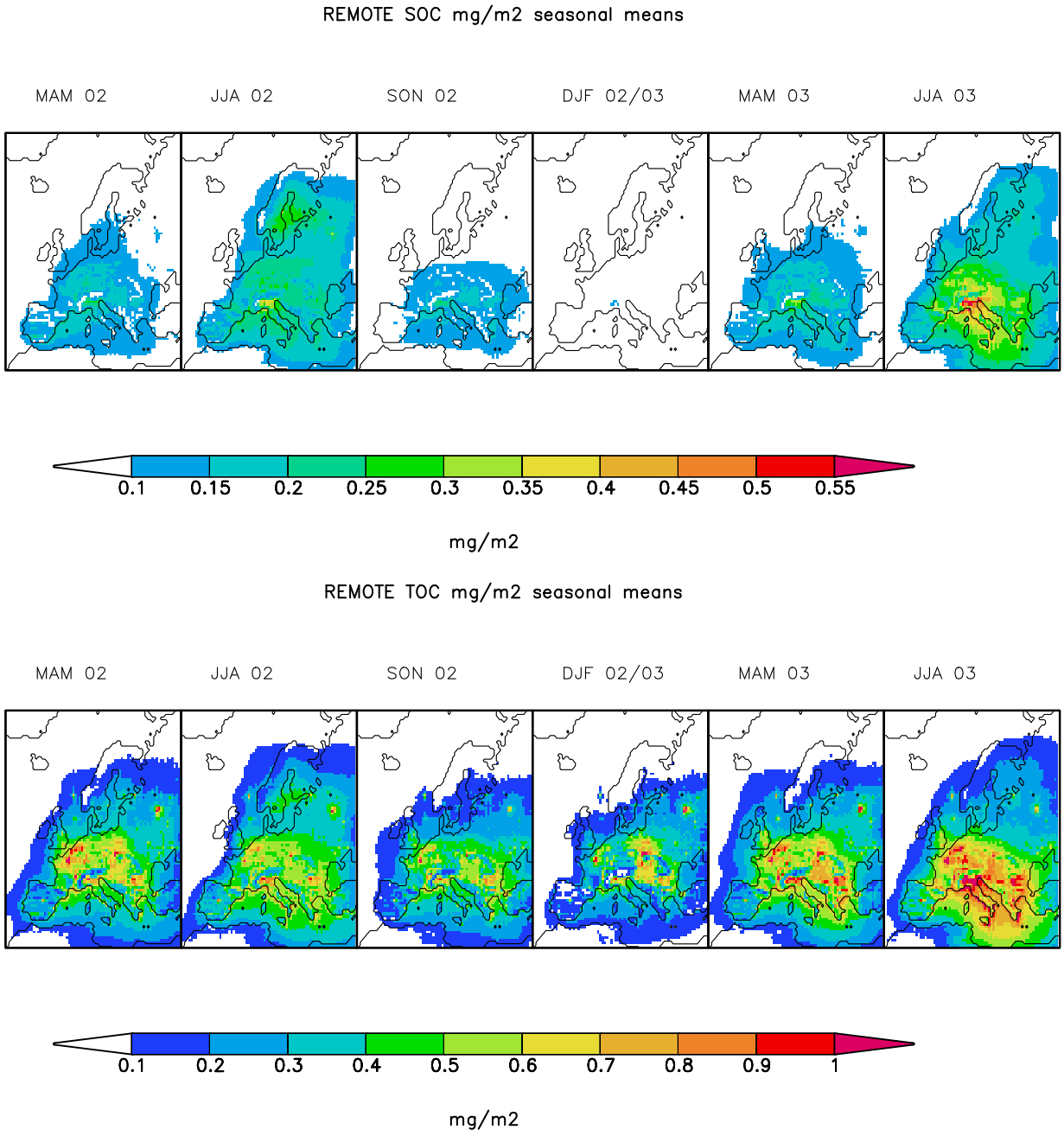

Figure 4.10: Modeled seasonal means of SOA (top) and TOC (bottom) column burden [mg(m^{-2})] for March-April-May (MAM), June-July-August (JJA), September-October-November (SON) and December-January-February (DJF), 2002–2003.

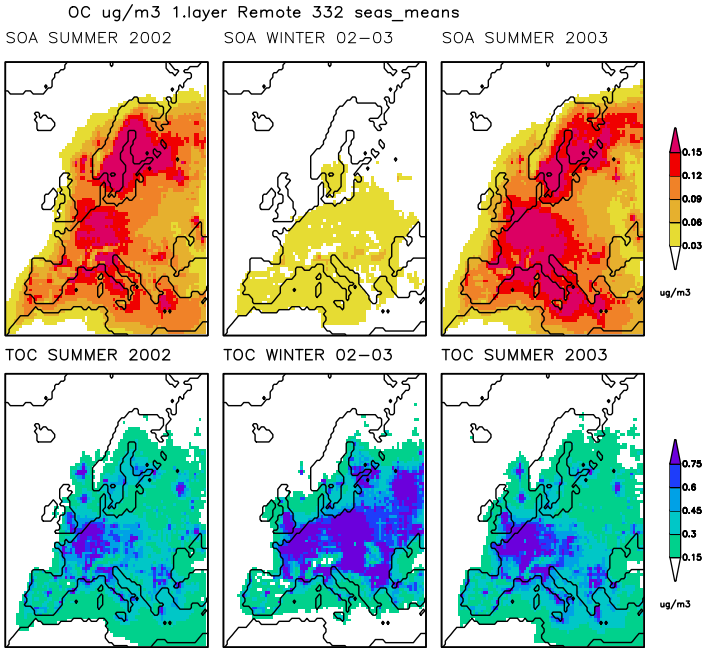

Figure 4.11: Modeled seasonal means of SOA (top) and TOC (bottom) surface concentration [μg(m^{-3})]. The scale for SOA is five times smaller than that for TOC.

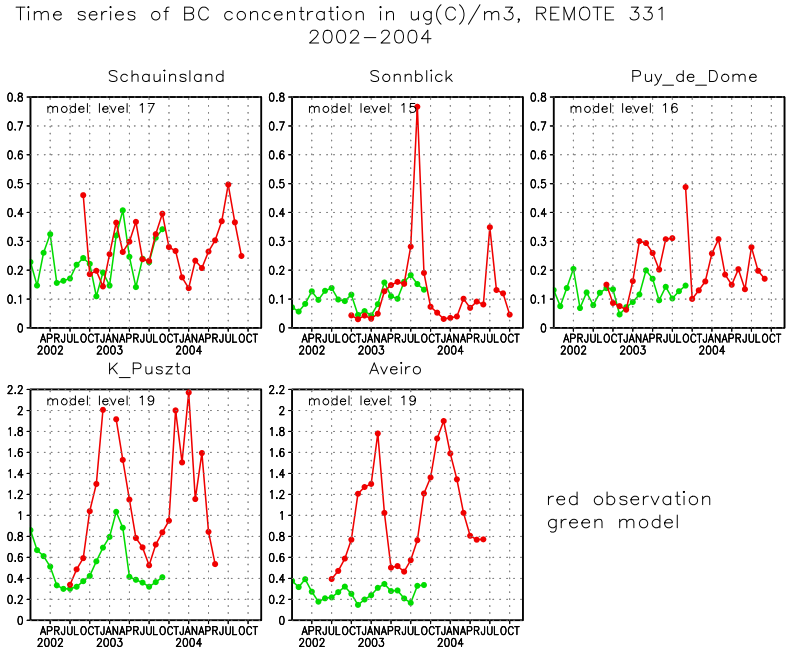

Figure 4.12: Observed (red) versus modeled (green) monthly mean time series of BC concentration [μg(S)m^{-3}] at five CARBOSOL sites: Schauinsland, Sonnblick, Puy de Dome, K-Puszta and Aveiro.

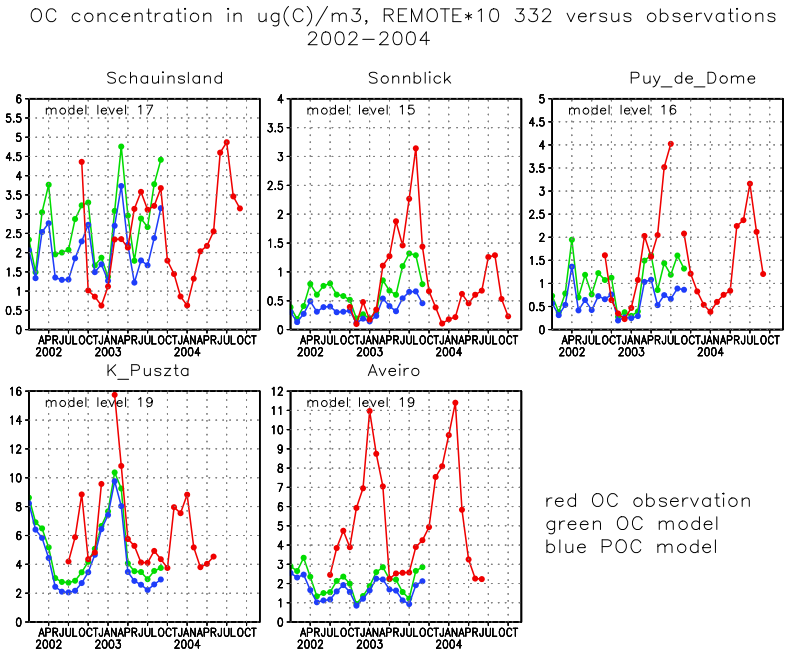

Figure 4.13: Observed monthly mean TOC concentration (red) versus modeled monthly mean TOC (green) and POC (blue) concentration multiplied by 10 [μg(S)m^{-3}] at five CARBOSOL sites: Schauinsland, Sonnblick, Puy de Dome, K-Puszta and Aveiro.

factor of 2 in summer, as well as at Aveiro by a factor of 3 in winter and almost 2 in summer. The POC from biomass burning is found to contribute over 90 % of the primary organic aerosols in Aveiro in winter, and approximately 60 % for other sites for winter and summer. Simulated SOA concentration is extremely underpredicted by one to two (at Aveiro) orders of magnitude (not shown). In summer, very high contribution of SOA from non-fossil sources was found in most CARBOSOL samples. This includes not only SOA from VOC emitted by vegetation, but also from VOC emitted by biomass burning. Thus, biomass burning emissions contribute not only to primary, but also to secondary carbonaceous aerosol concentration. It is important to mention, that the concept of SOA in (Gelencsér et al., 2006) differs from ours and includes condensation of directly emitted semi-volatile organic compounds at low ambient temperatures and also covers primary emissions from non-specific sources. That is why observed contribution of SOA remains relatively high during wintertime, and can not be directly compared with simulated SOA concentration.

Annual mean concentration of each aerosol species were also compared with mean values obtained by Putaud et al. (2004). In this work, chemical composition of aerosol samples collected from different European sites over the past decade have been analyzed. Table 4.3 shows the range of the absolute annual mean concentrations of sulfate, black and organic carbon aerosol in $PM_{2.5}$ from natural, rural and near-city sites compared to the simulated annual mean concentration.

The simulated annual mean for sulfate aerosol is within the range measured; black carbon

Author	Sulfate	BC	OC
Putaud et al. (2004) in $PM_{2.5}$	1–3	0.5–2	0–6
this study	1.42	0.18	0.23

Table 4.3: Annual mean surface concentration [$\mu g(m^{-3})$]

is underpredicted by at least a factor of 3, and organic carbon by an order of magnitude.

4.4 Direct shortwave radiative forcing

The REMOTE model results were further used in conjunction with the radiation model ORTM to calculate the direct radiative forcing due to different aerosols over Europe. The radiation flux density at the top of the atmosphere (TOA) was calculated with and without aerosols. The forcing is restricted to solar spectral range.

4.4.1 Externally mixed aerosols

Sulfate

Sulfate aerosol particles scatter shortwave radiation, so that a part of the incoming solar radiation is scattered back to space, resulting in a negative forcing at the top of the atmosphere (Haywood and Boucher, 2000). Direct radiative shortwave forcing of sulfate aerosol shows annual and inter-annual variabilities (Figure 4.14). The seasonal mean of the direct forcing of sulfate aerosol over Europe varies from –0.2 Wm^{-2} in winter to –1.5 Wm^{-2} in summer (Table 4.4). The forcing pattern is different for the same seasons of the different years: the mean values slightly vary with stronger forcing in spring and summer 2003, compared to 2002. In summer 2003, the maximum of –4.3 Wm^{-2} over the Mediterranean is significantly higher than the previous year.

Carbonaceous aerosols

The direct forcing of black and organic carbon was also determined using the ORTM model. Organic carbon scatters shortwave radiation, just like sulfate, and has a negative TOA forcing. Seasonal means for summer and winter of the direct forcing due to organic carbon are presented in Figure 4.15. The mean summer forcing of primary organic carbon is only –0.07 Wm^{-2} in 2002 and –0.08 Wm^{-2} in 2003; the mean winter forcing is –0.04 Wm^{-2} (Table 4.4). These values are negligible compared with the direct forcing of sulphate aerosols. Secondary organic carbon contributes to the OC forcing mainly in summer, with maximum contribution of up to –0.3 Wm^{-2} over Scandinavia in summer 2002 and over northern Italy in summer 2003.
Black carbon strongly absorbs shortwave radiation, thus its radiative TOA forcing is positive. Seasonal means for summer and winter of the direct forcing due to black carbon

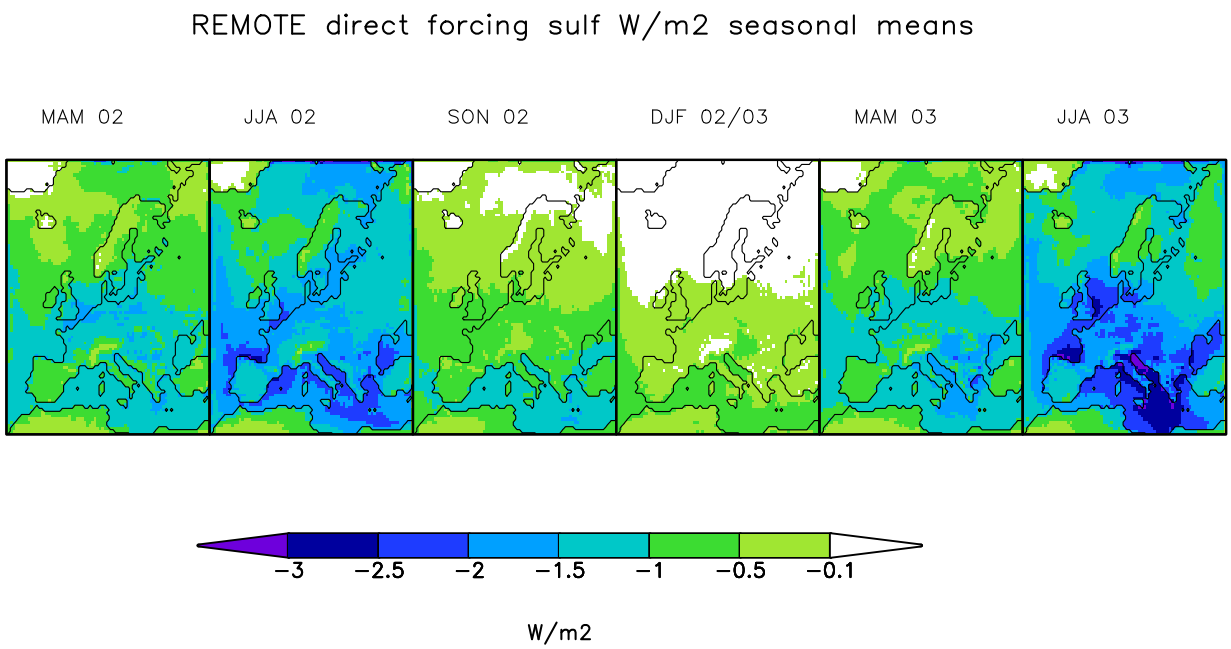

Figure 4.14: Seasonal mean direct radiative forcing of sulfate aerosol [Wm^{-2}] for March-April-May (MAM), June-July-August (JJA), September-October-November (SON) and December-January-February (DJF).

		Sulfate	BC	OC
MAM 02	mean	−0.8	+0.16	−0.12
	max	−2.4	+4.7	−1.0
JJA 02	mean	−1.4	+0.14	−0.14
	max	−3.3	+1.8	−1.0
SON 02	mean	−0.5	+0.07	−0.07
	max	−1.6	+1.0	−0.5
DJF 02/03	mean	−0.2	+0.09	−0.04
	max	−1.2	+2.2	−0.6
MAM 03	mean	−0.8	+0.18	−0.13
	max	−2.3	+3.5	−0.9
JJA 03	mean	−1.5	+0.16	−0.16
	max	−4.3	+2.1	−1.1

Table 4.4: Calculated seasonal mean and maximum values [Wm^{-2}] of the direct radiative forcing of each aerosol type for March-April-May (MAM), June-July-August (JJA), September-October-November (SON) and December-January-February (DJF).

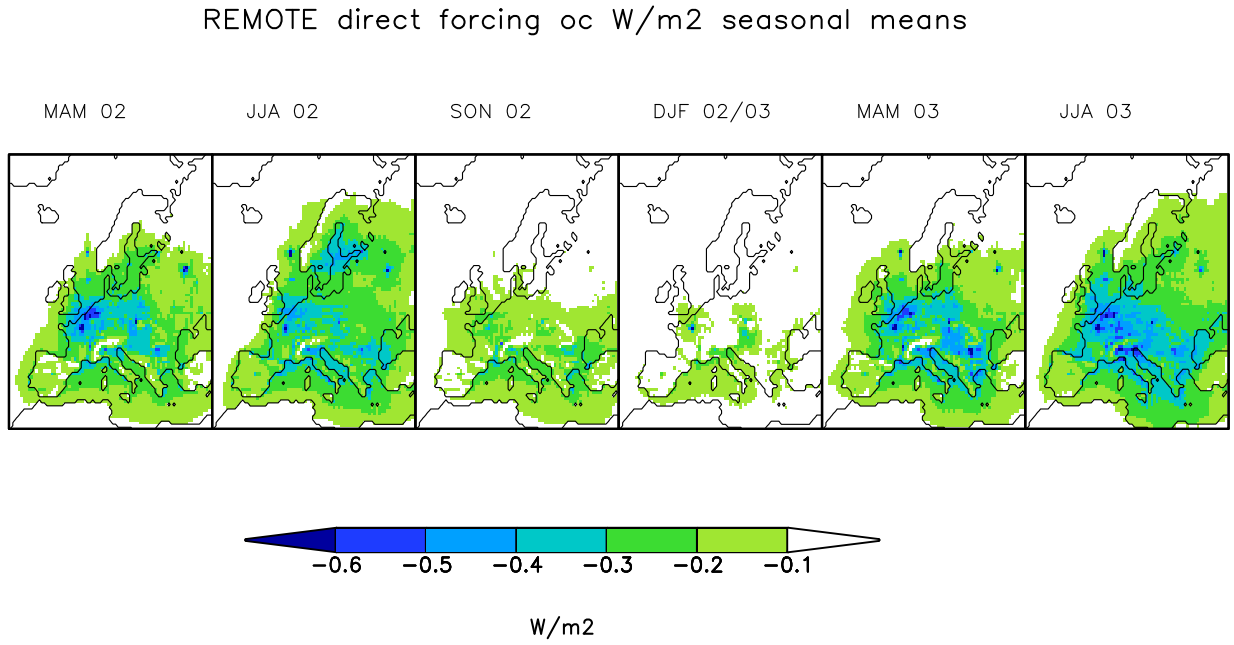

Figure 4.15: Seasonal mean direct radiative forcing of organic carbon [Wm^{-2}] for March-April-May (MAM), June-July-August (JJA), September-October-November (SON) and December-January-February (DJF), 2002-2003.

are presented in Figure 4.16. The mean forcing of BC aerosol has a maximum during spring with +0.16 Wm^{-2} in 2002 and +0.18 Wm^{-2} in 2003 (Table 4.4), with forcing maxima of +4.7 Wm^{-2} in 2002 and +3.5 Wm^{-2} in 2003 over north-western Russia. The mean forcing is weakest during fall with +0.07 Wm^{-2}. Concentration of both, black and organic carbon, is underestimated by the model, so the calculated forcing can only be regarded as a minimum estimate. In Figure 4.17 we show the total direct shortwave forcing over Europe for winter and summer, assuming externally mixed aerosols, by adding up the different aerosol forcings to obtain the total forcing. This assumption is only an approximation, since aerosols are mixed externally and internally, and the optical properties of internal mixtures are different and not necessarily additive.

The patterns of the seasonal mean forcing in summer and fall look very similar to the forcing of sulfate aerosols. Black and organic carbon nearly compensate each other, since their forcing is of the same magnitude, but opposite in sign. Only over some areas the negative forcing is slightly enhanced by organic carbon or reduced by black carbon. In winter and spring, the forcing of black carbon dominates over Eastern Europe. Here the emissions of black carbon due to domestic heating are responsible for the positive direct forcing of +0.1 to +0.5 Wm^{-2}, and up to +3 Wm^{-2} over strong emission sources.

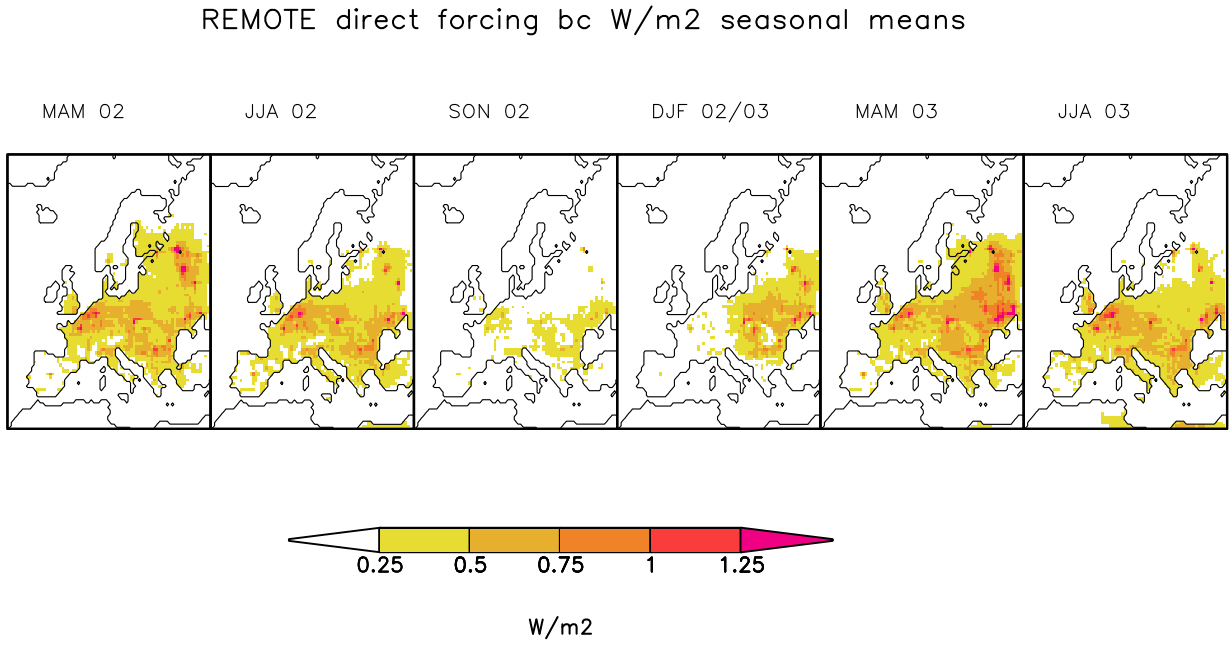

Figure 4.16: Seasonal mean direct radiative forcing of black carbon [Wm^{-2}] for March-April-May (MAM), June-July-August (JJA), September-October-November (SON) and December-January-February (DJF), 2002-2003.

4.4.2 Internally mixed aerosol particles

Estimates of the total aerosol forcing depend on the assumed mixing state of the aerosols (Lesins et al., 2002). At one extreme each aerosol component can be assumed to be physically separated form the other component creating an external mixture of chemically pure modes (Section 4.4.2). At the other extreme, the aerosols can be assumed to be internally mixed as a homogeneous material reflecting the chemical and physical average of all contributing components. The real mixed state can be expected to lie somewhere in between these two extremes. Even if the particles are individually pure when emitted, there are numerous processes in the atmosphere that can cause internal mixing: coagulation, cycling of aerosols through a cloud, aqueous reactions, gas-to-particle reaction onto existing particles (Lesins et al., 2002). Aged particles have been found to be internally mixed (e.g. Murphy and Thomson, 1997; Middlebrook et al., 1998). The optical properties of internally mixed particles depend on their chemical composition.

We have determined the total aerosol direct forcing assuming an internal mixing for all particles (Figure 4.18). Both positive and negative mean forcings exceed that of externally mixed aerosols. The negative forcing enhancement is mainly over water. The most interesting feature is the enhancement of the positive forcing in spring and winter. In spring, the forcing is positive over western Russia and the Alps, in winter over most of

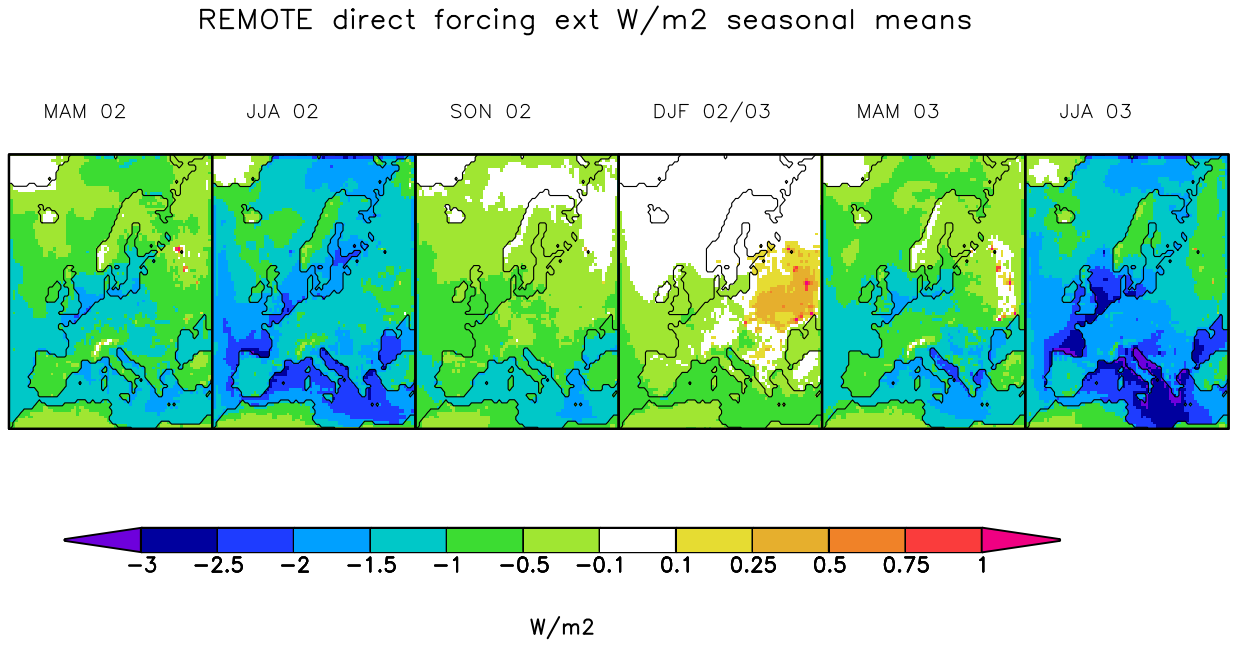

Figure 4.17: Seasonal mean direct radiative forcing of externally mixed aerosols [Wm^{-2}] for March-April-May (MAM), June-July-August (JJA), September-October-November (SON) and December-January-February (DJF), 2002-2003.

Europe.
According to our estimates, our model captures only 50 % of black and 10 % of organic carbon (Section 4.3.2). To determine a maximum estimate of the direct forcing over Europe, we have run a sensitivity experiment, whereby we have doubled the atmospheric concentration of black carbon and multiplied that of the organic carbon by a factor of 10, assuming internally mixed aerosols (Figure 4.19). Comparing the minimum estimate, where we have assumed externally mixed aerosols (Section 4.4.1), with this maximum estimate, we find the mean direct forcing doubled in spring and fall, and increased by a factor of 1.5 in summer and winter (Table 4.5). The regional seasonal maxima of both positive and negative forcing show much greater enhancement: a factor 4 for the negative forcing in spring, and a factor 11 for the positive maximum in fall.
Our forcing estimates have been compared to the results of other studies (Table 4.6). The annual mean direct forcing of externally mixed aerosols (–0.74 Wm^{-2}) compares well with the study of Koch et al. (2006) (–0.83 Wm^{-2}). A closer look reveals that this agreement is only due to averaging: Our sulfate forcing (–0.76 Wm^{-2}) is 1.4 times weaker than that of Koch et al. (2006) (–1.13 Wm^{-2}), just like the OC forcing (–0.1 Wm^{-2} vs. –0.5 Wm^{-2}), and our BC forcing is 4 times weaker (+0.11 Wm^{-2} vs. +0.45 Wm^{-2}). The opposite signs of the forcings set off the differences and the total mean forcing looks quite comparable. The same can be said about the good agreement between the mean internal direct forcing with that determined by Chung (–0.8 Wm^{-2} vs. –0.75

		Externally mixed	Internally mixed	Internally mixed, sensitiv.
MAM 02	mean	–0.8	–0.9	–1.5
	min	–2.4	–2.3	–9.7
	max	+3.6	+7.2	+12.9
JJA 02	mean	–1.4	–1.5	–2.4
	min	–3.4	–4.1	–10.4
	max	+0.1	+0.5	+0.6
SON 02	mean	–0.5	–0.6	–1.0
	min	–1.9	–2.2	–5.1
	max	+0.4	+0.8	+4.6
DJF 02/03	mean	–0.2	–0.1	–0.3
	min	–1.2	–1.2	–5.3
	max	+2.1	+4.0	+4.6
MAM 03	mean	–0.8	–0.8	–1.5
	min	–2.5	–2.7	–9.7
	max	+2.5	+4.9	+8.1
JJA 03	mean	–1.5	–1.7	–2.7
	min	–4.3	–5.5	–11.5
	max	+0.5	+0.8	+1.7

Table 4.5: Seasonal minimum, mean and maximum values [Wm^{-2}] of the direct radiative forcing of the total aerosol assuming external and internal mixing and for the sensitivity experiment for March-April-May (MAM), June-July-August (JJA), September-October-November (SON) and December-January-February (DJF), 2002-2003.

Wm^{-2}). Comparing the forcing exerted by the individual aerosol compounds reveals that BC forcing estimate of Chung (+ 1.43 Wm^{-2}) is 13 times higher than estimated in this study, being close to the forcing computed by Hohenegger and Vidale (2005) with distribution of Tanré et al. (1984) (+ 1.2 Wm^{-2}). The BC distribution in the study of Chung was calculated based on emissions of 1984, which are a factor of 2 higher than emissions applied in this study. This alone can not explain such high difference in the forcing estimates. Differences in the optical parameters, the assumptions made about the particle size and the treatment of the relative humidity for the forcing calculations might serve as additional explanations. The forcing computed by Hohenegger and Vidale (2005) applying the distribution of Tanré et al. (1984) is positive, probably due to much higher contribution of BC to the total aerosol mass. The annual mean forcing computed by Hohenegger and Vidale (2005) with the GADS-aerosol distribution is 1.4 times weaker then ours (–0.5 Wm^{-2} vs.–0.76 Wm^{-2}). The European annual mean forcing computed by Bellouin et al. (2005) (–2.92 Wm^{-2}) from satellite measurements agrees well with the result of our sensitivity experiment (–2.36 Wm^{-2}). Again, this is only true for the average estimate. The forcing given by Bellouin et al. (2005) is negative all over Europe for all seasons (not shown), while forcing resulting from our sensitivity study is positive for large

Author	Aerosol type	mixing state	clear-sky	all-sky
this study	Sulfate		–1.34	–0.76
Koch et al. (2006)	Sulfate			–1.13
Chung[1]	Inorganic[2]			–2.94
this study	BC		+0.12	+0.11
Koch et al. (2006)	BC			+0.45
Chung[1]	BC			+1.43
this study	OC		–0.17	–0.10
Koch et al. (2006)	POC			–0.15
Chung[1]	POC			–0.47
this study	Sulf., BC and OC	extern	–1.39	–0.74
Koch et al. (2006)	Sulf., BC and POC	extern		–0.83
Chung[1]	Inorg.[2], BC and OC	extern		–1.98
Hohenegger and Vidale (2005) (based on GADS (Hess et al., 1998))	Sulf., BC and OC	extern		–0.5
Hohenegger and Vidale (2005) based on Tanré et al. (1984)	Sulf., BC and OC	extern		+1.2
this study	Sulf., BC and OC	intern	–1.41	–0.80
Chung[1]	Inorg.[2], BC and OC	intern		–0.75
this study, sens. study	Sulf. BC and OC	intern	–2.36	–1.38
Bellouin et al. (2005)	total aerosol	sat. meas.	–2.92	

[1] based on Chung and Seinfeld (2002) with the inorganic aerosol system simulated on-line following methodology of Adams et al. (1999, 2001) and with updated HNO_3 field from the Havard-GISS GCM Mickley et al. (1999)

[2] including SO_4, NH_4, NO_3

Table 4.6: Annual mean direct aerosol forcing over Europe, results from this study compared with other publications

areas of Europe in spring and winter (Figure 4.19). The forcing estimates presented here show a very large scatter due to different aerosol burden, chemical composition, mixing assumptions and assumptions about aerosol size distribution and optical properties.

4.5 Spatial and temporal variations of the aerosol load and forcing

4.5.1 Impact of emissions on the variation of the aerosol load

Figure 4.20 shows monthly mean emissions and respective atmospheric loads for black and primary organic carbon. The same emission inventory was applied 2002 and 2003, with an emission maximum in February and minimum in August for both carbonaceous species. In 2002, the burden maximum of both occurred in April, the minimum in November. The

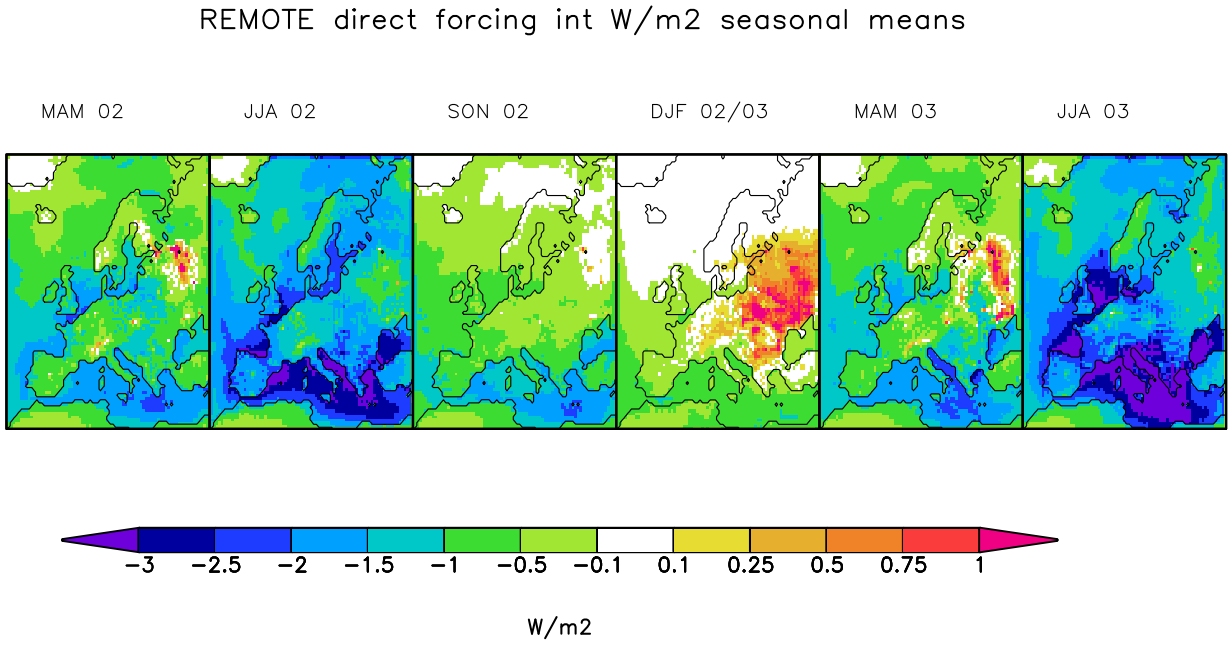

Figure 4.18: Seasonal mean direct radiative forcing of internally mixed aerosols [Wm^{-2}] for March-April-May (MAM), June-July-August (JJA), September-October-November (SON) and December-January-February (DJF), 2002-2003.

burden of BC in February (emission maximum) was much lower than in August (emissions minimum). The burden of POC for February and August were nearly the same for each year, but very different between years, despite consistently low emission levels in August. In 2003 the burden maximum for BC occurred in August, coinciding with emissions minimum; the burden maximum for POC occurred in March, with a secondary maximum in August. On the European average, the temporal variation of the atmospheric burden of primary carbonaceous aerosols show large inter-annual variability and do not primarily depend on the temporal variation of the emission sources.
Figure 4.21 shows the variability of the emissions of precursor gases SO_x and anthropogenic VOCs, and the column burden of secondary aerosols, sulfate aerosol and anthropogenic SOA. The temporal variation of sulfate shows an anti-correlation with SO_x emissions: here the emissions maxima in January coincide with burden minima, and the emissions minima in August with burden maxima for both years. The VOC emissions have a very different annual cycle compared to that of SO_x, with a maximum in March/April, a secondary maximum in October/November, a minimum in August and a secondary minimum in January. The secondary organic aerosol burden trend follows that of emissions from November to March; the trend is opposite otherwise. Despite the very different emission patterns, the annual cycle of SOA resembles that of sulfate. Both species are subjected to inter-annual variability, with higher aerosol loads in summer 2003 compared to 2002.

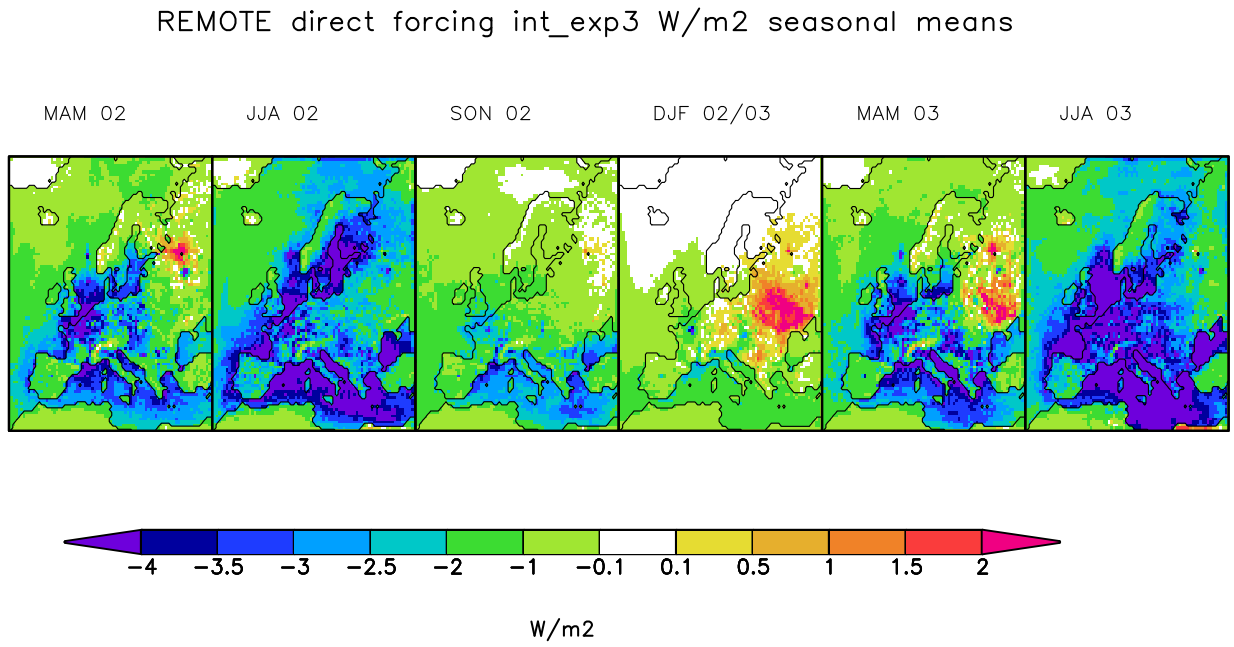

Figure 4.19: Seasonal mean direct radiative forcing of internally mixed aerosols [Wm^{-2}] in a sensitivity experiment with BC burden multiplied by 2, OC burden multiplied by 10; for March-April-May (MAM), June-July-August (JJA), September-October-November (SON) and December-January-February (DJF), 2002-2003.

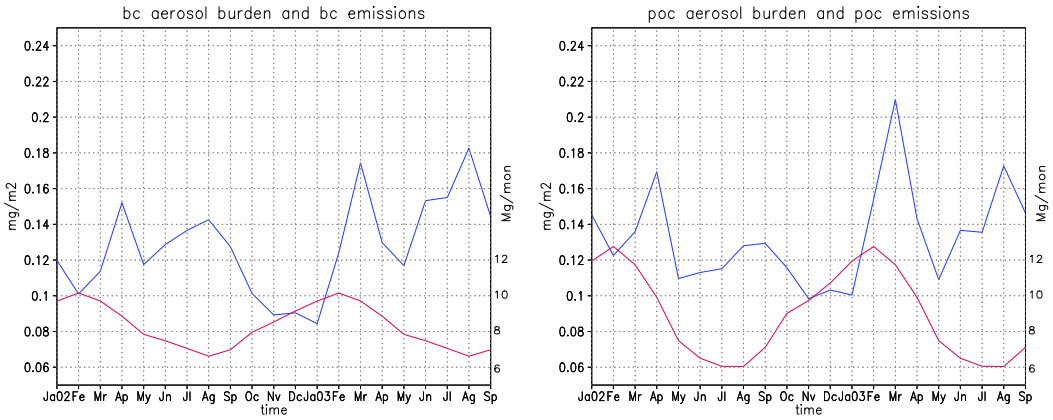

Figure 4.20: Time series of monthly mean emission fluxes [$Mg(mon^{-1})$ per grid cell], red, and primary aerosol column load [$mg(m^{-2})$], blue, both averaged over the model domain. BC (left), POC (right).

There is an enhanced aerosol burden for all species in April 2002 and in March 2003, that is not reflected in the emissions.

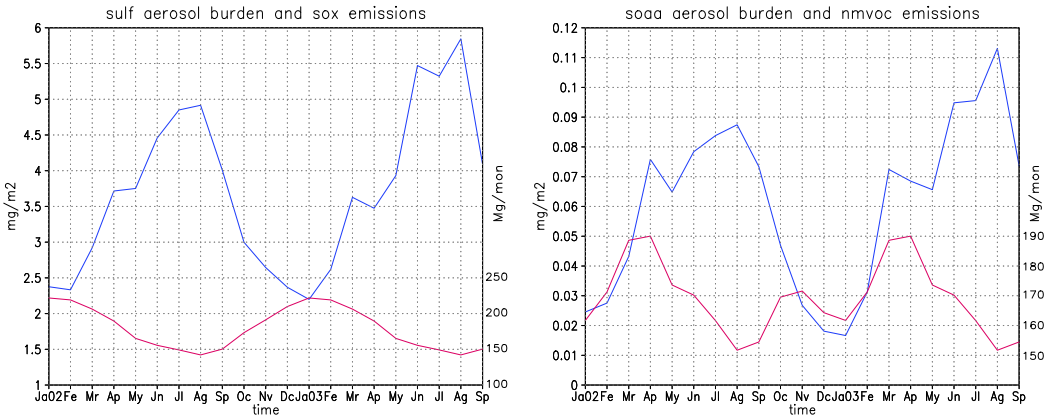

Figure 4.21: Time series of monthly mean emission fluxes of precursor gases [Mg(mon^{-1}], red, and secondary aerosol column load [mg(m^{-2})], blue, both averaged over the model domain. SO_x and sulfate (left) and VOC's and anthropogenic SOA (right).

4.5.2 Impact of meteorological conditions on variations of the aerosol load

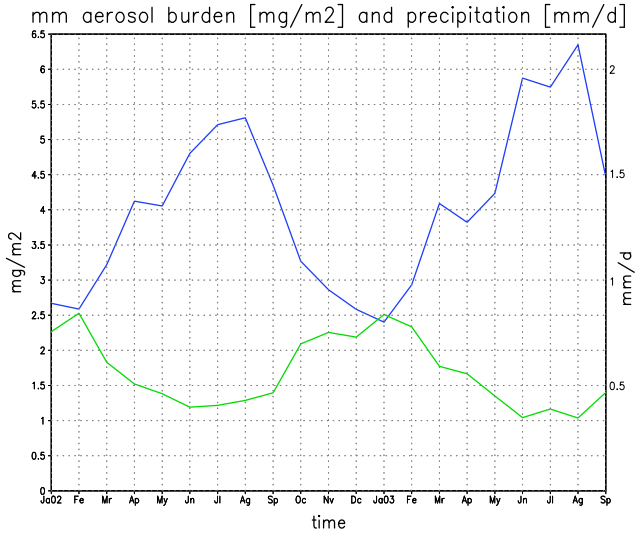

Figure 4.22: Time series of monthly mean precipitation [mm(d^{-1})], green, and total aerosol burden [mg(m^{-2})], blue, both averaged over the model domain.

The temporal and spatial variation in aerosol load is governed to great extent by meteorological conditions, which determine advection, turbulent diffusion, convective transport and dry and wet deposition. Wet deposition is the main removal process of aerosol from the atmosphere. The scavenging efficiency in the model depends on hygroscopisity of the particles and liquid water content in the atmosphere based on Kasper-Giebl et al. (2000)

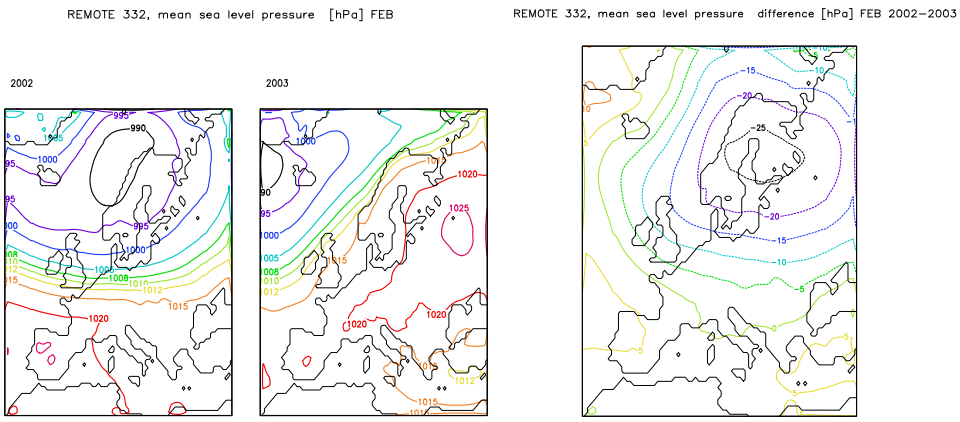

Figure 4.23: Monthly mean sea level pressure for February 2002 (left), 2003 (center), and difference 2002-2003 (right) [hPa].

and Hitzenberger et al. (2000). The scavenging efficiency for black carbon is assumed to be 3 times smaller then for hygroscopic particles (sulfate and organic carbon). Spatially averaged monthly mean aerosol load was found to strongly anti-correlate with monthly precipitation (Figure 4.22). Seasonal and inter-annual variability of the mean precipitation in Europe is directly reflected in the European mean pollution level with pollution maximum (precipitation minimum) in August 2003 and pollution minimum (precipitation maximum) in January 2003.
To illustrate the dependency of inter-annual variation of the aerosol burden on pressure, wind and regional precipitation patterns, we have analyzed February and August 2002 and 2003. These two months demonstrate high inter-annual variability in aerosol burden (Table 4.7).

Aerosol type	Feb. 02	Feb. 03	Aug. 02	Aug. 03
Sulfate	2.30	2.60	4.90	5.80
SOA	0.03	0.04	0.13	0.15
POC	0.12	0.15	0.14	0.17
BC	0.10	0.12	0.13	0.18

Table 4.7: Mean aerosol burden in February and August 2002 and 2003 [mg(m^{-2})].

February:
The general weather conditions of February 2002 were characterized by a low pressure system north of Scandinavia with steep pressure gradients over north-central Europe, transporting Northatlanic air masses with westerly winds towards the European continent (Figures 4.23 and 4.24). Strong advection occured in areas with strong emissions (Figures 4.2 and 4.7). A high pressure system with weak pressure gradients was located over southern Europe. In contrast, in February 2003, there was a blocking-high over western Russia, with calm winds, inducing very little advection. This high pressure system was

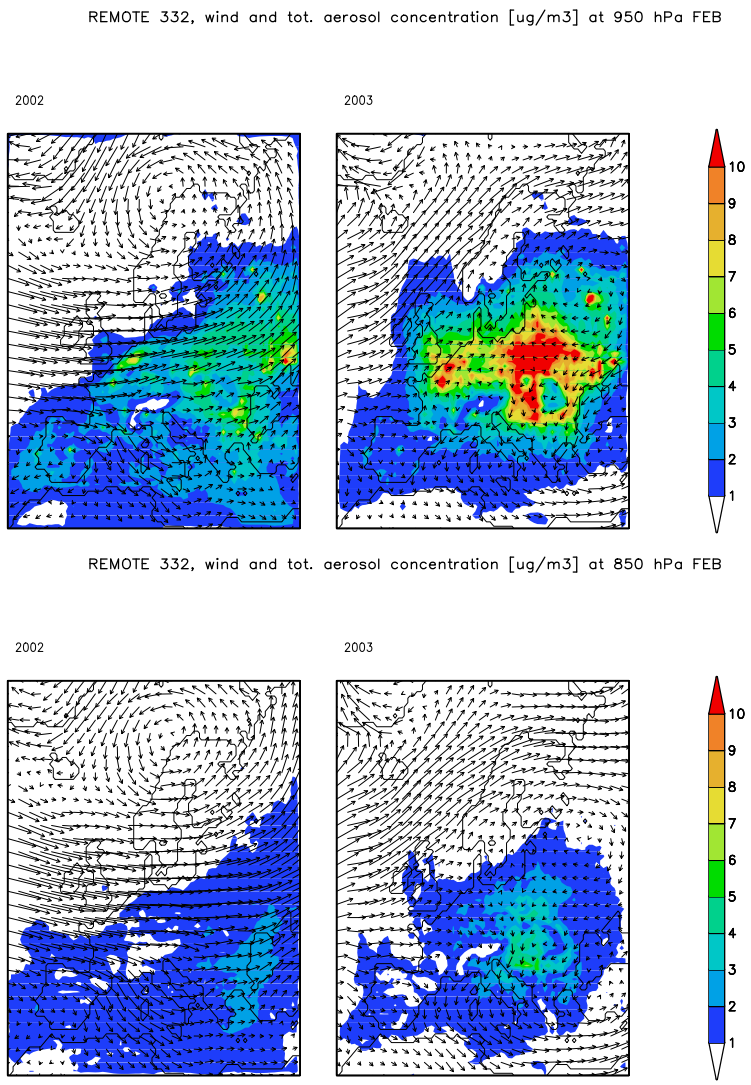

Figure 4.24: Monthly mean wind [mm(s^{-1})] at 950 hPa and surface aerosol concentration [μg(m^{-3})] (above); monthly mean wind [mm(s^{-1})] at 850 hPa and aerosol concentration at the corresponding model level [μg(m^{-3})] (bottom), in February 2002 (left), and February 2003 (right).

complemented by an Iceland low. Relatively unpolluted air from the North Atlantic could not reach the European continent, just striving the northern coasts. The main emission sources are located in the region of the blocking high. The difference plots of the sea level pressure and aerosol load between February 2002 and February 2003 reveal an anti-correlation, in areas with significant emission sources (Figures 4.23, 4.25). The regions of negative (positive) pressure differences show positive (negative) difference in aerosol load. There is also an anti-correlation between the aerosol load and precipitation differences in these two Februares(Figure 4.26). In February 2002, there was strong precipitation over northern Scandinavia, Russia, North UK and the Alpine Region (over 220 mm($month^{-1}$)),

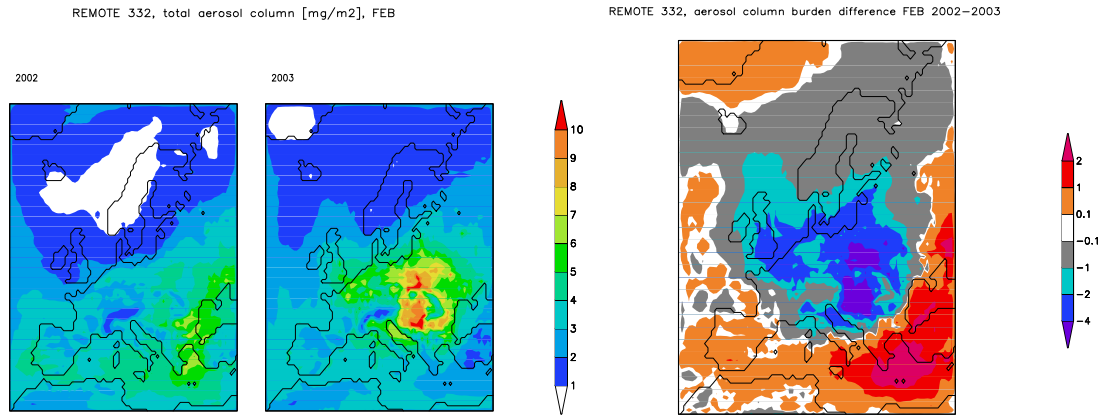

Figure 4.25: Monthly mean total aerosol column load for February 2002 (left), 2003 (center), and difference 2002-2003 (right) [mg(m^{-2})].

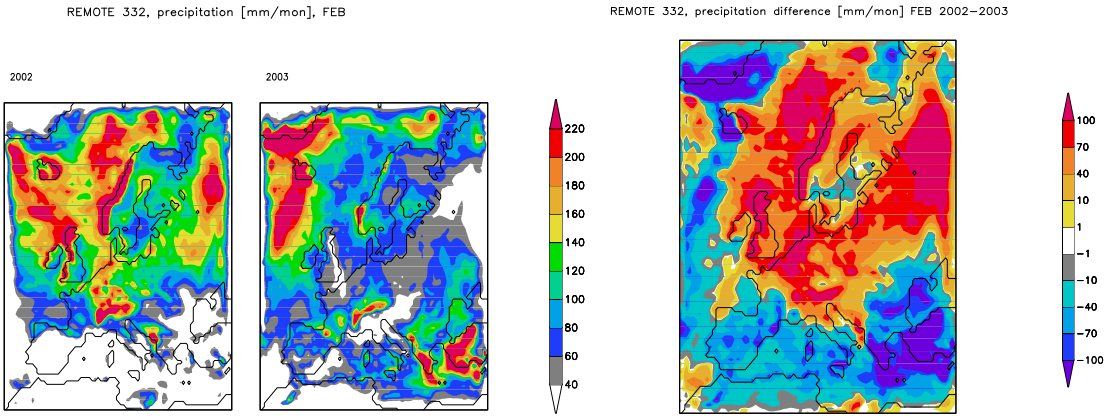

Figure 4.26: Monthly precipitation for February 2002 (left), 2003 (center), and difference 2002-2003 (right) [mm(mon^{-1})].

moderate precipitation over northern Europe, and little or no precipitation in the South. In February 2003, there was less precipitation over all of Europe, except in the South – where there was more precipitation over the Black Sea, the Balkans, Turkey and the eastern Mediterranean.

As a result of these weather conditions: strong advection, atmospheric instability and strong precipitation in February 2002 versus atmospheric stability of the blocking-high, low advection and low precipitation in February 2003, the aerosol load over central Europe, close to strongest emission sources, is 2 to 6 mg(m^{-2}) higher in February 2003 than in the previous year. Only over areas with stronger precipitation and higher sea level pressure in February 2003, as was found in the South, were the aerosol loads lower than in 2002 (1-2 mg(m^{-2}) less).

August:

The anti-correlation between the difference in sea level pressure and aerosol load observed

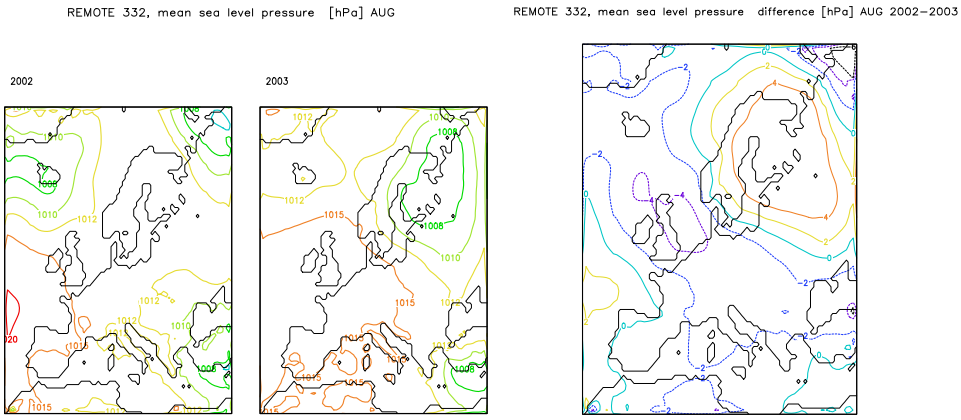

Figure 4.27: Monthly mean sea level pressure for August 2002 (left), 2003 (center), and difference 2002-2003 (right) [hPa].

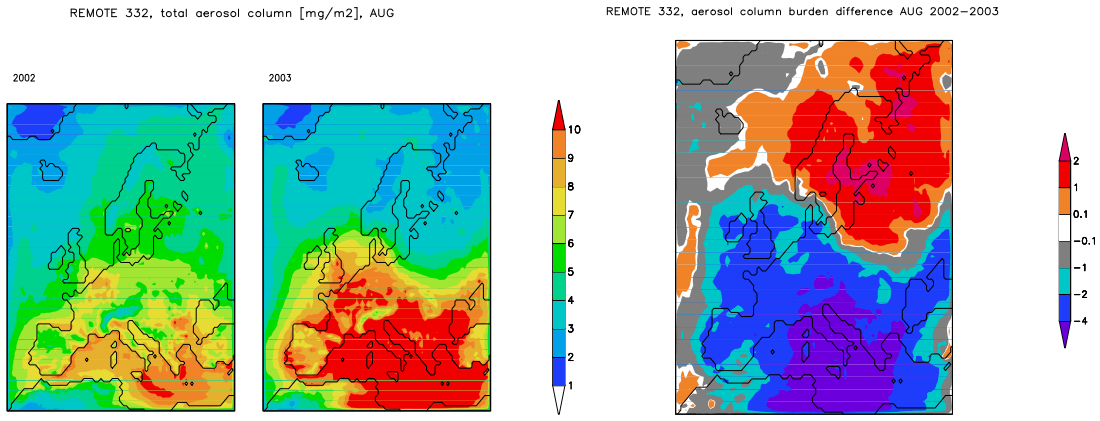

Figure 4.28: Monthly mean total aerosol column load for August 2002 (left), 2003 (center), and difference 2002-2003 (right) [mg(m^{-2})].

for the two Februares also holds true for August 2002 and 2003 (Figures 4.27 and 4.28). The magnitude of the difference in aerosol load is the same as in February, but the distribution is opposite: only Scandinavia and northern Russia were more polluted in August 2002 than in 2003. Central Europe was more polluted in August 2003, and the Mediterranean region shows 4-6 mg(m^{-2}) more aerosol burden than in the previous year. The winds were very calm for both years (Figure 4.29). The summer of 2003 was marked by semi-arid conditions almost all over Europe (Figure 4.30). August was the driest month with mean precipitation of less then 5 mm($month^{-1}$). It is important to mention that the arid conditions led to extended forest fires in Portugal, Spain and France, significantly enhancing pollution, but the biomass emissions are not included in our emission inventory. Hence, we expect the summer pollution in Southern Europe to be even higher then simulated. Only in Scandinavia, Russia and Ukraine did some precipitation fall. The precipitation pattern is almost exactly opposite to that of August 2002. The model does

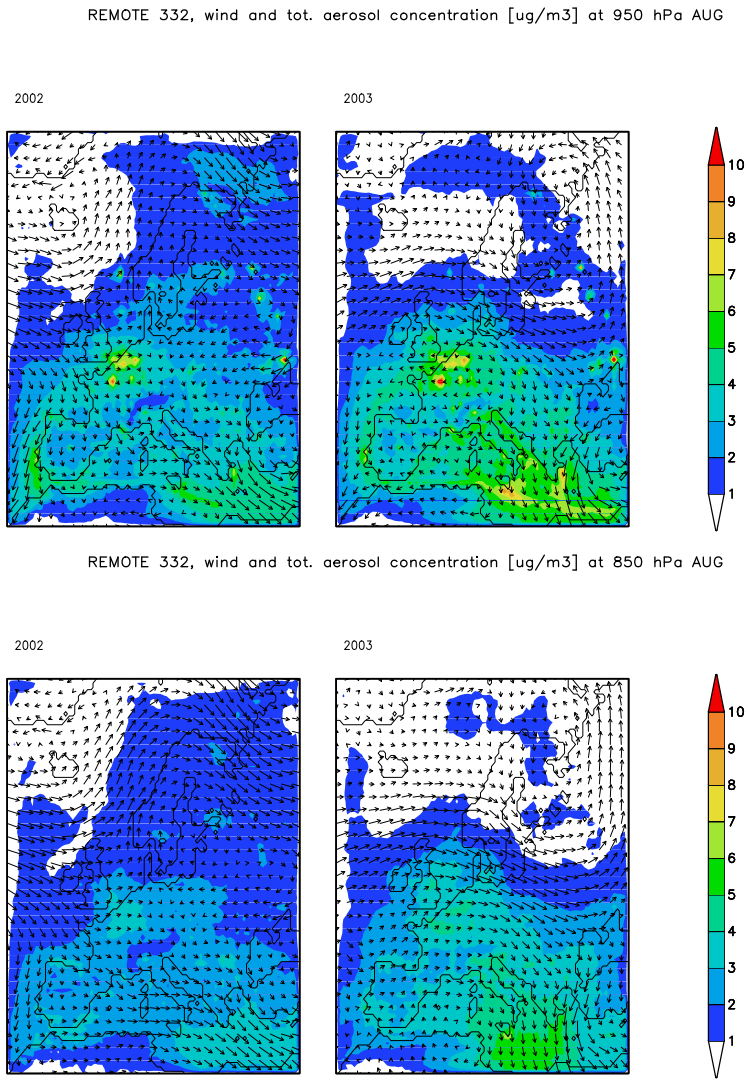

Figure 4.29: Monthly mean wind [mm(s^{-1})] at 950 hPa and surface aerosol concentration [μg(m^{-3})] (top); mothly mean wind at 805hPa and aerosol concentration [μg(m^{-3})] at the corresponding model level (bottom), in August 2002 (left), and August 2003 (right).

not capture the floods in August 2002, with the simulated precipitation amount is not unusual for this time of the year. The modeled precipitation pattern is strongly reflected in the aerosol load distribution. While the aerosol load is higher over Scandinavia and east-northern Russia in August 2002, the opposite is true for the rest of Europe in August 2003.

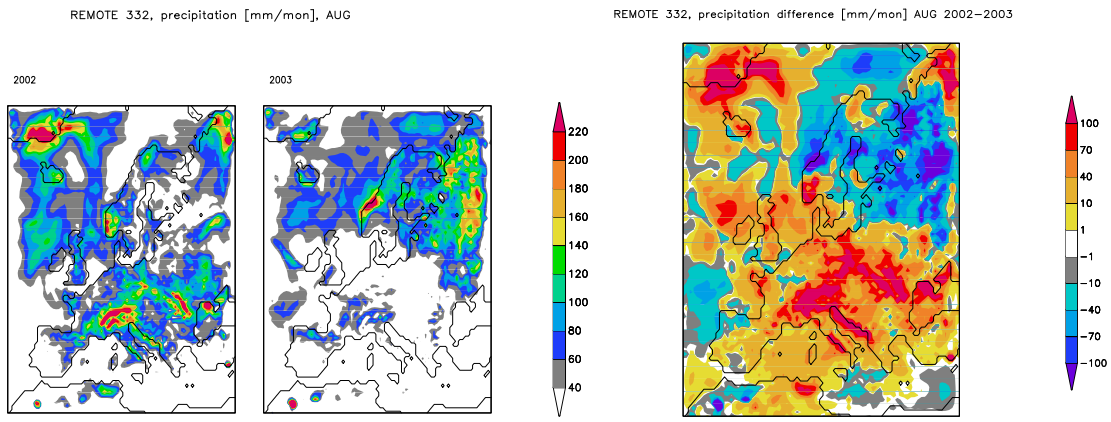

Figure 4.30: Monthly precipitation for August 2002 (left), 2003 (center), and difference 2002-2003 (right) [mm(mon^{-1})].

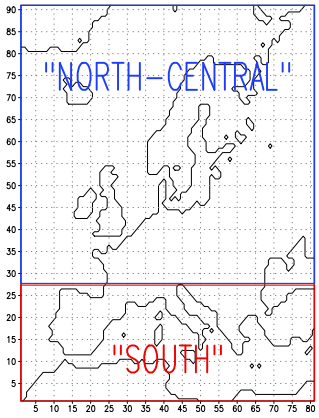

Figure 4.31: Map of the selected aereas 'North-Central' and 'South'.

4.5.3 Impact of meteorological conditions on the formation of secondary aerosols

We showed in Section 4.5.2, that atmospheric stability and precipitation play a key role for the spatial and temporal aerosol atmospheric burden variation. For secondary aerosol particles, the influence of meteorological conditions goes much further – the formation of these aerosols in the atmosphere depends on several meteorological parameters, including liquid water content, incoming solar radiation and air temperature. SO_2 is converted to sulfate via both aqueous and gaseous phase chemical reactions (Figure **??**). For conversion in cloud water, clouds and liquid water must be present. The regional patterns of total cloud cover and the vertically integrated liquid water content are very similar to that of precipitation; thus areas of aerosol formation in clouds overlap with those of aerosol removal by precipitation. To be able to distinguish the influence of each process, we have looked at different atmospheric levels. From the temporal variability of the

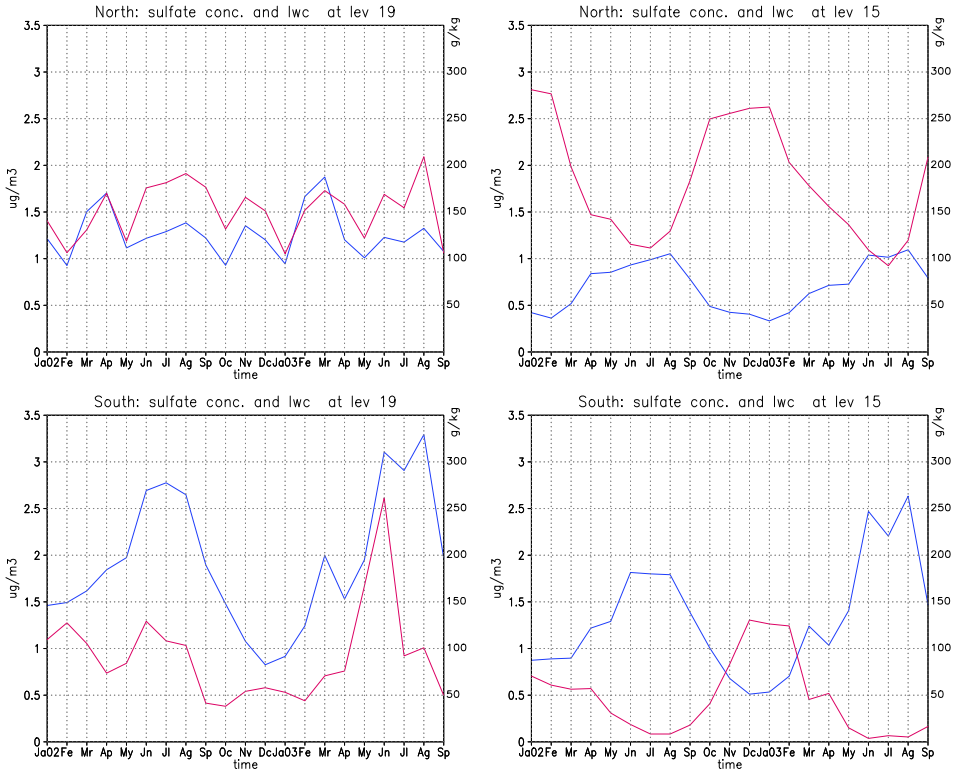

Figure 4.32: Time series of liquid water content [g(kg^{-1})], red, and sulfate aerosol concentration [μg(m^{-3})], blue, for 'North-Central' (top), and for 'South' (bottom), at the surface level (left) and at app. 800 hPa (right).

sulfate aerosol distribution, we can clearly distinguish between two regions (Figure 4.3): northern and central Europe (further called 'North-Central') and southern Europe (further called 'South') (Figure 4.31). For 'North-Central', sulfate concentration follows the trend in liquid water content in the lower atmosphere below the clouds (Figure 4.32, top left), showing the dependency of sulfate production on the availability of liquid water. At cloud level, as an example at app. 800 hPa (Figure 4.32. top right), the trend of sulfate concentration is quite opposite to that of liquid water content, indicating that removal processes dominate over production. For 'South', the opposite trend at the cloud level can also be found. The dependency of sulfate concentration on the liquid water content in the lower atmosphere however, is less significant, than in 'North-Central'. We conclude that the aqueous production of sulfate is the dominant formation mechanism in northern and central Europe in the lower atmosphere. At the cloud level, aerosol removal dominates over aerosol production. In southern Europe, aqueous production is by far less important. For sulfate and secondary aerosol production, photo-oxidation plays a major role. Availability of O_3, OH and NO_3 in the atmosphere depends on temperature and solar radiation. For 'North-Central', sulfate concentration is independent of surface solar radiation and air temperature (Figure 4.33). For 'South', the surface sulfate concentration shows significant dependency on the surface solar radiation and air temperature. We conclude that

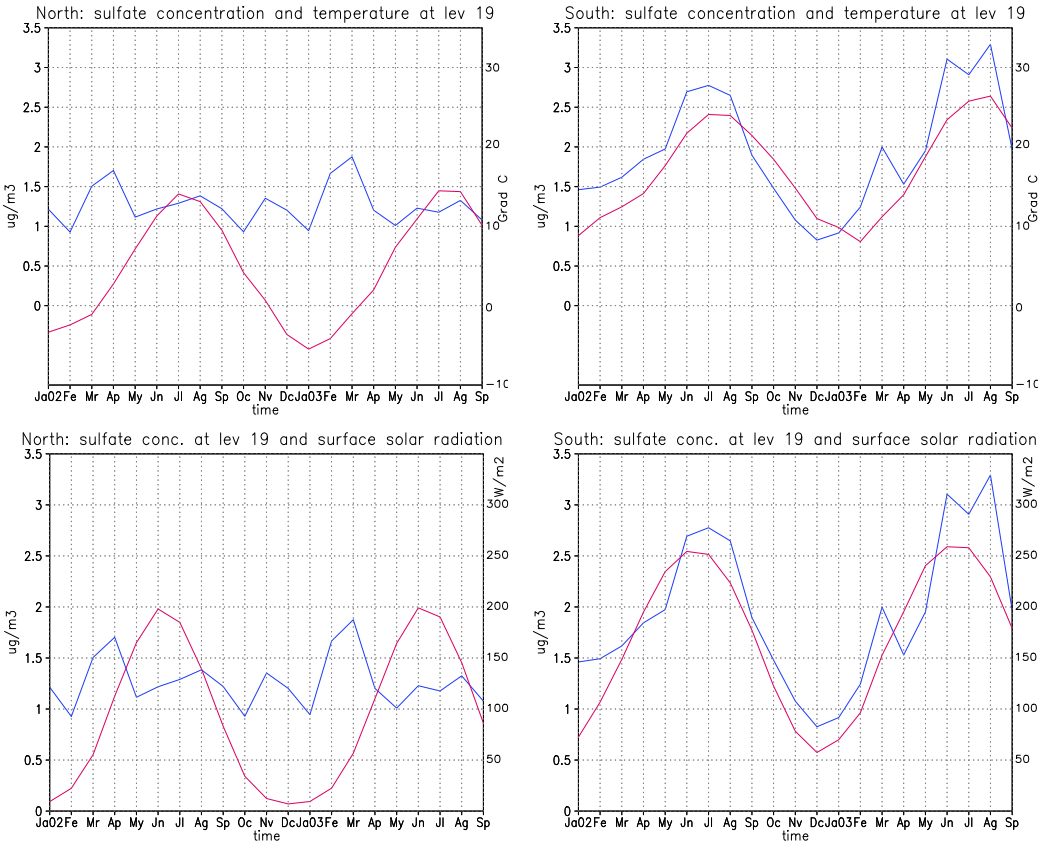

Figure 4.33: Time series of temperature [°C], red, and sulfate aerosol concentration [μg(m^{-3})], blue, for 'North-Central' (left) and 'South' (right) (top row). Timer series of surface solar radiation [Wm^{-2}], red, and sulfate aerosol concentration [μg(m^{-3})], blue, for 'North-Central' (left) and 'South' (right) (bottom row).

in southern Europe photo-oxidation is the dominant mechanism of sulfate production. Figure 4.34 shows the dependency of the surface SOA concentration on the air temperature surface solar radiation. Generally, enhanced temperatures lead to enhance SOA concentrations. (except in April 2002 and March 2003).

4.5.4 Variations in aerosol radiative forcing

In this section we analyze the spatial and temporal variation of the direct radiative forcing of internally mixed aerosol. Forcing efficiency (FE), defined as the ratio of the radiative forcing to the aerosol burden, is used a measure of the variation in aerosol forcing independent of the aerosol pollution levels Boucher and Theodore (1995). The forcing efficiency has a pronounced seasonal cycle with lowest values in November and December due to reduced incoming solar radiation (from –50 W(g aerosol)$^{-1}$ to +50 W(g aerosol)$^{-1}$ over most of Europe). In January to March, the positive FE over eastern Europe is strongest and reaches over +200 W(g aerosol)$^{-1}$. From May to August, the negative FE is much

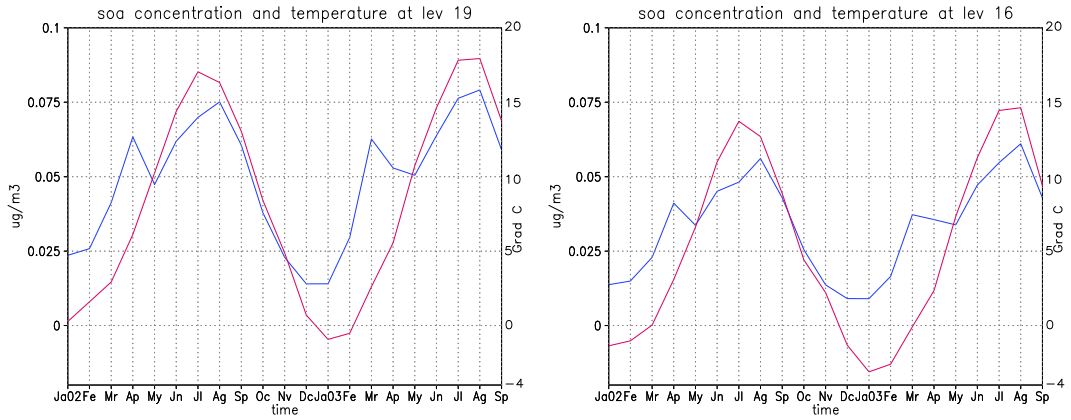

Figure 4.34: Time series of temperature [Grad C], red, and SOA concentration [μg(m^{-3})], blue, at the lowest (left) at app. 870 hPa.

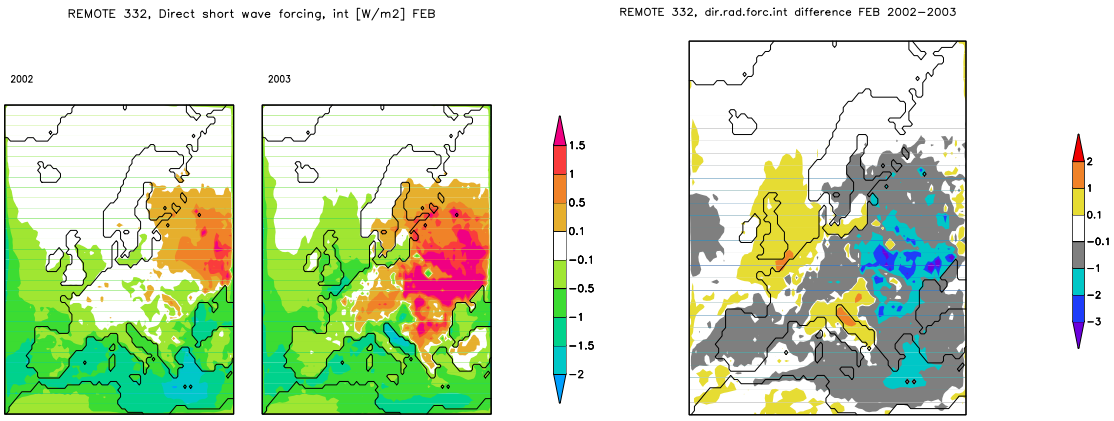

Figure 4.35: Monthly mean direct radiative forcing of internally mixed aerosol in February 2002 (left), and February 2003 (center) and the difference plot 2002-2003 (right) [Wm^{-2}].

stronger (below –350 W(g aerosol)$^{-1}$) over higher latitudes because of longer hours of daily solar radiation. The negative FE is higher over water than over land, and positive FE is stronger over ice and snow. We want to discuss the inter-annual variation of the radiative forcing and the forcing efficiency exemplarily for the months February and August 2002 and 2003.

February:

The aerosol forcing depends on the aerosol load. The direct radiative forcing of internally mixed aerosol is enhanced over central Europe in February 2003, because of the higher aerosol load compared to February 2002 (Figure 4.35). The difference plot of aerosol forcing is initially difficult to interprate, because the sign of the forcing varies. That is why comparison of different forcing distributions should be regarded carefully. The forcing changed signs from negative to positive over Greece and eastern Turkey between February 2002 and 2003, the areas with less aerosol burden in February 2003 than February

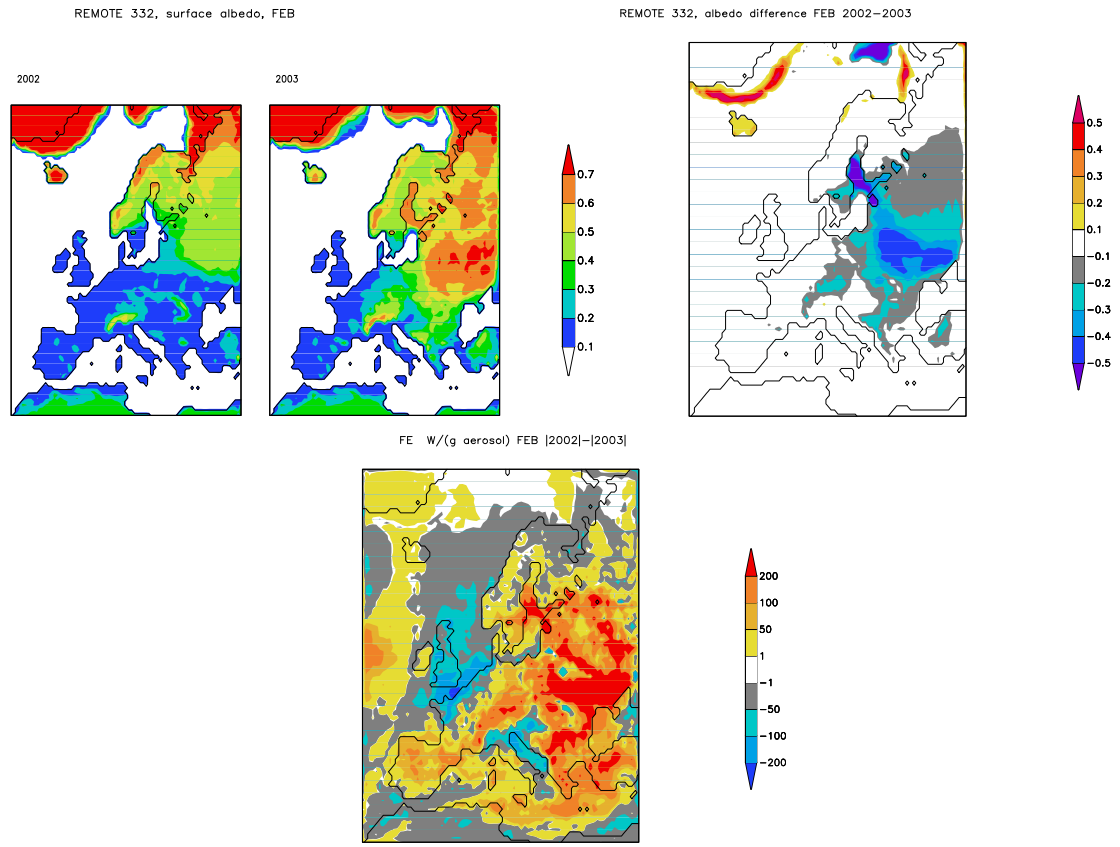

Figure 4.36: Monthly mean surface albedo, February 2002 and 2003 (left), surface albedo difference plot 2002-2003 (center), FE difference plot 2002-2003 [W(g aerosol)$^{-1}$] (right).

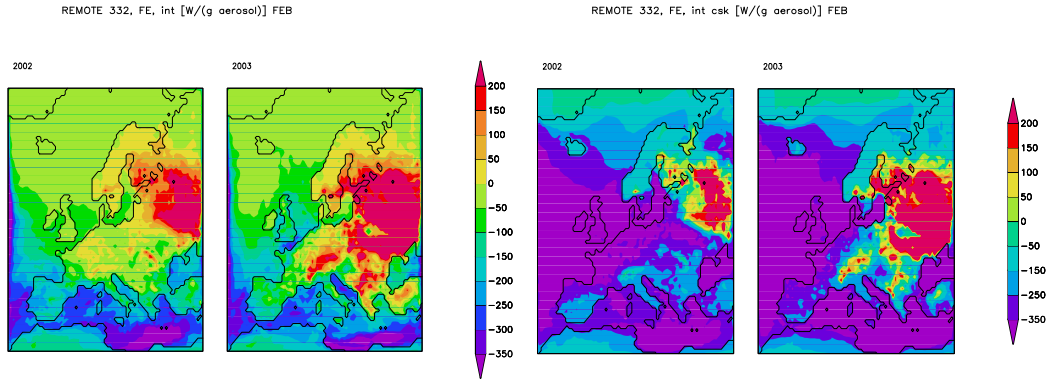

Figure 4.37: FE with clouds (left) and clear-sky (right) for February 2002 and 2003 [W(g aerosol)$^{-1}$].

2002. The reason for this is that the surface albedo in February 2003 is much higher over northern, eastern and south eastern Europe and over the Alps due to snow, and in northern Baltic Sea due to the sea-ice (Figure 4.36). The areas with enhanced surface

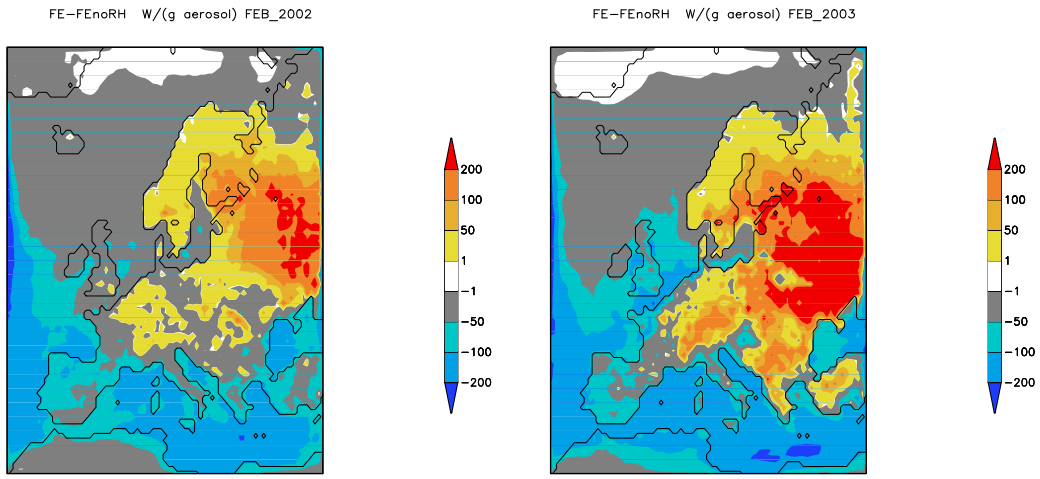

Figure 4.38: Difference of forcing efficiency with and without regarding relative humidity [W(g aerosol)$^{-1}$], February 2002 (left) and 2003 (right).

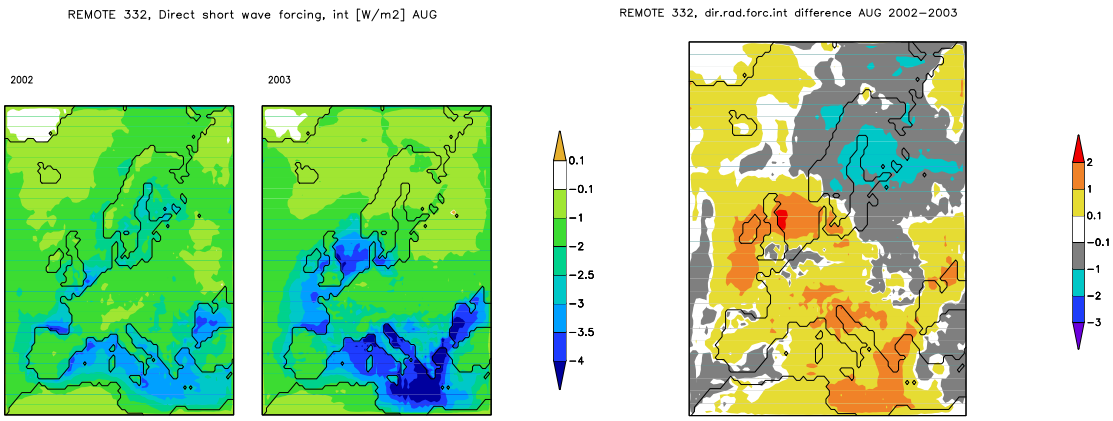

Figure 4.39: Monthly mean direct radiative forcing of internally mixed aerosol in August 2002 (left), and August 2003 (right) and the difference plot 2002-2003 [Wm^{-2}].

albedo correspond with the areas of increased positive forcing. This increase is larger for areas with higher aerosol burden.
Forcing efficiency is highly variable reaching from over +200 to below –350 W(g aerosol)$^{-1}$. Changes in surface albedo of 0.5 can cause an increase in positive FE of up to +200 W(g aerosol)$^{-1}$ over Eastern Europe and the Baltic Sea, and even change its sign from –100 to +100 W(g aerosol)$^{-1}$(Figure 4.36). This behavior is typical for partially absorbing aerosols (Haywood and Shine, 1995). The cloud albedo has similar effect on the FE (Figure 4.37). The presence of clouds reduces the negative and enhances the positive FE: over water, strong negative forcing of up to –350 W(g aerosol)$^{-1}$is reduced to –50 W(g aerosol)$^{-1}$, over western Europe and Scandinavia it changes sign from negative to positive, and over eastern Europe the positive forcing over is enhanced. Enhanced relative

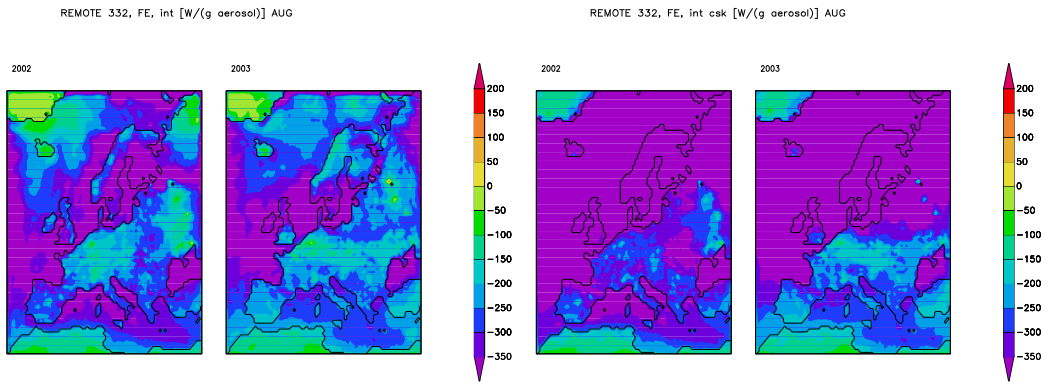

Figure 4.40: FE with clouds (left) and clear-sky (right) for August 2002 and 2003 [W(g aerosol)$^{-1}$].

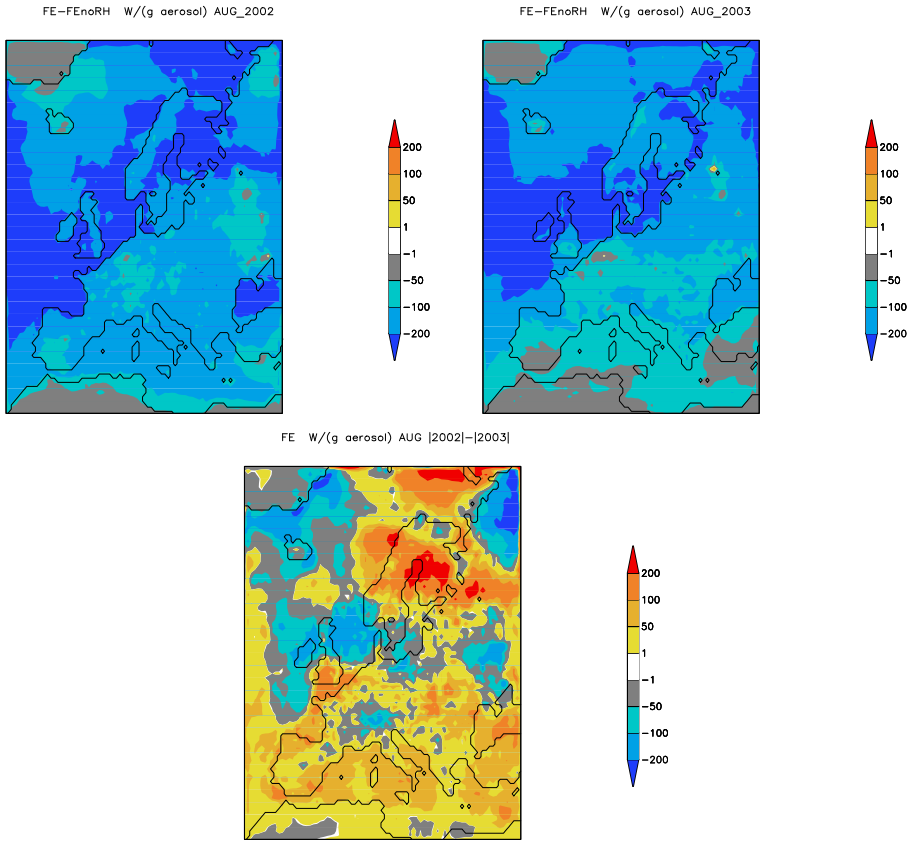

Figure 4.41: Difference of forcing efficiency with and without regarding relative humidity [W(g aerosol)$^{-1}$], August 2002 (top left) and 2003 (top right). Difference in all-sky forcing efficiency for August, 2002–2003 [W(g aerosol)$^{-1}$] (bottom).

humidity causes water uptake of aerosol particles, increasing their specific extinction. We have run a sensitivity test where the influence of the relative humidity on specific extinc-

tion was turned off and have calculated the FE for this simulation (Figure 4.38). Both positive and negative forcing efficiencies are affected - the forcing efficiency due to the relative humidity accounts for up to –200 W(g aerosol)$^{-1}$ over the Mediterranean Sea and up to +300 W(g aerosol)$^{-1}$ over eastern Europe. The effect is larger in February 2003 due to higher RH values.

August:

The direct radiative forcing is negative in August, except for a very small positive forcing in August 2003 over Cherepovec in Russia, one of the strongest emission sources of BC (Figure 4.39). The variation in forcing follows the trend of the aerosol burden. In August 2002, forcing is stronger over Scandinavia and north-western Russia; in 2003, over the rest of Europe. The forcing efficiency regionally varies between 0 and below –350 W(g aerosol)$^{-1}$. While clouds reduce the negative FE all over Europe in August 2002, in 2003 only northern Europe is affected (Figure 4.40). The reduction is most significant in August 2002 over the North Atlantic and northern Russia, from below –350 W(g aerosol)$^{-1}$ to –100 W(g aerosol)$^{-1}$. Over central Europe, all-sky FE is 50 to 100 W(g aerosol)$^{-1}$ weaker than the clear-sky FE. In August 2003, clouds change the sign of the forcing from negative to positive over Cherepovec in Russia. The effect of relative humidity over the North Atlantic and over higher latitudes is stronger in August than in February: in August, the relative humidity causes here an increase of FE of up to –300 W(g aerosol)$^{-1}$ (Figure 4.41). Similar to cloud cover, the relative humidity is lower over central and southern Europe in August 2003 compared to 2002, but the effect is opposite: clouds reduce the negative FE, relative humidity enhances both, negative and positive FE. Due to RH and clear-sky conditions, the FE in August 2002 is 100 to 150 W(g aerosol)$^{-1}$ stronger over Scandinavia compared to 2003 (Figure 4.41, bottom); the aerosol burden is also slightly higher (Figure 4.28). Together with stronger FE, this results in up to 2 Wm^{-2} stronger forcing over Scandinavia in August 2002 (Figure 4.39). Over the Mediterranean Sea, the FE in August 2002 is also stronger than in 2003 (50 to 100 W(g aerosol)$^{-1}$), mainly due to relative humidity. But the aerosol burden over the Mediterranean Sea in August 2002 is 4 mg(m^{-2}) lower than in 2003, thus the forcing is 1 to 2 Wm^{-2} weaker, despite the stronger FE.

4.6 Conclusions

The regional atmosphere-chemistry model REMOTE (Langmann, 2000) has been applied for two very different meteorological years to determine spatial and temporal variability of the aerosol column load and the aerosol direct forcing. Model results compared with measurements showed that sulfate aerosol concentrations and variability could be successfully simulated, but the simulation of the carbonaceous species remains a challenge. Carbonaceous compounds from fossil fuel are well predicted for some sites, while underpredicted by a factor of 2 to 3 for others. Carbonaceous emissions from biomass burning must be included in the model: their exclusion from our emissions partially explains the tremendous underprediction of total black and organic carbon concentrations. Gas-particle partitioning of oxidized semi-volatile organic compounds alone cannot explain the dominant contribution of SOA to total organic mass. Surprisingly high contribution

of SOA in winter observed in samples was not at all captured by the model. Secondary organic carbon is further underpredicted by the model due to missing formation processes that are yet not fully understood. Generally, we estimate the underprediction factor of total black carbon ranging from 2 to 5, and the underprediction factor of the organic matter to be an order of magnitude. The underprediction of black carbon also agrees with the study of Schaap et al. (2004), suggesting that BC emissions for Europe are underestimated by a factor of 2.

The temporal variability of emission sources of sulfate and primary carbonaceous aerosols are not directly reflected in the variability of the aerosol burden. Meteorological conditions play a major role in the spatial and temporal variations of the aerosol burden distribution. The main removal process of aerosol from the European atmosphere is wet deposition, thus the aerosol burden is very sensitive to precipitation. In general, pressure systems and corresponding winds control the advection and vertical diffusion and/or accumulation of aerosols. Blocking highs over areas of strong emissions enhance pollution levels substantially. Westerly winds from the North Atlantic, associated with strong pressure gradients, reduce pollution despite strong emissions. A combination of both removal by precipitation and enhanced advection can reduce the monthly mean burden by a factor of two, as was demonstrated for the month of February 2002 versus 2003. Semi-arid conditions in the summer of 2003 strongly affected the pollution levels, especially in lower latitudes. Despite the fact that extreme precipitation events in August 2002 could not be captured well by the model, and that the pollution from extended forest fires in August 2003 was not a part of the emission inventory, we found monthly mean pollution enhancement by a factor of 1.5. On a daily basis, the variation in pollution levels due to meteorological conditions is expected to be even more significant.

Meteorological conditions also substantially influence the formation of secondary aerosol particles. Availability of clouds and liquid water are found to govern sulfate production over northern and central Europe, while temperature and solar radiation to be the main contributors in southern Europe via photo-oxidation processes. The production of secondary organic aerosol in our model is mainly governed by the efficiency of photo-oxidation. To be able to predict pollution levels by modeling aerosol distribution, accuracy in emission sources, formation processes and simulated meteorological conditions are equally important.

The variability of aerosol radiative forcing depends directly on the aerosol distribution. The mixing state of the aerosol influences strength, regional distribution and the sign of the forcing, thereby regulating the forcing efficiency. The assumption of internally mixed aerosol particles leads to an enhancement of both negative and positive forcing efficiency, compared to the external mixture. Under an assumption of externally mixed aerosols the forcing is almost everywhere negative, with the absorbing black carbon overpowered by the scattering sulfate aerosol. When mixed internally, absorption of the aerosol is enhanced, resulting in positive aerosol forcing in spring and winter over eastern and south-eastern Europe.

The forcing efficiency also depends on meteorological parameters: the incoming solar radiation strength and daily duration determine the regional seasonality of the forcing efficiency. Over high latitudes, FE is almost negligible during winter and much stronger

during summer. During the cold season, direct forcing is also very sensitive to the surface albedo. Enhanced surface albedo due to snow cover and sea ice can turn the sign of the forcing from negative to positive and enhance the positive forcing. This was demonstrated exemplarily for February 2002 versus 2003: increased aerosol load in 2003 resulted in enhanced positive radiative forcing, because large parts of the continent were covered by snow in contrast to the warmer winter 2002. The effect reached very high latitudes despite the limited hours of solar radiation. In March, the aerosol burden in 2003 was even higher than in February, but this had very little effect on the forcing, because most parts of central Europe were snow free. For all seasons, relative humidity and cloud cover influenced the forcing efficiency. Clouds reduce the negative forcing efficiency by a factor of 1.5 to 2 and change the sign of the positive forcing efficiency from negative to positive. Relative humidity can cause an increase of forcing efficiency of up to +200 W(g aerosol)$^{-1}$ and over –200 W(g aerosol)$^{-1}$.
In a sensitivity study we derived the direct forcing of a 'realistic' aerosol burden, where we have adapted the underestimation factors from observations, 2 for black and 10 for organic carbon. The radiative forcing shows very high values for summer with –2.5 to –3 Wm^{-2} over most parts of Europe, –3.5 Wm^{-2} to –4 Wm^{-2} over the Mediterranean and the North Sea, and a high range for winter from –2 Wm^{-2} over the Mediterranean to +2 Wm^{-2} over the eastern Europe.

Acknowledgements
We thank Benedickt Schell for providing the SORGAM model, Martin Schultz and Ulrike Niemeier for providing the MOZART data, CARBOSOL team and Anne-G. Hjellbrekke for providing observation data, Nicolas Bellouin, Dorothy Koch, Cathy Hohenegger and Serena Chung for their forcing estimates, Melissa Pfeffer for reviewing the manuscript internally. This research was financially supported by EU project CARBOSOL.

Chapter 5

Conclusions and Outlook

The subject of this thesis is the past and present European atmospheric aerosol distribution and its direct radiative forcing, investigated by modeling. The regional atmosphere chemistry and aerosol model REMOTE was utilized for the present day aerosol distribution studies. Previously, REMOTE has been successfully applied to simulate short-time (days or months) pollution episodes to investigate the relative contribution of individual processes such as chemical transformations, transport and deposition to total atmospheric concentration changes (e.g. Langmann, 2000; Langmann and Bauer, 2002). The current study presents the first application of the model covering a long term period of nearly two years allowing to investigate seasonal and inter-annual variations of photo-chemistry and the aerosol distribution over Europe. REMOTE has been gradually modified to include primary and secondary carbonaceous aerosol species. The SORGAM model (Schell, 2000) was implemented into REMOTE for the treatment of the secondary organic aerosol formation. Emissions partitioning technique has been introduced in REMOTE for SO_x emissions, in order to trace back the origin of sulfate aerosols.
The evaluation of the model results against measurements showed a good agreement for the surface ozone, which plays an important role in the formation of the secondary aerosol species, and for the sulfate aerosol. Sulfate aerosol was underestimated for sites with strong contribution from ship emissions, possibly indicating an underestimation of the applied ship emission inventory dating back to 1990 for the year 2002. Black and organic carbon were strongly underestimated by REMOTE. The comparison with the source-apportionment analysis based on measurements revealed the importance of biomass burning emissions, which are neglected in the applied emission inventory. This can partly explain the underestimation of the carbonaceous species by the model. The understimation of SOA, especially in winter, indicates that beside the gas-particle partitioning of oxidized volatile organic carbons, other SOA formation processes may exist. Uncertainties associated with the VOC emissions could be additionally responsible for the underprediction of SOA. The aerosol yields applied in the model have been derived from chamber experiments and present an additional uncertainty. Updating the ship emission inventory and including biomass burning emissions in future simulations might largely improve the model performance for sulfate and primary carbonaceous aerosols. The inclusion of VOCs from biomass burning might increase SOA production. However, the SOA simulations can not be significantly improved until we can gain a better understanding about its for-

mation mechanisms.
REMOTE was found to be a useful tool for investigations of the contribution of different emission sources to the aerosol pollution, as was shown in the study of the Mediterranean pollution episode in summer 2002. Sulfate aerosol particles were traced back to their emission sources, showing that ship emissions of SO_x contribute up to 60-85 % to the surface sulfate concentration over the Western Mediterranean. Their contribution reached 58 % averaged over the Mediterranean region in summer. Ship emissions of NO_x were found to contribute to the formation of secondary trace gases hence considerably decreasing Mediterranean air quality in summer. Surface level concentration of nitric acid could be reduced by 66 % in a sensitivity simulation without ship emissions, concentration of hydroxy radical droped by 42 %, formaldehyde by 24 %, mean surface ozone by 15 %. Summertime meteorological conditions of the Mediterranean region, namely high solar radiation intensity and semi-aridity, were found mainly responsible for the enhanced sulfate aerosol formation and life time in the atmosphere. The pronounced seasonality of the sulfate aerosol burden over this region was found to be independent of the variability in SO_x emissions, because the ship emissions have been assumed to be temporally constant. Similar results have been found analyzing the dependency of the temporal variability of sulfate and carbonaceous aerosols on the variability of respective emission sources averaged over Europe for the two different meteorological years 2002 and 2003.
Meteorological conditions have been found to play a major role in the spatial and temporal variations of the aerosol burden distribution. The main removal process of aerosol from the European atmosphere is wet deposition, thus the aerosol burden is very sensitive to precipitation. Fox example, the aridity in August 2003 caused a pollution enhancement by a factor of 1.5 over the Mediterranean region compared to August 2002. In general, pressure systems and corresponding winds control the advection and vertical diffusion and/or accumulation of aerosols. Blocking highs over areas of strong emissions enhance pollution levels substantially. Westerly winds from the North Atlantic, associated with strong pressure gradients, reduce pollution despite strong emissions. A combination of both removal by precipitation and enhanced advection can reduce the monthly mean burden by a factor of two, as was demonstrated for the month of February 2002 versus 2003. Meteorological conditions also substantially influence the formation of secondary aerosol particles. Availability of clouds and liquid water were found to govern sulfate production over northern and central Europe, while in southern Europe, temperature and solar radiation are the main factors controlling sulfate production via photo-oxidation processes. The simulated production of secondary organic aerosol is mainly governed by the efficiency of photo-oxidation. To be able to predict pollution levels by modeling aerosol distribution, accuracy in emission sources, formation processes and simulated meteorological conditions is very important.
For the historical simulation of the sulfate aerosol distribution over Europe the influence of meteorological variability on sulfate aerosol formation and life time has not been considered. All simulations of the sulfate aerosol distribution from 1900 to 2000 have been based on the same meteorological year 1997. Taking into account the significant temporal and spatial evolution of the sulfur emission sources in the past 100 years, the influence of the meteorology is expected to be less significant than for the two year simulation period.

With this data, provided by the Norwegian Meteorological Institute, the historical evolution of the direct radiative sulfate aerosol forcing over Europe was calculated. An off-line radiation transfer model ORTM was utilized for the forcing calculations. The mean direct forcing has increased since the 1900's reaching its peak in the 1980's and then returning in present times to approximately the values of the 1950's. Historically, the wintertime maximum of the direct radiative aerosol forcing was always located over the Mediterranean Sea. The wintertime geographical forcing distribution is different from the distribution of the sulfate aerosol load. From the 1960's to the 1990's, the sulfate aerosol wintertime pollution maximum was located over central Europe, but low solar radiation during the cold season did not result in a significant forcing here. Low surface albedo over water additionally increased the negative direct forcing over the Black and Mediterranean Sea. In summer, where high latitudes receive more solar radiation, both the burden and the forcing maxima have experienced a shift from northwestern to southeastern Europe. At the beginning of the century, the summertime sulfate aerosol burden and its forcing over the Mediterranean mainly originated from volcanic sulfur emissions. Today, it is the most polluted region over Europe during summer, dominated by anthropogenic emissions. Geographical changes in sulfur emission distribution in the past century reduced the mean European sulfate aerosol forcing efficiency from –246 W(g sulfate)$^{-1}$ in the 1900's to –230 W(g sulfate)$^{-1}$ in the year 2000.

The historical simulations must be complemented with the inclusion of the highly absorbing black carbon aerosol. We expect the temporal and spatial historical evolution of black carbon emissions and the resulting distribution of the atmospheric burden to be quite different from that of sulfate. Thus the inclusion of black carbon might substantially alter the historical direct radiative forcing estimates. Regionally, the forcings might partially offset each other, high contribution of black carbon may also amplify the total aerosol absorption. The non-linearity of the aerosol burden response associated with emission changes as suggested by Stier (2004) can additionally affect the historical aerosol burden of sulfate and black carbon and the corresponding direct forcing.

The present day direct aerosol radiative forcing was found to strongly depend on the chemical composition of the atmospheric aerosol and on its mixing state. For this study, the ORTM model has been modified to include carbonaceous aerosols, and to determine the forcing of internally mixed aerosol particles. The chemical composition of the internally mixed aerosols for every grid box was determined from the volume of sulfate, BC and OC in 10 % intervals. The assumption of internally mixed aerosol particles leads to an enhancement of both negative and positive forcing efficiencies, compared to the external mixture. Under an assumption of externally mixed aerosols the forcing is almost everywhere negative, with the absorbing black carbon overpowered by the scattering sulfate aerosol. When mixed internally, absorption of the aerosol is enhanced, resulting in positive aerosol forcing in spring and winter over eastern and south-eastern Europe. During the cold season, direct forcing is also very sensitive to the surface albedo. Enhanced surface albedo due to snow cover and sea ice can change the sign of the forcing from negative to positive and enhance the positive forcing. This was demonstrated exemplarily for February 2002 versus 2003: increased aerosol load in 2003 resulted in enhanced positive radiative forcing, because large parts of the continent were covered by snow in contrast to

the warmer winter 2002. The effect reached very high latitudes despite the limited hours of solar radiation. In March, the aerosol burden in 2003 was even higher than in February, but this had very little effect on the forcing, because most parts of central Europe were snow free. For all seasons, relative humidity and cloud cover influenced the forcing efficiency. Clouds reduce the negative forcing efficiency by a factor of 1.5 to 2 and change the sign of the positive forcing efficiency from negative to positive. Relative humidity can cause an increase of forcing efficiency of up to +200 W(g aerosol)$^{-1}$ and over –200 W(g aerosol)$^{-1}$.

In a sensitivity study, the direct forcing of a 'realistic' aerosol burden has been derived, adapting the underestimation factors from observations, 2 for black and 10 for organic carbon. The radiative forcing shows very high values for summer with –2.5 to –3 Wm^{-2} over most parts of Europe, –3.5 Wm^{-2} to –4 Wm^{-2} over the Mediterranean and the North Sea, and a high range for winter from –2 Wm^{-2} over the Mediterranean to +2 Wm^{-2} over the eastern Europe.

The direct forcing obtained for the total aerosol is comparable with other estimates given in literature. Comparison of the forcing of individual aerosol compounds shows that the estimates derived in this study are lower than the values found in literature. Different emission inventories and meteorologies applied in the models and different size distributions and optical parameters assumed alter the direct forcing estimates. The treatment of the relative humidity in the ORTM can additionally result in an underestimation of the direct forcing. In ORTM, Mie calculations are applied for the dry particle size. The specific extinction obtained for a dry particle is then multiplied with an RH growth factor. This approach can lead to an underestimation of the direct forcing for high relative humidities. Future modifications of the model shall thus improve the treatment of relative humidity.

The aerosol forcing has been simulated diagnostically, neglecting the dynamical feedback of the atmosphere. To investigate the actual past and present impact of the atmospheric aerosol on the European climate, the direct radiative forcing has to be calculated prognostically. The first, second and semi-indirect radiative forcings must also be included in the future modeling work. Aerosol-cloud interaction studies with REMOTE have been carried out over Indonesia (Langmann, 2006). First attempts have been made to consider this interaction over Europe. A new cloud scheme with microphysical parameterization of the ice phase (Pfeifer, 2006) will be implemented in REMOTE in the near future, opening possibilities of investigating the aerosol-ice-cloud interactions. Sea salt aerosol and mineral dust have been recently included in the model. Currently, the size resolving aerosol model M7 (Stier, 2004; Vignati et al., 2004) is being implemented in REMOTE. The implementation of M7 combined with other developments listed here promises to gain a deeper insight in the microphysics of the atmospheric aerosol, its chemical composition and interactions with climate on the regional scale.

Bibliography

Ackerman, A. S., Toon, B. O., Stevens, D. E., Heymfield, A. J., Ramanathan, B., and Welton, E. J., Reduction of Tropical Cloudiness by Soot, *Science*, *288*, 1042–1047, 2000.

Ackermann, I., Hass, H., Memmesheimer, M., Ebel, A., Binkowski, F., and Shankar, U., Modal aerosol dynamics model for Europe: Development and first applications, *Atmos. Environ.*, *32*, 2981–2999, 1998.

Adams, P., Seinfeld, J., and Koch, D., Global concentrations of tropospheric sulfate, nitrate, and ammonium aerosol simulated in a general circulation model, *J. Geophys. Res.*, *104*(D11), 13791–13824, 1999.

Adams, P., Seinfeld, J., Koch, D., L., M., and Jacob, D., General circulation model assessment of direct radiative forcing by the sulfate-nitrate-ammonium-water inorganic aerosol system, *J. Geophys. Res.*, *106*(D1), 1097–1112, 2001.

Albrecht, B., Aerosols, cloud microphysics and fractional cloudiness, *Science*, *245*, 1227–1230, 1989.

Andersson-Skøld, Y. and Simpson, D., Secondary organic aerosol formation in Northern Europe: a model study, *J. Geophys. Res.*, *106*(D7), 7357–7374, 2001.

Andreae, M. and Crutzen, P., Atmospheric aerosols: biogeochemical sources and role in atmospheric chemistry, *Science*, *276*, 1052–1057, 1997.

Andreae, T., Andreae, M., and Ichoku, C., Light scattering by dust and anthropogenic aerosol at a remote site in the Negev desert, Israel, *J. Geophys. Res.*, *107*(D2), 4008, 2002.

Bardouki, H., Berresheim, H., Vrekoussis, M., Sciare, J., Kouvarakis, G., Oikonomou, K., Schneider, J., and Mihalopous, N., Gaseous (DMS, MSA, SO_2, H_2SO_4 and DMSO) and particulate (sulfate and methanesulfonate) sulfur species over the northeastern coast of Crete, *Atmos. Chem. Phys.*, *3*, 1871–1886, 2003.

Bellouin, N., Boucher, O., Haywood, J., and M.S., R., Global estimate of aerosol direct radiative forcing from satellite measurements, *Nature*, 2005.

Benedictow, A., 1999 meteorological fields produced by PARLAM-PS and used as input for Eulerian EMEP model. Documentation and characterization, Tech. rep., Norwegian Meteorological Institute, 2002.

Blanchard, D., The electrification of the atmosphere by particles from bubbles in the sea, *Prog. Oceanogr.*, *1*, 71–202, 1963.

Bond, T., Streets, D., Yarber, K., Nelson, S., Woo, J., and Klimont, Z., A technology-based global inventory of black and organic carbon emissions from combustion, *J. Geophys. Res.*, *109*(D14203), 2004.

Bott, A., A positive definite advection scheme obtained by non-linear re-normalization of the advection fluxes, *Mon. Weather Rev.*, 1989.

Bott, A., Reply in "Notes and Correspondence", *Mon. Weather Rev.*, *117*, 2633–2636, 1989.

Boucher, O. and Pham, M., History of sulfate aerosol radiative forcings, *Geoph. Res. Lett.*, *29*(9), 10.1029/2001GL014048, 2002.

Boucher, O. and Theodore, L. A., General circulation model assessment of the sensitivity of direct climate forcing by anthropogenic sulfate aerosols to aerosol size chemistry, *J. Geophys. Res.*, *100*(D12), 26,117–26,134, 1995.

Brenguier, J.-L., Pawlowska, H., Schüler, L., Preusker, R., Fischer, J., and Fouquart, Y., Radiative properties of boundary layer clouds: Droplet effective radius versus number concentration, *J. Atmos. Sci.*, *57*, 803–821, 2000.

Capaldo, K., Corbett, J., Kasibhatla, P., Fischbeck, P., and Pandis, S., Effects of ship emissions on sulfur cycling and radiative climate forcing over the ocean, *Nature*, *400*, 743–746, 1999.

Chang, J. S., Brost, R. A., Isaken, I. S. A., Madronich, S., Middleton, P., Stockwell, W. R., and Walcek, C. J., A three-dimensional Eulerian acid deposition model: physical concepts and formulation, *J. Geophys. Res.*, *92*, 14681–14700, 1987.

Chung, S. and Seinfeld, J., Global distribution and climate forcing of caronaceous aerosols, *J. Geophys. Res.*, *108*(D19), 2002.

Chylek, P. and Wong, J., Effect of absorbing aerosols on global radiation budget, *J. Geophys. Res.*, *100*, 16235–16232, 1995.

Chylek, P., Jennings, S., and Pinnick, R., *Encyclopedia of Atmospheric Sciences*, chap. Soot, Academic Press, Amsterdam, 2003.

Claeys, M., Graham, B., and Vas, G., Formation of secondary organic aerosols through photooxidation of isoprene, *Science*, *303*(1173-1176), 2004.

Cooke, W., Liosse, C., Cachier, H., and Feichter, J., Construction of a 1°x1° fossil fuel emission data set for carbonaceous aerosol and implementation and radiative impact in the ECHAM4 model, *J. Geophys. Res.*, 1999.

Corbett, J. and Koehler, H., Updated emissions form ocean shipping, *J. Geoph. Res.*, *108*(D20), 4650, 2003.

Crutzen, P., *Nucleation of atmospheric aerosols*, chap. The role of particulate matter in ozone photochemistry, pp. 268–270, Elsevier, 1996.

Crutzen, P. and Zimmermann, P., The changing photochemistry of the troposphere, *Tellus*, *43*(A-B), 136–151, 1991.

DeMott, P. J., Chen, Y., Kreidenweis, S. M., Rogers, D. C., and Sherman, D. E., Ice formation by black carbon particles, *Geoph. Res. Lett.*, *26*(16), 2429–2432, 1999.

Dusek, U., Secondary Organic Aerosol Formation Mechanisms and Source Contributions in Europe, Tech. rep., IIASA, Laxenburg, Austria, 2000.

Ekman, A. and Rodhe, H., Regional temperature response due to indirect suflate aerosol forcing: impact of model resolution, *Clim. Dyn.*, *21*, 1–10, 2003.

Endresen, O., Sørgård, E., Sundet, J., Dalsøren, S., Isaksen, I., Berglen, T., and Gravir, G., Emissions from international sea transport and environmental impact, *J. Geophys. Res.*, *108*, 4560, 2003.

EPA, National Air Pollutant Emission Trends: 1900-1998, EPA 454/R-00-002, 2000.

Fabian, P., Atmosphäre und Umwelt, Springer Verlag, Berlin, 1993.

Fagerli, H., unpiblished, 2006.

Fagerli, H., Simpson, D., and Aas, W., Model performance for sulphur and nitrogen compounds for the period 1980 to 2000, in *In Transboundary Acidification, Eutrophication and Ground Level Ozone in Europe. EMEP Status Report 1/2003, Part II Unified EMEP Model Performance*, edited by L. Tarrasón, pp. 1–66, Norwegian Meteorological Institute, 2003.

Fagerli, H., Simpson, D., and Tsyro, S., Unified EMEP model: Updates, in *EMEP Report 1/2004, Transboundary acidification, eutrophication and ground level ozone in Europe. Status Report 1/2004*, pp. 11–18, Norwegian Meteorological Institute, 2004.

Fagerli, H., Simpson, D., and Jonson, J., PART II. EMEP Unified model performance, *in preparation*, 2006.

Feichter, J., Lohmann, U., and Schult, I., The atmospheric sulfur cycle in ECHAM-4 and its impact on the shortwave radiation, *Clim. Dym.*, *13*, 235–246, 1997.

Feichter, J., Roeckner, E., Lohmann, U., and Liepert, B., Nonlinear aspects of the climate responce to greenhouse gas and aerosol forcing, *J. Clim.*, *17*, 2384–2398, 2004.

Formenti, P., Andreae, M., Andreae, T., Galani, E., Vasaras, A., Zerefos, C., Amiridins, V., Orlovsky, L., Karnieli, A., Wendisch, M., Wex, H., Holen, B., Maenhaut, W., and Lelieveld, J., Aerosol optical properties and large scale transport of air masses: Observation at a coastal and a semiarid site in the eastern Mediterranean during summer 1998, *J. Geophys. Res.*, pp. 9807–9826, 2001.

Gelencsér, A., May, B., Simpson, D., Puxbaum, H., Wagenbach, D., Pio, C., Kasper-Giebl, A., and Legrand, M., Source apportionment of $PM_{2.5}$ organic aerosol in Europe: primary vs. secondary, natural vs. anthropogenic, fossil vs. biogenic origin, *to be submitted to J. Geoph. Res.*, 2006.

Gilgen, H., Wild, M., and Ohmura, A., Means and trends of shortwave irradiance at the surface estimated from global energy balance archive data, *J. Clim.*, *11*, 2042–2061, 1998.

Giorgi, F., X, B., and Qian, Y., Direct radiative forcing and regional climatic effects of anthropogenic aerosols over east Asia: a regional coupled climate-chemistry/aerosol model study, *J. Geophys. Res.*, *107*, 2002.

Giorgi, F., Bi, X., and Qian, Y., Indirect versus direct effects of anthropogenic sulfate on the climate of east Asia as simulated with a regional coupled climate-chemistry/aerosol model, *Clim. Change*, *58*, 345–376, 2003.

Guenther, A., Monson, R., and Fall, R., Isoprene and monoterpene emission rate variability: Observations with eucalyptus and emission rate algorithm development, *J. Geoph. Res.*, *96*(D6), 10799–10808, 1991.

Guenther, A., Zimmermann, P., Harley, P., Monson, R., and Fall, R., Isoprene and monoterpene emission rate variability: Model evaluations and sensitivity analyses., *J. Geoph. Res.*, *98*(D7), 12608–12617, 1993.

Hansen, J., Bond, T., Cairns, B., Gaeggler, H., Liepert, B., Novakov, T., and Schichtel, B., Carbonaceous Aerosols in the Industrial Era, *EOS*, *85*(25), 241–248, 2004.

Hass, H., Ebel, A., Feldmann, H., Jakobs, H., and Memmesheimer, M., Evaluation studies with a regional chemical transport model (EURAD) using air quality data from the EMEP monitoring network, *Atmos. Environ.*, *27A*, 867–887, 1993.

Hass, H., Jakobs, H., and Memmesheimer, M., Analysis of a regional model (EURAD) near surfacs gas concentrations predictions using observations from networks, *Met. atmos. Phys.*, *57*, 173–200, 1995.

Hass, H., van Loon, M., Kessler, C., Stern, R., Matthijsen, J., Sauter, F., Zlatev, Z., Langner, J., Foltescu, V., and Schaap, M., Aerosol Modelling: Results and Intercomparison from Europea Regional-scale Modelling Systems. A contribution to the EUROTRAC-2 subproject GLOREAM, Tech. rep., EUROTRAC ISS, Munich, 2003.

Haywood, J. and Boucher, O., Estimates of the direct and indirect radiative forcing due to tropospheric aerosols: A review, *Rev. of Geoph.*, *38*, 513–543, 2000.

Haywood, J. and Shine, K., The effect of anthropogenic sulfate and soot on the clear-sky planetray radiation budget, *Geophys. Res. Lett.*, 1995.

Haywood, J. M., Robert, D. L., Slingo, A., Edwards, J. M., and Shine, K. P., General circulation model calculations of the direct radiative forcing by anthropogenic sulfate and fossil-fuel soot aerosol, *J. Clim.*, *10*, 1562–1577, 1997.

Hering, S., Appel, D., Cheng, W., Slaymeh, F., Cadle, S., Mulawa, A., Cahill, T., Eldred, R., Surovik, M., Fitz, D., Howes, J., Knapp, K., Stockburger, L., Turpin, B., Huntzicher, J., Zhang, X., and McMurry, P., Comparison of sampling methods for carbonaceous aerosol in ambient air, *Aerosol Sci. Technol.*, *12*, 200–213, 1990.

Hess, M., Koepke, P., and Schult, I., Optical properties of aerosols and clouds: The software pacage OPAC, *Bull. Am. Meteorol. Soc.*, *79*, 831–844, 1998.

Hesstvedt, E., Hov, O., and Isaksen, I., Quasy steady-state approximations in air pollution modelling: Comparison of two numerical schemes for oxidant prediction, *Int. J. Chemical Kinetics*, *10*, 971–994, 1978.

Hitzenberger, R., Berner, A., Kromp, R., Kasper-Giebl, A., Limbeck, A., Tschrwenka, W., and H., P., Black carbon and other species at a high-elevation European site (Mt. Sonnblick (3106 m a.s.l., Austria): Concentration and scavenging efficiencies, *J. Geophys. Res.*, *105*(D20), 24637–24645, 2000.

Hjellbrekke, A.-G., Data report 2002, acidifying and eutrophying compounds, Tech. Rep. EMEP/CCC Report 1/2004, EMEP, Norway, 2004.

Hjellbrekke, A.-G. and Solberg, S., Acidifying and eutrophying compounds, Tech. rep., EMEP, Norway, 2004.

Hohenegger, C. and Vidale, P., Sensitivity of the Eeropean climate to aerosol forcing as simulated with a regional model, *J. Geophys. Res.*, *110*, 2005.

Hongisto, M., Sofiev, M., and Joffre, S., Hilatar, a limited area simulation model of acid contaminants, Part ii, *Atmos. Environ.*, *37*, 1535–1547, 2003.

Horowitz, L., Waltern, S., Mauzerall, D., Emmons, L., Rasch, P., Granier, C., Tie, X., Lamrque, J.-F., Schultz, M., and Brasseur, G., A global simulation of tropospheric ozone and related tracers: Description and evaluation of MOZART, version 2, *J. Geoph. Res.*, *105*(D4), 4399–4407, 2003.

IPCC, IPCC Third Assessment Report. Climate Change 2001: The Scientific Basis, Tech. rep., Cambridge University Press, 2001.

Jacob, D., A note to the simulation of the annual and inter-annual variability of the water budget over the Baltic Sea drainage basin, *Met. and Atmos. Phys.*, *77*, 61–73, 2001.

Jacobson, M., Strong radiative heating due to the mixing state of black carbon in atmospheric aerosols, *Nature*, *409*, 695–697, 2001.

Jacobson, M., Hannson, H., Noone, K., and Charlson, R., Organic atmospheric aerosols: Review and state of science, *Rev. Geophys.*, *38*, 267–294, 2000.

Jonson, J., Simpson, D., Fagerli, H., and Solberg, S., Can we explain the trends in European ozone levels?, *Atmos. Chem. Phys.*, accepted for publication in Atmos. Chem. and Physics, 2006.

Kanakidou, M., Seinfeld, J., Pandis, S., Barnes, I., Dentener, F., Facchini, M., van Dingenen, R., Ervens, B., Nenes, A., Nielsen, C., Swietlicki, E., Putaud, J., Balkanski, Y., Fuzzi, S., Horth, J., Moortgat, G., Winterhalter, R., Myhre, C., Tsigaridis, K., Vignati, E., Stephanou, E., and Wilson, J., Organic aerosol and global climate modelling: a review, *Atmos. Chem. Phys. Discuss.*, *4*, 5855–6024, 2004.

Kasper-Giebl, A., Koch, A., Hitzenberger, R., and Puxbaum, H., Scavenging efficiency of "Aerosol Carbon" and sulfate in supercooled clouds at Mt. Sonnblick (3106 m a.s.l., Austria, *J. Atmos. Chem.*, *35*(1), 33–46, 2000.

Kaufman, Y., Tanré, D., and Boucher, O., A satellite view of aerosols in the climate system, *Nature*, *419*, 215–223, 2002.

Khain, A., Rosenfeld, D., and Pokrovsky, A., Simulating convective clouds with sustained supercooled liquid water down to -37.5 °C using a spectral microphysical model, *Geophys. Res. Lett.*, *28*, 3887–3890, 2001.

King, M., Kaufman, Y., Tanré, D., and Nkajima, T., Remote sensing of tropospheric aerosols: Past, present and future, *Bull. Am. Meteorol. Soc.*, *80*, 2229–2259, 1999.

Koch, D., Bond, T., Streets, D., and Unger, N., Global impact of aerosols from particular source regions and sectors, *J. Geophys. Res.*, submitted, 2006.

Koepke, P., Hess, M., Schult, I., and Shettle, E., Global aerosol data set, *Fourth International Aerosol Conference*, 1994.

Kouvarakis, G., Tsigaridis, K., Kanakidou, M., and Mihalopous, N., Temporal variations of surface regional background ozone over Crete Island in the southwestern Mediterranean, *J. Geophys. Res.*, *104*(D4), 4399–4407, 2000.

Krüger, O. and Grassl, H., The indirect aerosol effect over Europe, *Geophys. Res. Lett.*, *29*, 2002.

Langmann, B., Numerical modelling of regional scale transport and photochemistry directly together with meteorological processes, *Atmos. Environ.*, *34*, 3585–3598, 2000.

Langmann, B., Rauchpartikel in der Atmospäre: Modellstudien am Beispiel indonesischer Brände, Habilitationsschrift, Max-Planck-Institut for Meteorology, Hamburg, Germany, 2006.

Langmann, B. and Bauer, S., On the importance of reliable initial and boundary concentrations of ozone for regional scale air pollution modelling, *J. Atmos. Chemistry*, *42*, 71–90, 2002.

Langmann, B., Herzog, M., and Graf, H. F., Radiative forcing of climate by sulfate aerosols as determined by a regional circulation chemistry transport model, *Atmos. Environ.*, *32*(16), 2757–2768, 1998.

Langmann, B., Bauer, S., and Bey, I., The influence of the global photochemical composition of the troposphere on European summer smog, Part I: Application of a global to mesoschle model chain, *J. Geophys. Res.*, *108*(D4), 4146, 2003.

Lave, L. and Seskin, P., An Analysis of the Association Between U.S. Mortality and Air Pollution, *J. Am. Statist. Ass.*, *68*(342), 1973.

Lawrence, M. and Crutzen, P., Influence of NO_x emissions from ships on thropospheric photochemistry and climate, *Nature*, *402*, 167–170, 1999.

Lelieveld, J. and Dentener, F., What controls tropospheric ozone?, *J. Geophys. Res.*, 2000.

Lelieveld, J., Berresheim, H., Borrmann, S., Crutzen, P., Dentener, F., Fischer, H., Feichter, J., Flatau, P., Heland, J., Holzinger, R., Korrmann, R., Lawrence, M., Levin, Z., Marcowicz, K., Mihalopoulos, N., Minikin, A., Ramanathan, V., De Reus, M., Roelofs, G., Scheeren, H., Sciare, J., Schlager, H., Schultz, M., Siegmund, P., Steil, B., Stephanou, E., Stier, P., Traub, M., Warneke, C., Williams, C., and Ziereis, H., Global air pollution crossroads over the Mediterranean, *Sciance*, *298*(5594), 794–799, 2002.

Lenoble, J. and Brogniez, C., A comparative review of radiation aerosol models, *Contr. Atmos. Phys.*, *57*, 1–20, 1984.

Lesins, G., Chylek, P., and Lohmann, U., A study of internal and external mixing scenarios and its effect on aerosol optical properties and direct rediative forcing, *J. Geophys. Res.*, *107*(doi.10.1029/2001JD000973), 1227–1230, 2002.

Li, J., Wong, J., Dobbie, J., and Chýlek, P., Parameterization of the optical properties of sulfate aerosols, *J. Atmosph. Sci.*, 2001.

Liepert, B., Feichter, J., Lohmann, U., and Roeckner, E., Can aerosols spin down the water cycle in a warmer and moister world?, *Geophys. Res. Lett.*, *31*, L06207, 2004.

Likens, G. and Bohrmann, F., Acid rain: a serious regional environmental problem, *Science, New Series*, *184*, 1176–1179, 1974.

Limbeck, A., Kulmala, M., and Puxbaum, H., Secondary organic aerosol formation in the atmosphere via heterogeneous reaction of gaseous isoprene on acidic particles, *Geophys. Res. Lett.*, *30*, 2003.

Lin, W. and Gao, J., Acid deposition and intergrated zoning control in China, *Environ. Management*, 2002.

Lloyd's Register of Shipping, London, Marine exhaust Emissions Research Program, 1995.

Lloyd's Register of Shipping, London, Marine exhaust Emissions Quantification Study - Baltic Sea., Final Report 98/EE77036, 1998.

Lloyd's Register of Shipping, London, Marine exhaust Emissions Quantification Study for the Mediterranean Sea, 1999.

Lohmann, U., A glaciation indirect aerosol effect caused by soot aerosols, *Geophys. Res. Lett.*, *29*, 1052, 2002.

Madronich, S., Photodissociation in the atmosphere, 1. actinic flux and the effects of ground reflections and clouds, *J. Geophys. Res.*, *92*(D8), 9740–9752, 1987.

Majewski, D., The Europa Modell of the Deutsche Wetterdienst, *Seminar Proccedings ECMWF*, *2*, 147–191, 1991.

Marmer, E. and Langmann, B., Impact of ship emissions on Mediterranean summertime pollution and climate: A regional model study, *Atmos. Environ.*, *39*, 4659–4669, 2005.

Marmer, E., Langmann, B., Hungershöfer, K., and Trautmann, T., Present-day aerosol forcing due to sulfate, black and organic carbon, *in preparation*, 2006.

Mellor, B. and Yamada, T., A hierarchy of turbulence closure models for planetary boundary layers, *J. Atmos. Sc.*, *31*, 1791–1806, 1974.

Memmesheimer, M., Tippke, J., Ebel, A., Hass, H., Jakobs, H., and Laube, M., On the use of EMEP emission inventories for European scale air pollution modelling with the EURAD model, *EMEP Workshop on Photooxidant Modelling for Long-Range Transport in Relation to Abatement Strategies*, *16-19*, 307–324, Berlin, Germany, 1991.

Menon, S., Hansen, J., Nazarenko, L., and Luo, Y., Climate effects of black carbon aerosols in China and India, *Science*, *297*, 2250–2253, 2002.

Mesinger, F. and Arakawa, A., Numerical methods used in atmospheric models, *Garp publications Series*, 1976.

Mickley, L., Murti, P., Jacob, D., Logan, J., Koch, D., and D.(1999), R., Radiative forcing from tropospheric ozone calculated with a unified chemistry-climate model, *J. Geophys. Res.*, 1999.

Middlebrook, A., Murphy, D., and Thomson, D., Observations of organic material in individual marine particles at Cape Grim during the First Aerosol Characterization Experiment (ACE 1), *J. Geophys. Res.*, *103*, 16475–16483, 1998.

Mihalapous, N. and de Reus, M., Mediterranean intensive oxidant study (MINOS 2001), *Atm. Chemist. and Phys., Special Issue*, 2004.

Murphy, D. and Thomson, D., Chemical composition of single aerosol particles at Idaho Hill, *J. Geophys. Res.*, *102*, 6341–6368, 1997.

Myhre, C. and Nielsen, C., Optical properties in the uv and visible spectral region of organic acids relevant to tropospheric aerosols, *Atmos. Chem. Phys. Discuss.*, *4*, 3013–3043, 2004.

Myhre, G., Stordal, F., Restad, K., and A., I. I. S., Estimates of the direct radiative forcing due to sulfate and soot aerosols, *Tellus*, *50B*, 463–477, 1998.

Myhre, G., A., M., and Stordal, F., Historical evolution of radiative forcing of climate, *Atmos. Environ.*, *35*, 2361–2373, 2001.

Mylona, S., Sulphur dioxide emissions in Europe 1880-1991 and their effect on sulphur concentrations and depositions, *Tellus.*, *48B*, 662–689, 1996.

Nemesure, S., Wagner, R., and Schwartz, S. E., Direct shortwave forcing of climate by the anthropogenic sulfate aerosol: sensitivity to particle size, composition and relative humidity, *J. Geophys. Res.*, *100*, 26,105–26,116, 1995.

Novakov, T., Ramanathan, V., Hansen, J., Kirchstettter, T., Sato, M., Sinton, J., and Sathaye, J., Large historical changes of fossil fuel black carbon aerosols, *Geophys. Res. Lett.*, *30*(6), 1324, 2003.

Odum, J., Jungkamp, T., Griffin, R., Flagan, R., and Seinfeld, J., The atmospheric aerosol formation potential of whole gasoline vapor, *Science*, *274*, 96–99, 1997.

Odum, J., Jungkamp, T., Griffin, R., Forstner, J., Flagan, R., and Seinfeld, J., Aromatics, reformulated gasoline and atmospheric organic aerosol formation, *Environ. Sci. Technol.*, *31*, 1890–1897, 1997.

Pekkanen, J., Peters, A., Hoek, G., Tiittanen, P., Brunekreef, B., de Hartog, J., Heinrich, J., Ibald-Mulli, A., Kreyling, W., Lanki, T., Timonen, K., and Vanninen, E., Particulate Air Pollution and Risk of ST-Segment Depression During Repeated Submaximal Exercise Tests Among Subjects With Coronary Heart Disease. The Exposure and Risk Assessment for Fine and Ultrafine Particles in Ambient Air (ULTRA) Study, *Circulation*, *106*, 933, 2002.

Penner, J., Chuang, C., and Grant, K., Climate forcing by carboaceous and sulfate aerosols, *Clim. Dyn.*, *14*, 836–851, 1998.

Penner, J., Andreae, M., Annegarn, H., Barrie, L., Feichter, J., Hegg, D., Jayaraman, A., Leatch, R., Murphy, D., Nganga, J., and Pitari, G., *Climate change 2001: The scientific basis*, chap. Aerosols, their direct and indirect effects, Cambridge University Press, 2001.

Pfeifer, S., *Modeling cold cloud processes with the regional climate model REMO*, Ph.D. thesis, Fachbereich Geowissenschaften der Universität Hamburg, 2006.

Pio, C., Legrand, M., Oliveira, T., Afonso, J., Santos, C., Fialho, P., Barata, F., Puxbaum, H., Gelencser, A., Preunkert, S., and Schock, M., Climatology of aerosol composition (organic versus inorganic) at non-urban areas on a West-East transect across Europe, *to be submitted to J. Geophys. Res.*, 2006.

Pope, C., Cancer, cardiopulmonary mortality, and long-term exposure to fine particulate air pollution, *Journal of the American Medical Association*, *287*, 1132–1141, 2002.

Putaud, J., Raes, F., Van Dingenen, R., Bruegemann, E., Facchini, M., Decesrai, S., Fuyyi, S., Gehrig, R., Hueglin, C., Laj, P., Lorbeer, G., Maenhaut, W., Mihalopous, N., Mueller, K., Yuerol, X., Rodriguez, S., Schneider, J., Spindler, G., ten Brik, H., Tørseth, K., and Wiedensohler, A., A European aerosol phenomenology–2: chemical characteristics of particulate matter at kerbsite, urban, rural and background sites in Europe, *Atmos. Environ.*, *38*, 2579–2595, 2004.

Qian, Y., Leung, L., Ghan, S., and Giorgi, F., Regional climate effects of aerosols over China: modeling and observations, *Tellus*, 2003.

Ravishankara, A., Heterogeneous and multiphase chemistry in the troposphere, *Science*, *276*, 1058–1066, 1997.

Roeckner, E., The atmospheric general circulation model ECHAM4: Model description and simulation of present-day climate, MPI Report 218, Max-Planck-Institut für Meteorologie, Hamburg, 1996.

Rosenfeld, D., TRMM Observed First Direct Evidence Of Smoke From Forest Fires Inhibiting Rainfall, *Geophys. Res. Lett.*, *26*, 3105–3108, 1999.

Schaap, M., Denier van Der Gon, J., Visschedijk, A., van Loon, M., ten Brink, H., Dentener, F.J. nad Putaud, J.-P., Guillaume, B., Liousse, C., and Builtjes, P., Anthropogenic Black Carbon and Fine Aerosol Distribution over Europe, *J. Geophys. Res.*, 2004.

Scheeren, H., Lelieveld, J., Roelofs, G., Williams, J., Fischer, H., de Reus, M., de Gouw, J. A., Warneke, C., Holzinger, R., Schlager, H., Kluepfel, T., Bodler, M., van der Veen, C., and Lawrence, M., The impact of monsoon outflow from India and Southeast Asia in the upper troposphere over the eastern Mediterranean, *Atm. Chemist. and Phys.*, *3*, 1589–1608, 2003.

Schell, B., *Die Behandlung sekundärer organische Aerosole in einem komplexen Chemie-Transport-Modell*, Ph.D. thesis, University of Cologne, Germany, 2000.

Schnaiter, M., Linke, C., Moehler, O., Naumann, K. H., Saathoff, H., Wagner, R., and Schurath, U., Absorbtion amplification of black carbon internally mixed with secondary organic aerosol, *J. Geophys. Res.*, *107*(D19), 2005.

Sciare, J., Bardouki, H., Moulin, C., and Mihalopoulos, N., Aerosol sources and their contribution to the chemical composition of aerosols in the Eastern Mediterranean Sea during summer, *Atm. Chemist. and Phys.*, *3*, 291–302, 2003.

Seinfeld, J. and Pandis, S., *Atmospheric Chemistry and Physics: From Air Pollution to Climate Change*, John Wiley and Sons, New York, 1998.

Seinfeld, J. H., ed., *Direct aerosol forcing*, Air Pollution as a Climate Forcing: A Workshop, New York, N.Y., Goddard Institute for Space Studies, 2002.

Simpson, D., Fagerli, H., Jonson, J., Tsyro, S., Wind, P., and Tuovinen, J.-P., The EMEP Unified Eulerian Model. Model Description, EMEP MSC-W Report 1/2003, Norwegian Meteorological Institute, 2003.

Simpson, D., Tuovinen, J.-P., Emberson, L., and Ashmore, M., Characteristics of an ozone deposition module II: sensitivity analysis, *Water, Air and Soil Pollut.*, *143*, 123–137, 2003.

Simpson, D., Fagerli, H., Hellsten, S., Knulst, K., and Westling, O., Comparison of modelled and monitored deposition fluxes of sulphur and nitrogen to ICP-forest sites in Europe, *Biogeosciences*, submitted, 2006.

Smolarkiewitz, P., A simple posititve definite advection scheme with small implicit diffusion, *Monthly Weather Rev.*, *111*, 476–479, 1983.

Sokolik, I. and Toon, O., Direct radiative forcing by anthropogenic airborne mineral aerosols, *Nature*, *381*, 681–683, 1996.

Solmon, F., Giorgi, F., and Liousse, C., Aerosol modelling for regional climate studies: application to anthropogenic particles and evaluation over a European/African domain, *Tellus*, *58B*, 51–72, 2006.

Stier, P., *Towards the Assessment of the Aerosol Radiative Effects: A Global Modelling Approach*, Ph.D. thesis, Fachbereich Geowissenschaften der Universität Hamburg, 2004.

Stockwell, W., Middleton, P., Chang, J., and Tang, X., The second generation regional acid deposition model: Chemical mechanism for regional air quality modeling, *J. Geoph. Res.*, *95*(D10), 16343–16367, 1990.

Stoddart, J., Jeffries, D., Lkewolle, A., Clair, T., Dillon, P., Driscoll, C., Fortius, M., Johannessen, M., Kahl, J., Kellogg, J., Kemp, A., Mannio, J., Monteith, D., Murdoch, P., Patrick, S., Rebsdorf, A., and Skjelkv, B., Regional trends in aquatic recovery from acidification in North America and Europe, *Nature*, 1999.

Strader, R., F., L., and Pandis, S., Evaluation of secondary organic aerosol formation in winter, *Atmos. Environ.*, *33*, 4849–4863, 1999.

Swedish NGO Secretariat on Acid Rain, Environmental NGO recommendations on COM (2002) 595 as regards the sulfur content of marine fuels, 2003.

Tanré, D., Geleyn, J., and J., S., First results of the introduction of an advanced aerosol-radiation interaction in the ECMWF low resolution global model, in *Aerosols and Their Climatic Effects: Proceeding of the Meetings of Experts*, edited by H. Gerber and A. Deepak, pp. 133–177, Williamsburg, VA, USA, 1984.

Tegen, I., Koch, D., Lacis, A. L., and Sato, M., Trends in tropospheric aerosol loads and corresponding impact on direct radiative forcing between 1950 and 1990: A model study, *J. Geophys. Res.*, *105*, 26,971–26,989, 2000.

The European Environmental Bureau (EEB), The European Federation for Transport and Environment (T&E), Seas at Risk (SAR), and The Swedish NGO Secretariat on Acid Rain, Air pollution from ships, A briefing document by The European Environmental Bureau (EEB), The European Federation for Transport and Environment (T&E), Seas at Risk (SAR) and The Swedish NGO Secretariat on Acid Rain. Available on http/:www.eeb.org/activities/air/publications.htm, 2003.

Tiedtke, M., A comprehensive mass flux scheme for cumulus parameterization in large-scale models, *Monthly Weather Review*, *117*, 1778–1800, 1989.

Tuovinen, J.-P., Ashmore, M., Emberson, L., and Simpson, D., Testing and improving the EMEP ozone deposition module, *Atmos. Environ.*, *38*, 2373–2385, 2004.

Turpin, B., Saxena, P., and Andrews, E., Measuring and simulating prticulate organics in the atmosphere: problems and prospects, *Atmos. Environ*, *34*, 2983–3013, 2000.

Twomey, S., Pollution and the planetary albedo, *Atmos. Environ.*, *8*, 1251–1256, 1974.

UNECE/EMEP, *EMEP/CORINAIR Emission Inventory Guidebook - 3rd edition October 2002 UPDATE*, EEA (European Environment Agency), 2002.

van Aardenne, J., Dentener, F., Olivier, J., Goldewijk, C., and Lelieveld, J., A 1 degrees x 1 degrees resolution data set of historical anthropogenic trace gas emissions for the period 1890-1990, *gbc*, *15*(4), 909–928, 2001.

van Loon, M., Ackermann, I., Schaap, M., and Builtjes, P., Primary and secondary aerosol simulation using LOTOS, *J. Aerosol Sci.*, *31*(Suppl.1), S52–S53, 2000.

Veefkind, J., de Leeuw, G., Durkee, P., Russel, P., Hobbs, P., and Livingston, J., Aerosol optical depth retireved using ATSR-2 and AVHRR data during TARFOX, *J. Geophys. Res.*, *104*, 2253–2260, 1999.

Vestreng, V., Review and Revision. Emission data reported to CLRTAP, Tech. Rep. EMEP-MSCW Status Report 2003, Technical Report Note 1/2003, Norwegian Meteorological Institute, Oslo, Norway, 2003.

Vestreng, V. and Semb, A., in preparation, 2006.

Vestreng, V., Adams, M., and Goodwin, J., Inventory Review 2004. Emission data reported to CLRTAP and under the NEC directive, EMEP/EEA Joint Review Report, Tech. Rep. EMEP-MSCW Report 1/2004, Norwegian Meteorological Institute, Oslo, Norway, 2004.

Vignati, E., Wilson, J., and Stier, P., M7: a size resolved aerosol mixture module for the use in global aerosol models, *J. Geophys. Res.*, *109*, 2004.

Walcek, C. J., Brost, R. A., Chang, J. S., and Wesely, M. L., SO_2, sulfate and HNO_3 depostition velocities computed using regional landuse and meteorological data, *Atmos. Environ.*, *20*, 949–964, 1986.

Wehrli, C., Extraterrestrial solar spectrum, Tech. Rep. Publication no. 615, World Radiation Center, Davos, Switzerland, 1985.

Wesley, M., Parameterization of surface resistances to gaseous dry deposition in regional-scale numerical models, *Atmos. Environ.*, *23*, 1293–1304, 1989.

WHO, World Health Report 2002, Tech. rep., World Health Organization, Geneva, 2002.

Wiedinmeyer, C., Guenther, A., Harley, O., Hewitt, N., Geron, C., Artaxo, P., Steinbrecher, R., and Rasmussen, R., *Emissions of Atmospheric Trace Compounds*, chap. Global Organic Emissions from Vegetation, pp. 115–170, Kluwer Academic Publishers, Dordrecht, The Netherlands, 2004.

Acknowledgements

First of all I would like to thank my supervisor Bärbel Langmann for the world's best supervision! I don't think I would have decided to go for my PhD without you encouraging me, sharing your knowledge, experience, without your moral support and fundings! I had to give up otherwise.

I sincerely want to thank Hans Graf and Hartmut Grassl for their supervision, ideas and moral support.

A lot of thanks goes to my office made Melissa Pfeffer, for all the discussions, revisions and most of all for the correct English! Not only that, also the good time we had sharing the office for all these years.

Also all the other colleagues from the old Schlump, Anita and Steven, Manu and Angelika. I am going to miss you guys!

I want to thank Stefan Kinne and Martin Schulz for revisions and sharing of their ideas that helped to improve this work.

Thanks to all the co-authors Katja, Hilde, Vigdis and Andras for their contribution and an excellent co-operation.

Thanks to the CARBOSOL partners for providing the measurement data and for the good project co-operation and to Benedikt Schell for the SORGAM code.

I want to thank CIS for their support, and privately Rainer for fixing my home computer.

I finally have to thank all my wonderful friends who were there for me in good and in bad times! And my family for their love and patience! My loving parents, who have always always supported and encouraged me, and my very best children, Dalia and Nesta, who were my main motivators through out the time!!!

THANK YOU!!!

MPI-Examensarbeit-Referenz:
Examensarbeit Nr. 1-82 bei Bedarf bitte anfragen:
MPI für Meteorologie, Abtlg.: PR, Bundesstr. 53, 20146 Hamburg

MPI-Report-Referenz:
MPI-Report Nr. 1-351 bei Bedarf bitte anfragen:
MPI für Meteorologie, Abtlg.: PR, Bundesstr. 53, 20146 Hamburg

---

Beginn einer neuen Veröffentlichungsreihe des MPIM, welche die vorherigen Reihen "Reports" und "Examensarbeiten" weiterführt:

„Berichte zur Erdsystemforschung" , „*Reports on Earth System Science*", ISSN 1614-1199
Sie enthält wissenschaftliche und technische Beiträge, inklusive Dissertationen.

Berichte zur Erdsystemforschung Nr.1 Juli 2004	**Simulation of Low-Frequency Climate Variability in the North Atlantic Ocean and the Arctic** Helmuth Haak
Berichte zur Erdsystemforschung Nr.2 Juli 2004	**Satellitenfernerkundung des Emissionsvermögens von Landoberflächen im Mikrowellenbereich** Claudia Wunram
Berichte zur Erdsystemforschung Nr.3 Juli 2004	**A Multi-Actor Dynamic Integrated Assessment Model (MADIAM)** Michael Weber
Berichte zur Erdsystemforschung Nr.4 November 2004	**The Impact of International Greenhouse Gas Emissions Reduction on Indonesia** Armi Susandi
Berichte zur Erdsystemforschung Nr.5 Januar 2005	**Proceedings of the first HyCARE meeting, Hamburg, 16-17 December 2004** Edited by Martin G. Schultz
Berichte zur Erdsystemforschung Nr.6 Januar 2005	**Mechanisms and Predictability of North Atlantic - European Climate** Holger Pohlmann
Berichte zur Erdsystemforschung Nr.7 November 2004	**Interannual and Decadal Variability in the Air-Sea Exchange of CO2 - a Model Study** Patrick Wetzel
Berichte zur Erdsystemforschung Nr.8 Dezember 2004	**Interannual Climate Variability in the Tropical Indian Ocean: A Study with a Hierarchy of Coupled General Circulation Models** Astrid Baquero Bernal
Berichte zur Erdsystemforschung Nr9 Februar 2005	**Towards the Assessment of the Aerosol Radiative Effects, A Global Modelling Approach** Philip Stier
Berichte zur Erdsystemforschung Nr.10 März 2005	**Validation of the hydrological cycle of ERA40** Stefan Hagemann, Klaus Arpe and Lennart Bengtsson
Berichte zur Erdsystemforschung Nr.11 Februar 2005	**Tropical Pacific/Atlantic Climate Variability and the Subtropical-Tropical Cells** Katja Lohmann
Berichte zur Erdsystemforschung Nr.12 Juli 2005	**Sea Ice Export through Fram Strait: Variability and Interactions with Climate**- Torben Königk
Berichte zur Erdsystemforschung Nr.13 August 2005	**Global oceanic heat and fresh water forcing datasets based on ERA-40 and ERA-15** Frank Röske

MPI-Examensarbeit-Referenz:
Examensarbeit Nr. 1-82 bei Bedarf bitte anfragen:
MPI für Meteorologie, Abtlg.: PR, Bundesstr. 53, 20146 Hamburg

MPI-Report-Referenz:
MPI-Report Nr. 1-351 bei Bedarf bitte anfragen:
MPI für Meteorologie, Abtlg.: PR, Bundesstr. 53, 20146 Hamburg

Berichte zur Erdsystemforschung Nr.14 August 2005	**The** HAM**burg** O**cean** C**arbon** C**ycle Model HAMOCC5.1 - Technical Description Release 1.1** Ernst Maier-Reimer, Iris Kriest, Joachim Segschneider, Patrick Wetzel
Berichte zur Erdsystemforschung Nr.15 Juli 2005	**Long-range Atmospheric Transport and Total Environmental Fate of Persistent Organic Pollutants - A Study using a General Circulation Model** Semeena Valiyaveetil Shamsudheen
Berichte zur Erdsystemforschung Nr.16 Oktober 2005	**Aerosol Indirect Effect in the Thermal Spectral Range as Seen from Satellites** Abhay Devasthale
Berichte zur Erdsystemforschung Nr.17 Dezember 2005	**Interactions between Climate and Land Cover Changes** Xuefeng Cui
Berichte zur Erdsystemforschung Nr.18 Januar 2006	**Rauchpartikel in der Atmosphäre: Modellstudien am Beispiel indonesischer Brände** Bärbel Langmann
Berichte zur Erdsystemforschung Nr.19 Februar 2006	**DMS cycle in the ocean-atmosphere system and its response to anthropogenic perturbations** Silvia Kloster
Berichte zur Erdsystemforschung Nr.20 Februar 2006	**Held-Suarez Test with ECHAM5** Hui Wan, Marco A. Giorgetta, Luca Bonaventura
Berichte zur Erdsystemforschung Nr.21 Februar 2006	**Assessing the Agricultural System and the Carbon Cycle under Climate Change in Europe using a Dynamic Global Vegetation Model** Luca Criscuolo
Berichte zur Erdsystemforschung Nr.22 März 2006	**More accurate areal preciption over land and sea, APOLAS Abschlussbericht** K. Bumke, M. Clemens, H. Graßl, S. Pang, G. Peters, J.E.E. Seltmann, T. Siebenborn, A. Wagner
Berichte zur Erdsystemforschung Nr.23 März 2006	**Modeling cold cloud processes with the regional climate model REMO** Susanne Pfeifer


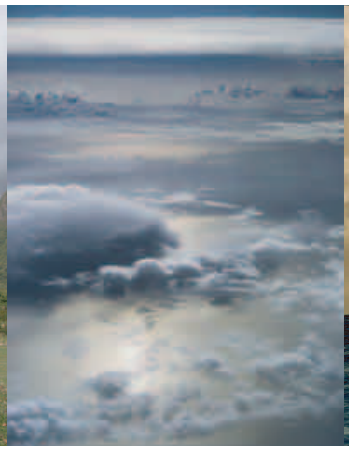


ISSN 1614-1199